Multi-scale models of T cell activation

By
Huan Zheng

B.S.E in Chemical Engineering
with Certificate in Applied and Computational Mathematics
Princeton University, 2005

Submitted to the Department of Chemical Engineering in partial fulfillment of the requirements for the degree of

DOCTOR OF PHILOSOPHY
in Chemical Engineering
at the
Massachusetts Institute of Technology

July 2010
[September 2010]

Signature of Author: _____
Department of Chemical Engineering
July, 2010

Certified by: _____
Arup K. Chakraborty
Robert T. Haslam Professor of Chemical Engineering
Professor of Chemistry and Biological Engineering
Thesis Superviser

Accepted by: _____
William M. Deen
Carbon P. Dubbs Professor of Chemical Engineering
Graduate Officer of the Department

This doctoral thesis has been examined by a Committee of the Department of Chemical Engineering as follows:

Professor K. Dane Wittrup _____
C.P. Dubbs Professor of Chemical Engineering
Committee Chairman

Professor Arup Chakraborty _____
Robert T. Haslam Professor of Chemical Engineering
Professor of Chemistry and Biological Engineering
Thesis Superviser

Professor Darrell Irvine _____
Associate Professor of Materials Science
and Biological Engineering
Committee Member

Professor Mehran Kardar _____
Professor of Physics
Committee member

Abstract

The overarching theme of this thesis is to develop and apply multi-scale computational techniques adopted from physical sciences to study a key phenomenon underlying the adaptive immune response: the activation of T cells. The specific objectives are: 1) develop efficient and versatile computational frameworks to study multi-scale biological systems in silico; 2) obtain mechanistic insights into how T cells are triggered in vivo.

The first problem investigated in this thesis addressed a controversy regarding when and how T cells alter migratory patterns in lymphoid tissues, as observed in intravital microscopy experiments. By developing a lattice-based model for T cell migration coupled with a mechanistically motivated simple scheme for T cell activation, I showed that the quantity and quality of cognate antigen (Ag) presented by dendritic cells (DC) dictate such changes. The results from theoretical and computational analyses were not only in agreement with synergistic experiments, but also made predictions that have been tested positively. Furthermore, I identified a consolidated measure of Ag quantity and quality, which provides a unifying conceptual framework for considering diverse future experimental results.

The results from this study also suggested that T cells may integrate sub-optimal signals derived from successive encounters with DCs to achieve full activation. However, an underlying molecular mechanism that may confer such "short term memory" of exposure to Ag is not known. I explored the possibility that the hysteresis resulting from positive feedback regulation of the catalytic conversion of a G-protein RasGDP to RasGTP in the T cell receptor (TCR) membrane-proximal signaling network may enable such "short term memory". I developed a multiscale computational model that combines stochastic simulations of the TCR membrane-proximal signaling network with T cell migration. The results showed that this hysteresis can enable T cells to integrate signals derived from weakly stimulatory DCs and may greatly enhance the detection sensitivity during disease onset when Ag presentation is low. The computational framework developed in this study can be readily adapted to examine diverse biological systems where signaling and cell motion need to be studied simultaneously. For example, the model was modified to investigate a DC-mediated mechanism for signal integration, and our results suggest that this mechanism is less likely.

Initial steps were also taken to construct a macroscopic model that aims to study how T cell activation impacts observations at the organismic level. Preliminary results for how microscopic receptor-ligand interactions affect the proliferation of different T cell types are presented. Directions for future research are suggested based on these findings.

To those who dare to challenge and persist

Acknowledgements

Reflecting on my academic journey, I have too many people to thank. First and foremost, my deepest gratitude goes to my uncle and his family for giving me the opportunity to pursue higher education in the US and many things beyond. I must also acknowledge my *alma mater*, Princeton University, in particular, the faculty at the Chemical Engineering and the Mathematics Department, who prepared and inspired me to pursue advanced education.

During my years at MIT, the growth in my intellectual capacity and character was positively influenced by many people I interacted with. For this my great appreciation goes to my thesis adviser Prof. Arup Chakraborty, who not only identified challenging problems and secured excellent resources for my PhD studies, but also gathered a group of diverse talents both at MIT and nationwide in a network of active collaborations. Among them I'd like to specially thank Dr. Sarah E. Henrickson and Prof. Uli von Andrian at Harvard Medical School, Scott Weber and Prof. Paul Allen at Washington University in St. Louis, Dr. Janelle Waite and Prof. Michael Dustin at NYU Medical School.

I am profoundly grateful for the support from my Thesis Committee members: Prof. Darrell Irvine, Prof. Mehran Kardar, Prof. K. Dane Wittrup and Prof. George Stephanopoulos. Their diverse expertise and perspectives helped to greatly enrich this thesis and my educational experience. To Prof. Kardar I owe my greatest joy in a classroom setting. It is a highlight in my twenty-one years' of formal schooling to have witnessed his supreme command and graceful delivery of some of the most challenging subjects I have ever studied. I deeply appreciate the kindness of Prof. K. Dane Wittrup, for assuming the duty of my committee chair so that my PhD defense could proceed timely.

The past and present members of the Chakraborty Lab at MIT collectively form my fondest memories of MIT. I have learned enormously from them about all aspects of life, and I will miss their company very dearly as I depart. In particular, Bo and Jayajit were extremely helpful in the beginning of my career as a graduate student. Steve, Vincent, Abhishek, Chris, Andrej, Elizabeth, Arvind and Misha offered critical help in the final preparation of my thesis and defense. I also thank Jason Locasale and Fei for their continued concern and encouragements for me, long after they have left the lab. My trajectory at MIT closely paralleled that of Chris Govern. To Chris I'd like to say: thank you for the companionship during our shared trials and tribulations, and best of luck!

Many thanks to Diego for being the most reliable and responsive resource for mathematics and computer programming, along with good humor, music and photography, steadfastly through the years. Also special thanks to Joel, for being not only the best roommate, but also a great friend whose daily encouragements gave me much anchor. And I'm deeply grateful for Stephen, who shouldered the weight of my agony during the final months of this arduous journey, when many a time the prospects of failure overwhelmed me. Many others who supported me during the most difficult final phase of my PhD studies include Karen, Sabrina, Christoph, Gary, Matt, Jason W. and Cindy. Gary's perseverance in music studies taught me not to shy away from the less

familiar intellectual territories. Jason deserves a special mention for his consistent effort to enhance my command of the English language, which culminated in the proofreading of passages from this hastily written thesis. I must also acknowledge Dr. Xiaolu Hsi and Dr. Marilyn Wilson at MIT, whose help and support were crucial in the self-explorations I undertook in my final year here. My mother traveled across an ocean to Cambridge to be with me during the final push of thesis writing. My strength and courage descended from hers. No words can convey how much she means to me.

A final special note is for my piano teacher, Ms Eleanor Perrone, who has always embraced me with the sympathy characteristic of a great artist, and an almost unconditional conviction in my abilities, even when I myself had grave doubts. Empowered by the musical language she taught me, I was able to recover solace, peace and confidence on the darker days of graduate school. And in the final months of my PhD studies, I relied on the greatest lesson I had learned from her: in pursuit of the purest of sounds our hearts can hear, one shall never relent.

Cambridge, MA
July, 2010

---

* My PhD studies were made possible thanks to the generous financial support by the Robert T. Haslam Presidental Fellowship at MIT, and NIH grant PO1 AI071195-01.

Table of Contents

Chapter 1 Introduction

1.1 Background and scope

As experimental tools and techniques become increasingly more sophisticated, biology has transformed from a descriptive, phenomena-centric field into one that is extremely data-rich. Not only does this change greatly improve our ability to build and test mechanistic hypotheses, it also simultaneously calls for investigations in which theory and experiments are brought together in a complementary fashion.

Physics, mathematics and engineering are beginning to provide powerful tools for the studying of biological systems. Not only can we borrow established methods from the physical sciences to process the rich data made available by new experimental techniques, we also can apply the "reductionist" abstract thinking common in physical sciences for extracting mechanistic principles. For example, signal transduction has been modeled as a network of chemical reactions and mathematically as a system of Ordinary Differential Equations (ODEs). In dealing with small number of signaling molecules where fluctuation may dictate the dynamics, stochastic differential equations (SDEs) have shown success (1-4). Mendelian genetics is essentially a set of probabilistic arguments. Methods developed in statistical physics for analyzing complex molecular systems and their macroscopic behaviors can be especially useful, if adapted for appropriate biological systems.

Among various biological contexts of interest, the adaptive immune system is a particularly important one. On the one hand, adaptive immunity confers higher vertebrates the ability to mount pathogen-specific immune response and retain long-lasting immune memory. On the other hand, autoimmune diseases may arise from the erroneous functioning of the adaptive immune system. Thus, a better understanding of the mechanisms underlying various immune responses is imperative for the development of treatment and prevention strategies for both infectious and autoimmune diseases.

To obtain such understanding, one must overcome many barriers, one of which results from the multi-scale nature of many phenomena and their underlying

mechanisms. Many processes critical in the functioning of adaptive immunity involve dynamical events that interact with one another while individually operating on vastly different time- and length-scales. Using conventional experimental approaches, it is difficult to examine these diverse time- and length-scales in a systematic and unified manner. Certain other disciplines, such as the physical sciences and computer science, have developed a rich repository of analytical tools for multi-scale systems. Thus, an inter-disciplinary approach toward problems in the immune system has great potential. While still a relatively recent phenomenon, there have been a number of successful studies wherein experiments and theory have been fruitfully paired to reveal mechanistic principles of scales ranging from the molecular to the level of the entire organism (5-8).

Among the array problems in immunology, an especially important one concerns how T cells are activated *in vivo* by their cognate antigens. In this complex sequence of events, dynamical processes operate on vastly different time- and length-scales, anywhere from molecular signaling events happening within seconds to the proliferation and circulation of T cells that take place over many days. Only when we examine the coupling of different time- and length-scales simultaneously do mechanistic insights emerge.

Such an undertaking is fraught with such difficulties, especially were one to rely solely on conventional approaches. Experimentally, it is typically difficult if not impossible to track simultaneously both the molecular signaling events within a cell and the cell's motion. In other words, we usually are not able to observe the "coupling" of different scales directly in experiments. Computational models, on the other hand, may permit the exact tracking of all events that individual cells or molecules participate. Statistical analyses can be performed to identify underlying correlations if any "coupling" exists.

Secondly, the extraordinary complexity of the immune system combined with our lack of comprehensive knowledge often result in a large combinatorial of possible mechanisms for any given phenomenon, none of which is significantly more plausible than others. On what basis can individual mechanisms be validated or rejected? Often, technical limitations such as the lack of appropriate animal model or biochemistry assay present enormous barriers for experimental testing, as will be discussed later in Chapter 3. Even when such experiments are possible, because animal experiments tend to be expensive

and time-consuming, an attempt to screen through all candidate mechanisms experimentally is, cost-wise, prohibitive. Using efficient implementation of a computational model, however, the duration of an in silico "experiment" is typically a small fraction of a physical experiment. Computational studies can be used to systematically test and improve candidate mechanisms, the results of which may provide helpful suggestions for more efficient experimental schemes.

Computational studies of T cell triggering *in vivo* pose significant challenges. For example, the need for computational tractability means that the models can only be a condensed version of the biology they represent. The challenge is to judiciously "pick and choose" the most relevant biological processes to be incorporated into the model, such that we can answer the sought-after questions without compromising computational feasibility. Such models have the additional advantage of being more likely to produce experimentally testable hypotheses. In the case of a multi-scale system, however, the balance of biological relevance and computational feasibility is even more daunting. Here, one may need to tailor different computational treatments for disparate time- and length-scales (e.g. deterministic vs. stochastic). Due to these barriers, multi-scale computational models have not seen much application in immunology.

In this thesis, I will discuss two such computational frameworks I have developed for examining T cell triggering *in vivo*. Besides providing new mechanistic insights, the multi-scale features of these undertakings constitute new additions to the toolbox for studying the immune system. These computational frameworks are versatile and can be easily adapted for other similar biological systems. My goal in this endeavor is thus not only to improve our understanding of T cell triggering in vivo, but more importantly to expand our repertoire of modeling techniques for multi-scale biological systems in general.

Guided by these objectives, this thesis is organized as follows. After a background discussion and overview of the scope of this thesis, in the remainder of Chapter 1 I will provide a brief introduction on the immune system with the specific focus on how dynamical events on vastly different time- and length-scales collectively enable various important immune functions. Chapters 2 and 3 will both examine how T cells detect antigen in vivo but with different focuses. The study in Chapter 2 predated that in

Chapter 3 and was in close synergy with a set of microscopy experiments that imaged dynamics on the cellular- and tissue-level. The corresponding model was developed for the same time- and length-scales. After a separate study from our lab (9) discovered a hysteretic signaling module in the TCR signaling network, I was able to incorporate these newly delineated intracellular dynamics and expand the earlier model to combine the simulation of stochastic molecular signaling network with simultaneous cell migration. Results from this study have motivated new experiments. Furthermore, this multi-scale computational framework can be generally applied to study other biological systems where cell migration dynamics are coupled with intracellular or inter-cellular signaling. Chapter 4 will first provide a summary on the investigations completed so far, then describe a third problem, which entails the integration of dynamics from a much longer time- and length- scale. Some initial modeling and results will also be presented, as the basis for discussion of possible future directions.

Various theoretical and computational analyses have been conducted for each of these studies. For the study in Chapter 2, a lattice-based Monte Carlo simulation was developed to describe the isotropic diffusive motion of T cells. Partial Differential Equations (PDEs) were used to carry out a mean-field analysis and produce some interesting mechanistic insights. For the study in Chapter 3, I expanded upon the original Monte Carlo simulation to allow for efficient simulation of diffusion in free space, instead of a lattice. This migration model was then adapted to simultaneously simulate intracellular signaling by incorporating a fast implementation of the Gillespie Algorithm, Stochastic Signaling Compiler (SSC). Probabilistic analysis of the numerical results was performed by way of a Markovian probability analysis. For the preliminary investigation of the problem presented in Chapter 4, a system of Delayed Differential Equations (DDEs) were implemented using MATLAB®.

1.2 The adaptive immune system on many scales

The immune system consists of innate and adaptive immunity. Innate immunity provides a highly effective first defense against invading pathogens by recognizing generic

molecular patterns presented by pathogens. Such recognition is not pathogen-specific, and can be evaded by some bacteria and all viruses via mutation. Jawed vertebrates have the additional defense of adaptive immunity, which responds to invading pathogens in a pathogen-specific manner, and maintains a memory of past infections, which allows for a faster and more efficient response should a second infection occur. In this section, I will provide a summary of some important processes pertinent to an adaptive immune response. The focus will be on processes that are investigated in this thesis. They are organized into different time- and length-scales, from the smallest to the largest. I hope to not only show the biological background of this thesis, but also highlight how closely integrated these dynamical events are, despite their disparate scales. I also hope to underscore the importance of a multi-scale perspective toward understanding the adaptive immune system.

1.2.1 The molecular level

T cells are the central orchestrators of cell-mediated or adaptive immunity. They are responsible for the detection and defense against invading pathogens, or antigens (Ag). They bear specialized T cell receptors (TCR) on their surface, which can interact with cognate peptide major histocompatibility complex (pMHC) on the surface of antigen presenting cells (APCs). Most of the APCs are dendritic cells (DCs).

Typically, there are $\sim 10^5$ MHC molecules on the surface of an APC. The vast majority of these MHC molecules present endogenous peptide fragments, which, bar the case of autoimmunity, do not trigger adaptive immune responses (10). Irvine and coworkers have shown that as few as 1 antigenic pMHC could stimulate TCR for Ca2+ flux, and ~10 pMHCs can elicit the formation of the immune synapse and sustained signaling (explained below) (11).

Upon detection of cognate Ag, TCRs initiate a cascade of signaling events that ultimately lead to both short-term and long-term immune responses. Ca2+ ion flux due to TCR signaling can appear within 1-2 minutes after TCR-pMHC engagement (11). TCRs, co-receptors and adhesion molecules such as LFA-1 may co-localize to form a highly structured synapse at the interface between the two interacting cells. Other early

markers, including CD69 and CD25, of T cell activation are also upregulated on T cell surface rather quickly. This implies that the signal generated on the cell surface upon TCR-pMHC binding propagates through the extremely complex intracellular signaling networks very rapidly. Indeed, many steps in the signaling network involve a few molecules interacting over extremely short time-scales.

Other essential molecular signaling events include the change in adhesion properties and cytokine secretion, both of which can happen on the time-scale of minutes. Interleukin-2 (IL-2) is one of the earliest cytokines to be produced by activated CD4+ T cells (see chapter 4 for more details). The mRNA transcripts for IL-2 can appear within 10 min of CD4+ T cell activation. Changes in T cells' surface adhesion are thought to result from integrins interacting with their ligands, most notably LFA-1 and its ligand ICAM. Though unsolved questions remain regarding how TCR signaling rapidly upregulates the affinity of LFA for ICAM, experiments have shown that this upregulation can happen within 1 second of LFA activation (12).

1.2.2 The cellular and tissue level

Many dynamical events at the molecular level culminate in changes in T cells' behaviors or properties at a higher level. Here I would like to highlight the characteristic scales at the cellular and tissue level to contrast those discussed previously.

At the cellular level, TCR signaling leads to re-organization of the cytoskeleton, which then causes cell morphology to change from an amoeboid shape to one that is more spherical. T cells' motility pattern thus switches from a rapid, diffusive motion punctuated with transient interactions with DCs to one where stationary T cells engage DCs for long periods of time. Interactions between adhesion molecules such as LFA-1 and ICAM are instrumental in facilitating these changes at the cellular level.

The distance over which a DC can interact with a T cell can be large, since DCs extend out long dendrites, some as long as 20μm (more than one cell-length), which sweep around the cell body, in an attempt to capture T cells as they pass by (13). The interactions between a T cell and a DC can be as brief as a few minutes or long and stable (e.g. (14, 15), see Chapter 2 for more details).

Another important cellular event during T cell activation is cell proliferation. A multitude of signaling events leads to the production of new cellular materials and the division into two daughter cells. At the peak of proliferation, an activated T cell can divide once every 6h. The division itself takes roughly half an hour. The polarity of this division has been linked to the lineage commitment of daughter cells (16). After the primary immune response, most activated T cells undergo apoptosis, which, again, is due to the transduction of apoptotic signals.

1.2.3 The tissue level

Adaptive immunity takes place in many different tissues. Here I will restrict my discussion to the ones most relevant for T cell triggering. T cell triggering occurs in secondary lymphoid organs (SLO), such as lymph nodes (LN), spleens and Peyer's patches, with LN being the most important site of defense battles. The most central function of LN is to provide an interface between the lymphatic and blood circulation to facilitate immune surveillance. Lymphatic and blood circulation carry extracellular fluid and lymphocytes, respectively, to the LN. In this manner, soluble or cell-associated Ags are collected from all over the body and presented to the T cells to initiate immune responses. To accommodate such function, the LNs have highly organized and specialized internal architecture. It is estimated that a typical LN contains ~10^9 cells per gram mass, around 45% of which are T cells, 25% B cells and the remaining 15% mostly DCs. In other words, there are ~ 10^8 $CD4^+$ or $CD8^+$ T cells and ~ 10^7 DCs per gram mass (17). Note that the relative abundance of a particular clone of T cells will increase significantly due to vigorous proliferation in the primary response. Within 6-8 days, CD8+ T cells may increase in number by 15,000-fold (18). These cells migrate at different speeds and interact with each other both directly via physical contact and indirectly via cytokines and chemokines. The flow rate into and out of LN is about 10^6 cells per hour (17). Each T cell has only about 20-24 hours of residence in a LN to search for cognate Ag, otherwise it leaves without being activated (19). In mice LN, the frequency of a particular TCR clone is about 50 cells out of 5 million cells in total (20). Combining this low precursor frequency

with the constraint on search time, the detection of Ag becomes a "needle in a hay stack" problem (see Chapter 2).

Finally, the presentation of cognate pMHC by DCs may also change, typically over the time-scale of several hours, up to 1 day. Earlier studies have shown that agonist peptide may dissociate from pMHC. Measured half-lives range from 2 to 7 hours (21). After acquiring antigenic materials, DCs take about 18h to circulate into the LN (14), where they may take an additional several hours to become fully mature, which allows for more effective pMHC presentation to T cells (22). The significance of these processes will be discussed in Chapter 2 and 3.

1.2.4 The organism level

The various aspects of adaptive immunity are integrated at the organism level, though during T cell triggering, most activities are restricted to within the site of Ag detection, namely the SLOs. Here, I will briefly touch upon the events that occur after T cell triggering in SLOs, and comment on their implications in the context of this thesis.

Activated T cells proliferate vigorously for several days before exiting via blood circulation. This is partly due to the changes in chemokine receptors on the surface of T cells, which are altered as a consequence of T cell activation. The new combination of homing receptors direct activated T cells away from SLOs and toward peripheral tissues, where they perform effector functions for days to come. After the primary response, while most effector cells die, a small fraction remains as memory cells, which can be activated much more rapidly should a later infection by a similar pathogen occur. Such immune memory can persist for many years. What are the connections between T cell triggering and these events that occur much later in time and much further away from the site of T cell triggering? There is evidence that suggests the commitment toward either an effector or memory lineage takes place during the initial triggering of T cells (16, 23, 24). Thus, early events that occur locally and rapidly can have far-reaching consequences.

I hope this brief introduction has highlighted the plurality of time- and length-scales involved in this thesis. The more we can approach adaptive immunity from a global

perspective, the better we can appreciate its intricate orchestration, but the level of difficulty also exponentially increases. Statistical physics and chemical kinetics have unique advantages in addressing such difficulties, as they have extensively dealt with macroscopic observables that are governed by collective microscopic events. In the next 3 chapters, I will describe 3 instances of their application to immunology.

References

1. Gillespie, D. T. 2007. Stochastic Simulation of Chemical Kinetics. *Annu. Rev. Phys. Chem.* 58:35-55.
2. Gillespie, D. T. 1977. Exact stochastic simulation of coupled chemical reactions. *The Journal of Physical Chemistry* 81:2340-2361.
3. Gillespie, D. T. 1976. A general method for numerically simulating the stochastic time evolution of coupled chemical reactions. *Journal of Computational Physics* 22:403-434.
4. van Zon, J. S., and P. R. ten Wolde. 2005. Simulating Biochemical Networks at the Particle Level and in Time and Space: Green's Function Reaction Dynamics. *Phys. Rev. Lett.* 94:128103.
5. Chakraborty, A. K., and J. Das. 2010. Pairing computation with experimentation: a powerful coupling for understanding T cell signalling. *Nat Rev Immunol* 10:59-71.
6. Chakraborty, A. K., and A. Ko≈°mrlj. 2009. Statistical Mechanical Concepts in Immunology. *Annu. Rev. Phys. Chem.* 61:283-303.
7. Perelson, A. S. 2002. Modelling viral and immune system dynamics. *Nat Rev Immunol* 2:28-36.
8. Borghans, J. A. M., and R. J. d. Boer. 2007. Quantification of T-cell dynamics: from telomeres to DNA labeling. *Immunol. Rev.* 216:35-47.
9. Das, J., M. Ho, J. Zikherman, C. Govern, M. Yang, A. Weiss, A. K. Chakraborty, and J. P. Roose. 2009. Digital Signaling and Hysteresis Characterize Ras Activation in Lymphoid Cells. *Cell* 136:337-351.
10. Sykulev, Y., M. Joo, I. Vturina, T. J. Tsomides, and H. N. Eisen. 1996. Evidence that a Single Peptide-MHC Complex on a Target Cell Can Elicit a Cytolytic T Cell Response. *Immunity* 4:565-571.
11. Purbhoo, M. A., D. J. Irvine, J. B. Huppa, and M. M. Davis. 2004. T cell killing does not require the formation of a stable mature immunological synapse. *Nat Immunol* 5:524-530.
12. Pasvolsky, R., V. Grabovsky, C. Giagulli, Z. Shulman, R. Shamri, S. W. Feigelson, C. Laudanna, and R. Alon. 2008. RhoA Is Involved in LFA-1 Extension Triggered by CXCL12 but Not in a Novel Outside-In LFA-1 Activation Facilitated by CXCL9. *J Immunol* 180:2815-2823.
13. Bousso, P., and E. Robey. 2003. Dynamics of CD8(+) T cell priming by dendritic cells in intact lymph nodes. *Nat. Immunol.* 4:579-585.
14. Mempel, T. R., S. E. Henrickson, and U. H. von Andrian. 2004. T-cell priming by dendritic cells in lymph nodes occurs in three distinct phases. *Nature* 427:154-159.
15. Miller, M. J., O. Safrina, I. Parker, and M. D. Cahalan. 2004. Imaging the single cell dynamics of CD4(+) T cell activation by dendritic cells in lymph nodes. *Journal of Experimental Medicine* 200:847-856.
16. Chang, J. T., V. R. Palanivel, I. Kinjyo, F. Schambach, A. M. Intlekofer, A. Banerjee, S. A. Longworth, K. E. Vinup, P. Mrass, J. Oliaro, N. Killeen, J. S. Orange, S. M. Russell,

W. Weninger, and S. L. Reiner. 2007. Asymmetric T Lymphocyte Division in the Initiation of Adaptive Immune Responses. *Science*:1139393.
17. Young, A. J. 1999. The physiology of lymphocyte migration through the single lymph node in vivo. *Seminars in Immunology* 11:73-88.
18. Bevan, M. J. 2004. Helping the CD8+ T-cell response. *Nat Rev Immunol* 4:595-602.
19. Halin, C., M. L. Scimone, R. Bonasio, J.-M. Gauguet, T. R. Mempel, E. Quackenbush, R. L. Proia, S. Mandala, and U. H. von Andrian. 2005. The S1P-analog FTY720 differentially modulates T-cell homing via HEV: T-cell-expressed S1P1 amplifies integrin activation in peripheral lymph nodes but not in Peyer patches. *Blood* 106:1314-1322.
20. Young, A. J. 1999. The physiology of lymphocyte migration through the single lymph node in vivo. *Semin. Immunol.* 11:73-83.
21. Henrickson, S. E., T. R. Mempel, I. B. Mazo, B. Liu, M. N. Artyomov, H. Zheng, A. Peixoto, M. P. Flynn, B. Senman, T. Junt, H. C. Wong, A. K. Chakraborty, and U. H. von Andrian. 2008. T cell sensing of antigen dose governs interactive behavior with dendritic cells and sets a threshold for T cell activation. *Nat. Immunol* 9:282-291.
22. Hugues, S., L. Fetler, L. Bonifaz, J. Helft, F. Amblard, and S. Amigorena. 2004. Distinct T cell dynamics in lymph nodes during the induction of tolerance and immunity. *Nat. Immunol.* 5:1235-1242.
23. Kaech, S. M., E. J. Wherry, and R. Ahmed. 2002. Effector and memory T-cell differentiation: implications for vaccine development. *Nat Rev Immunol* 2:251-262.
24. Williams, M. A., and M. J. Bevan. 2007. Effector and Memory CTL Differentiation. *Annu. Rev. Immunol.* 25:171-192.

Chapter 2

How antigen quantity and quality determine T-cell decisions in lymphoid tissues

As a first step in a multi-scale examination of T cell triggering in vivo, I studied how the quantity and quality of antigen present in lymphoid tissues may affect T cells' decision to stop on the surface of their cognate dendritic cells and become activated. This question served as a good starting point for a multitude of reasons. First of all, it does not require the detailed knowledge on the molecular signaling network involved in T cell triggering, thus the implementation is relatively simple. Secondly, a wealth of intravital imaging data was available to guide the development of a good model for T cell migration. In particular, Sarah E. Henrickson and Uli von Andrian at Harvard Medical School studied a highly analogous experimental system while the in silico model was being developed. Synergy between our experimental and computational approaches was greatly productive. The collaboration is covered in this chapter, as well as two publications (1, 2).

2.1 Introduction

Recent multiphoton and confocal microscopy experiments have produced vivid images of the migration of T cells in lymphoid tissues during antigen recognition (3-17). For both CD4 and CD8 T cells, the motility characteristics change with time. Initially, T cells move quite rapidly upon entering the lymph node (LN). In the presence of cognate antigen, after a few hours, antigen-specific T cells slow down and make stable contacts with dendritic cells (DCs) presenting cognate antigen (3, 8-12, 14, 15). In CD8 T cells, these two stages of different T cell motility have been labeled "phase one" and "phase two" behavior (9). It seems reasonable to assume that phase one corresponds to a period during which T cells "hunt" for antigen, whereas phase two is a period of time required for signaling processes that result in full commitment to activation (9, 11). An important open question is which factors determine the time required for the transition from phase one to phase two? This is important as this decision predicates T cell activation and the initiation of an immune response.

Several hypotheses could be considered to address this question. One is that T cells may go through such motility changes by default (9). This hypothesis implies that all antigen-specific T cells in the LN would transition into phase two synchronously, and that the time at which this happens should be independent of antigen dose or stimulatory potency. However, it seems more likely that this transition is linked to signaling events stimulated by interactions of T cell receptor molecules (TCR) on the surface of T cells with cognate, peptide-loaded major histocompatibility (pMHC) molecules expressed on DCs. This suggests a second hypothesis: the transition from phase one to phase two is influenced by the nature of cognate pMHC ligands, their expression levels on DC surfaces, and the number of DCs in the LN that bear cognate antigen. In this case, the time at which a particular T cell transitions from phase one to phase two type behavior depends on its history of interactions with DCs, which is stochastic in nature but also have a relatively broad distribution over time. We also explored the consequences of summation of multiple interactions with APCs on the duration of phase one. We have studied how all of these variables collectively define the duration of phase one using computer simulations and theoretical calculations.

Migrating T cells stochastically encounter DCs bearing antigen, which, in turn, can stimulate a stop signal with some probability thereby leading to sustained contacts. We find that the average antigen dose per DC, the number of DCs bearing antigen, and the characteristics of the TCR-pMHC interaction determine the mean time required for a transition from phase one to phase two. Our results on how antigen dose per DC and numbers of antigen bearing DCs affect the duration of phase one are in excellent agreement with experimental observations described by Mempel et al. (9) and Henrickson et al.(18). Importantly, theoretical analyses of the computational and experimental results provide a conceptual framework to understand how the consequences of changing one measure of antigen dose or type on the duration of phase one depend on the values of other related quantities that also play a role in T cell activation *in vivo*. We find that an interplay between two time-scales which encapsulate the effects of antigen characteristics and amount is important. One of the time-scales is the half-life of the pMHC complex, which characterizes its stability. The other time-scale

characterizes typically how long it takes for a productive T cell – DC encounter to occur. Results for the duration of phase one obtained by varying diverse measures of antigen quantity and type collapse onto one consolidated "master" curve when antigen quality and type is measured by the ratio of these two time-scales. The mechanistic principle embodied in this result should help guide future experimentation, because it shows how the effect of changing one variable is influenced by other relevant parameters.

2.2 Model and simulation method

2.2.1 Model development

Beltman et al. (19, 20) have studied T cell migration in a realistic representation of the densely packed physical environment of the LN using a computational method based on the cellular Potts model. These simulations faithfully reproduce many experimentally observed quantities that characterize T cell motility, such as velocity distributions, T cell/DC scanning frequencies, etc.. These studies also suggest that changes in velocity distributions observed upon transition to phase two type behavior require strong adhesion and stop signals from cognate DCs. Quantitative recapitulation of the experimental and computational facts regarding T cell motility (e.g., velocity distributions) is not the purpose of our *in silico* studies. While our investigations are closely synergistic with experiments (18), our purpose is to glean qualitative mechanistic principles that determine the duration of phase one. Specifically, we aimed to elucidate how variables such as cognate pMHC dose per DC, number of cognate DCs, stability of pMHC, etc., influence this duration. This goal guided the choice of the model that we simulated and analyzed.

We use a lattice representation of the space corresponding to the LN (Fig. 2.1) with periodic boundary conditions in which the edges of the box (e.g., left and right or top and bottom) are essentially pasted together. Thus, for example, when a cell exits the box on the left it reappears on the right. This enables simulation of the large spatial extent of the LN (~1 mm^3) with no collisions of T cells with the faces of the simulation box. Each type of cell (e.g., a T cell or a DC) can occupy one of the lattice sites. Motile cells can hop from one lattice site to a neighboring one. This discrete, rather than continuous,

representation of space dramatically reduces the computational power required to simulate the effects of specific parameters characterizing antigen dose and type on the duration of phase one. The lattice representation does not lead to artifacts as long as the properties of interest are manifested on long time and length scales (21) (and one other condition noted later is met). As we focus on the transition from phase one to phase two behavior, which occurs on a time-scale that far exceeds the microscopic time associated with cell motion between lattice sites and signaling events during transient T cell – DC encounters, a lattice representation is appropriate. We also note that while our stochastic simulations allow us to examine the important effects of fluctuations, the average values of the simulation results agree with those obtained from a mean field treatment that does not use a lattice representation. Therefore, for the qualitative results that we seek, the lattice representation seems adequate.

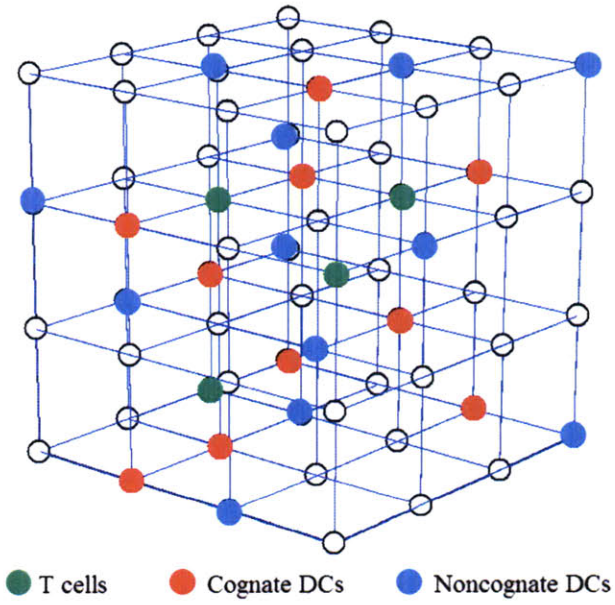

Figure 2. 1: Lattice representation of the volume in the LN that is subject to computer simulations. Cognate and noncognate DCs and T cells are shown schematically.

The lattice is 30×30×30 units in size. Only antigen-specific T cells were explicitly simulated to obtain the results shown here. Simulations wherein non-cognate T cells were included showed that the results were affected only when there were vastly many

non-cognate T cells, at lower levels the results are unaffected by their presence (see Appendix).

The T cells can be either motile or arrested. Intravital microscopy data suggest that T cells move in a directed fashion over distances of the order of 10 μm before changing direction randomly (4, 6, 9-11, 22). On large length and time-scales, the statistical features of the motion are those characteristic of a random walk. Experiments also show that the average speed of migrating T cells is on the order of 10μm/min. In view of these facts, we consider the spacing between points on the lattice to be 10μm and the elementary time step to be one minute. This means that our simulation box is approximately 300μm×300μm×300μm in size. Our simulation results apply also to other choices of the average directional movement (e.g. 20μm), because such changes would require a simple rescaling of the lattice dimension (20μm instead of 10μm). The simulation period of 1440 elementary steps corresponds to a 24-hour residence period of T cells in the LN (23). This simulation period is chosen because if T cells do not get activated and up-regulate CD69 (24), they migrate out of the LN after approximately 24 hours (23).

We consider two types of DCs, those bearing cognate pMHC ligands (cognate DCs) and those that do not display these molecules. Since intravital multiphoton microscopy results have shown that DCs are far less motile than T cells (6, 7, 10), in all our simulations the DCs are immobile. This will not affect qualitative results because the motion of DCs simply affects the frequency of T cell – DC encounters. It can be rigorously proven that in a system where the DCs are immobile, the T cell – DC encounter frequency equals that where they are allowed to move, if the motility coefficient characterizing T cell motion is taken to be the sum of that for T cells and DCs. As we discuss later, the encounter frequency does not limit the transition from phase-one to phase-two behavior, thus accounting for the slow movement of DCs is not important for the issues we study. Therefore different choices and/or random distributions of T cell speeds (e.g., centered around 10μm/min) will also not have an important effect.

A larger number of non-cognate DCs create more barriers for T cell migration, resulting in a lower T cell motility coefficient. Thus, we adjusted the number of non-cognate DCs to obtain a motility coefficient consistent with the experimentally measured values (9-11). A motility coefficient of $11\mu m^2/min$ was obtained with 3000 non-cognate DCs placed in the lattice. The numbers of cognate DCs and T cells span a range of values (from 100 to 1000 for DCs, 250 to 750 for T cells) in our simulations in order to examine their effects on the time at which a transition from phase one to phase two behavior occurs.

Henrickson et al. measured that a typical LN imaged in the experiments is approximately $1mm^3$ in volume, of which roughly 5-10% is the volume where relevant migration takes place. They also estimated that 300 cognate DCs are scattered therein, resulting in a density of 3000-6000 cognate DCs per $1mm^3$. Since our entire lattice is scaled to be $0.027mm^3$, the appropriate number of cognate DCs in the lattice should be on the order of 100 cells. Most of our simulations have been carried out with 100 cognate DCs and 500 cognate T cells, and qualitative results do not change upon varying these cell counts (see Appendix).

We have carried out simulations wherein the total number of DCs and T cells occupy as much as 50% of the available volume, which is lower than the fraction of space occupied by cells in a normal LN (25, 26). Simulations with higher densities of cells become computationally intensive. If we explicitly simulated all the non-cognate DCs and T cells, the following artifact of the lattice representation (which makes the simulations computationally tractable) would render the results less meaningful. Since we model T cells as hard objects that cannot occupy sites already inhabited by other T cells, including a very large number of non-cognate T cells and DCs would lead to a "jamming" of the lattice, in which case no cell would move. In reality, of course, space is continuous and T cells are deformable, and so such a jamming does not occur in the LN. Our goal is to determine qualitative mechanisms via which T cell motility is influenced by cognate pMHC. These qualitative mechanisms should not be affected by using fewer cells so that the jamming artifact is not manifested.

At the beginning of a simulation, all cells are placed randomly on the lattice, and all T cells are motile. T cell motion is simulated using a Monte-Carlo algorithm (see Simulation

Method). In short, a T cell is picked randomly, and an attempt is made to displace it in a random direction. If the chosen target site on the lattice is not occupied by another T cell, then the T cell moves to the new location. T cells are allowed to occupy the same site as a DC because they have been observed to sit on the surface of DCs and scan for antigen (5, 6, 8-12, 15). In addition, DCs have been observed to extend out multiple dendrites from their center of mass and these protrusions are longer than 10μm (9, 10). Since a DC can interact simultaneously with several T cells, and encounters between DCs and T cells can occur simultaneously at several dendrites (6, 9-11), in our model, T cells at the 6 lattice points surrounding a DC can simultaneously interact with it and scan for antigen. Along with the fact that T cells can co-occupy the same lattice point as a DC, in principle, a large number of T cells (exceeding 6) are allowed to scan a DC simultaneously, as observed in experiments. Experiments have also shown that the brief contacts during phase one last for about 3 minutes (4, 6, 9-11, 27), which we model by introducing a scanning time equal to 3 Monte-Carlo steps (this corresponds to approximately 3 minutes). T cells that encounter a DC do not move until this scanning time period has elapsed. Varying the length of scanning time does not alter the results qualitatively (see Appendix).

During the scanning period, interactions between the TCR and pMHC on DCs as well as integrins, co-stimulatory molecules, and cytokines result in intracellular signaling events that could lead to a stop signal (28). It remains an open question whether T cells can integrate signals from multiple serial encounters with cognate DCs (15, 17, 27, 29), or a threshold level of signaling must result from encounters with a single DC (8, 30-34). We consider both scenarios, one in which T cells can integrate signals from serial encounters with DCs, and in the other, any signaling resulted from a T cell–cognate DC encounter is "forgotten" instantly after the T cell disengages.

In the latter situation, if a T cell encounters a cognate DC, signaling can lead to a stop signal with a probability equal to k (implemented as part of the Monte-Carlo algorithm described below). This probability is related to the characteristics of the TCR–pMHC interaction and the level of pMHC expression on the surface of the DC. Our model for T cell migration must be linked to molecular signaling models (e.g. (35-40)) in order to properly link k to these quantities, which reflect antigen quality and quantity. While such

a sophisticated multi-scale model is under development, in the present study, we adopt a simpler approach. We model the relationship between k and antigen concentration by a sigmoidal curve, which exhibits a threshold antigen concentration above which k is large and below which k is small (Figure 2.2). This shape is chosen because experimental results for markers of T cell signaling/activation exhibit such dose-response curves (e.g. (36, 41)). The value of k is zero when the antigen concentration is zero, and approaches one for large values of the antigen dose. A function with a sigmoidal shape was used to interpolate values of k between these asymptotes (see section 2.2.2 Simulation methods). Different TCR–pMHC-binding characteristics alter the threshold concentration defined by the sigmoidal curve and its sharpness. While the results in the main text are for a particular choice of the location and sharpness of the threshold of this sigmoidal curve, we found that changing the values of these variables only results in quantitative, rather than qualitative, differences (see Appendix).

To study situations where T cells can integrate signals from multiple DCs, the probability of generating a stop signal (k) upon a particular T cell - DC encounter is modeled to depend upon the history (or experiences) of that particular T cell as it migrates through the LN. The specific way in which k depends on history in our simulations is described in the context of our results.

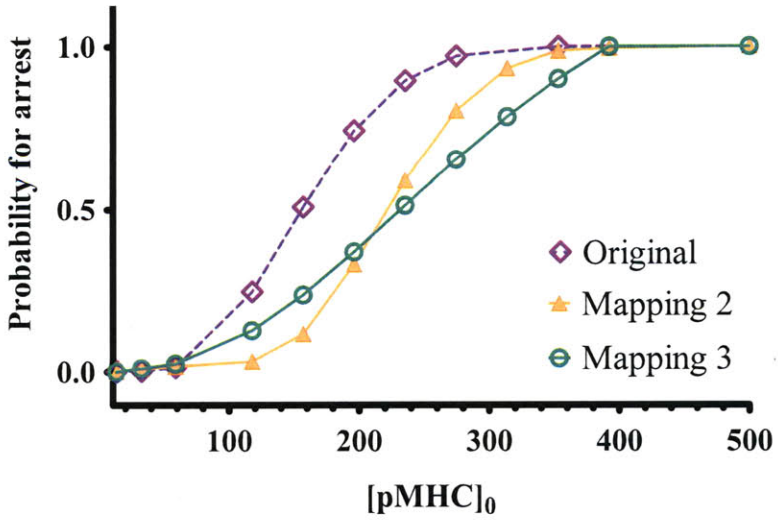

Figure 2. 2: Probability for T cells to receive a stop signal upon encountering a cognate DC (k) plotted against the concentration of pMHC on DCs after pulsing with peptide prior to adoptive

transfer. Original mapping (green circles) corresponds to the mapping used for the results presented in the text, as described in Materials and Methods. To demonstrate how such mapping can be varied, two alternatives are shown. Alternative 1 (orange triangles) is a mapping with the pMHC threshold moved to the right (i.e., a higher initial loading of pMHC is needed for the same probability of stopping), while alternative 2 (purple circles, dotted line) maintains the original threshold location but exhibits a sharper response. As a consequence, k increases more sharply as the initial pMHC concentration is increased.

Most intravital microscopy experiments are conducted several hours after antigen (peptides targeted to DCs, protein and adjuvant injected subcutaneously, or adoptively transferred antigen pulsed DCs) is injected into mice (3-16) and the transition from phase one to phase two type behavior can occur several hours after T cells enter the LN (9, 11, 15). Thus, an important variable is the time-scale over which cognate peptides are lost from MHC molecules. As we shall see, this variable can have an important effect on the time corresponding to a transition from phase one to phase two. This effect is studied in the computer simulations by varying the characteristic time-scale, τ, which describes the first order dissociation process via which the antigen concentration on DCs decreases over time.

2.2.2 Simulation methods

For each Monte-Carlo move (42) a random integer drawn from a uniform distribution of integers from 1 to N (where N is the number of T cells) is used to pick a T cell, and an attempt is made to displace it to a neighboring lattice point in a randomly chosen direction. If the chosen T cell has not yet received a stop signal, and the proposed location is not occupied by another T cell, the T cell moves to the new location. Otherwise, the move is rejected and the T cell stays in place.

A T cell–DC encounter occurs when a T cell either moves to a lattice point directly occupied by a DC, or is at the site immediately adjacent a DC site. When a T cell encounters a DC, it waits (and scans for antigen) for 3 time steps (other values were tested as shown in Table 2). When a T cell contacts a cognate DC, it can receive a stop signal with some time-dependent probability, $k(t)$ (see above). In the case without memory, $k(t)$ is calculated using the pMHC concentration of the DC, $p(t)$, with which the T

cell is currently interacting. Following experimental observations (36, 41), *k(t)* is related to *p(t)*, using the sigmoidal function shown below:

$$k(t)=\begin{cases} 4\times10^{-3}\,p(t) & p(t)\le 3 \\ \dfrac{1.2218\,p(t)^2-1.9878\,p(t)}{734.118-19.7905\,p(t)+p(t)^2} & 3<p(t)<30 \\ 1 & p(t)>30 \end{cases} \qquad \text{Eq. 2. 1}$$

Note that in the above expressions, the time, *t*, refers to the time after the DCs have arrived in the LN (e.g., approximately 18 hours after pulsing DCs with peptides and injection in to animals in the experimental studies of Henrickson et al. (18). To trace back to the initial pMHC loading on DC surfaces, $[\text{pMHC}]_0$, one needs to account for the loss of peptides during the 18 hours, which can be estimated as $[\text{pMHC}]_0=p(\text{t})\exp(-18/\tau)$, where τ is the time-scale of pMHC loss in units of hours, and we have used values for τ reported in the caption of Figure 3. Changing the values of the constants in Eq. 2.1 represents changing the TCR-pMHC binding characteristics as it alters the threshold antigen dose and sharpness of the relationship between *k* and antigen dose. We also performed simulations with either the threshold location or sharpness altered (see Results and Appendix for details).

In the case without memory, at the beginning of each elementary time step, $p(t)$ and $k(t)$ are updated. When a T cell – cognate DC encounter occurs, a uniform random number (r) between 0 and 1 is generated and compared with the current value of k(t). If $r \le k$ the T cell receives a stop signal. If $r > k$, the T cell waits one step and repeats the activation attempt in the next step, with the same value of *k* as in the previous step. This procedure is chosen because we imagine that pMHC loss from the T cell – DC contact zone is unlikely. If no arrest occurred after 3 steps have elapsed, the T cell starts migrating again. T cells in contact with non-cognate DCs cannot receive a stop signal. We have also examined the case in which peptide loss is allowed in the contact zone, as well as the scenario where it is only possible to deliver a stop signal during the first scanning step. In both cases, the qualitative results (see Appendix) do not change.

This simulation protocol is modified slightly to incorporate signal integration, i.e. the "memory" effect. The details will be discussed in the next section along with relevant results.

Table 2.1: Definition of symbols used to represent important quantities.

Symbol	Description	Units
D	Motility coefficient	$\mu m^2/min$
K	Probability of a stop signal upon a T cell-DC encounter; depends upon TCR-pMHC binding characteristics and concentration of antigenic pMHC per DC	min^{-1}
p	Concentration of cognate-pMHC on DC surface	Number / DC
t	Time	Hours
ρ	Density of cognate DCs in the LN	Number $/\mu m^3$
τ	Characteristic time-scale for peptide dissociation from MHC groove	Hours
τ_e	Average time for T cell to encounter a cognate DC via motion characterized as a random walk	Hours
τ_s	Characteristic time required for a productive T cell – DC encounter; depends upon TCR-pMHC binding characteristics, number of cognate DCs in LN, and pMHC concentration on DC surface	Hours

2.3 Results

We have considered situations where T cells can and cannot integrate signals from serial encounters with DCs. We begin by reporting results from simulations and theoretical calculations where naïve, recirculating T cells do not exhibit a "memory" of past encounters with cognate antigen-bearing DCs in the LN.

2.3.1 Ag dose and quality determines the transition from phase one to phase two

In our simulations, antigen quality and quantity are determined by three variables: (1) the initial concentration of cognate pMHC ligands on DC surface and their TCR binding characteristics, which determines the probability (k) that a particular T cell – cognate DC encounter will result in a stop signal; (2) the stability of complexes formed between the cognate peptide and MHC proteins; (3) the density (or number) of DCs in lymphoid tissue that present these ligands.

The amount of cognate pMHC on DC surfaces, and hence the value of k, changes with time as peptides dissociate from the MHC groove. The stability of the pMHC complex is described by the parameter τ, which is the time associated with peptide dissociation from the pMHC complex. This parameter, along with the initial concentration of antigen loaded onto DCs before adoptive transfer, determines the antigen concentration displayed on DC surfaces at any given time. The density (related simply to the number) of cognate DCs in the LN is described by a single parameter (ρ).

Figure 2.3a and 2.3c show that the fraction of T cells arrested before the exit time (24 hours) has elapsed depends on antigen quality and quantity. The fraction of T cells arrested increases as the initial antigen loading and the density of cognate DCs are increased. This is because a higher density of cognate DCs (e.g. 300 vs. 100 cognate DCs per lattice) increases the probability of T cell – cognate DC encounter, while higher antigen concentration on DCs corresponds to a higher probability for the T cell to receive a stop signal (i.e., higher k). Varying the exit time between 10 and 27 hours led to barely any change in the results (see Appendix for discussion). Note also that since the arrested cells are the ones most likely to commit to full activation (28), late activation markers (e.g. proliferation) likely change in ways that parallel the changes in the fraction of arrested cells; thus, the fraction of arrested cells can be considered to be a measure of late markers of activation.

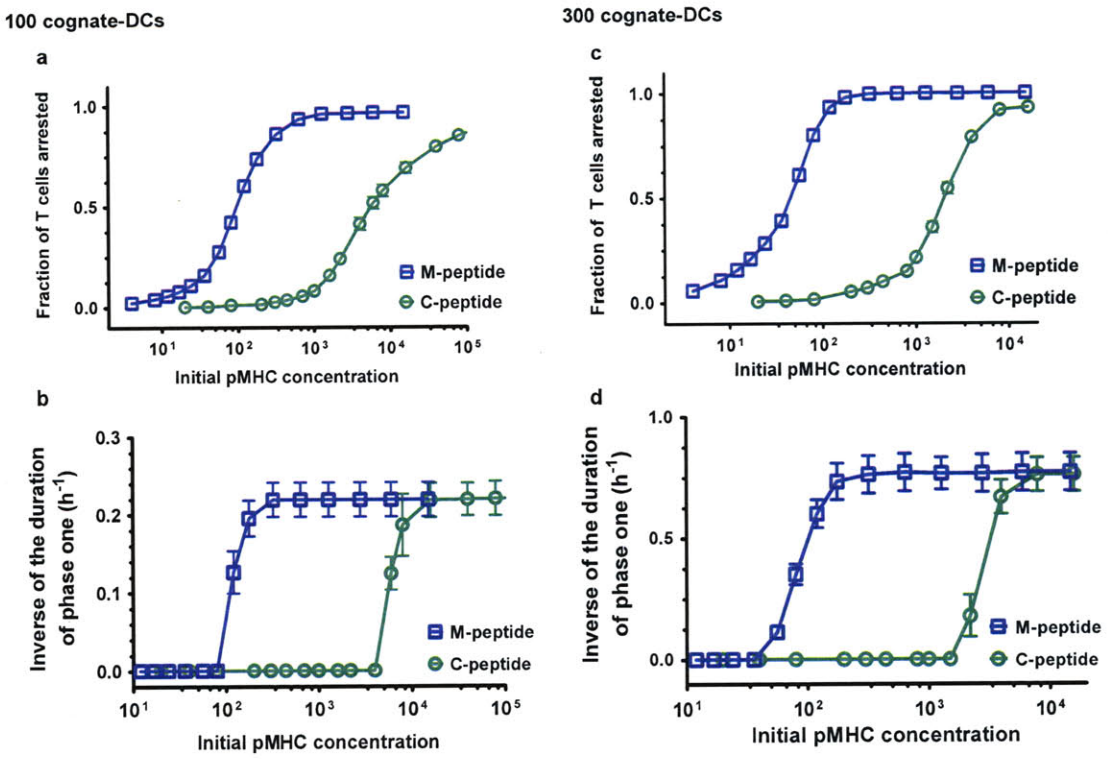

Figure 2. 3: Antigen dose and type determine the transition from phase-one- to phase-two-type behavior. Computer simulation results for the fraction of T cells that have been arrested before the exit time has elapsed (a and c) and the inverse of the mean duration of phase one (b and d) as a function of the concentration of pMHC on DCs prior to adoptive transfer into recipients. The duration of phase one is defined as the time required for 50% of the T cells to make sustained contacts with DCs, as described in the text. The relationship between the units of concentration on the abscissa of the graphs and the concentrations of peptides used to pulse DCs in experiments carried out by Henrickson et al. (22) is described in the text. If a transition to phase two does not occur prior to exit, the duration of phase one is taken to be infinite, in which case the inverse of the duration of phase one is zero, as seen in panels b and d. Results for two pMHC ligands, characterized by different half-lives of the pMHC complex, are shown. The values of the half-life that were used are approximately 6 h and 2.35 h, since that roughly corresponds to the experimentally determined pMHC half-lives for the M peptide and C peptide, respectively (22). These peptides are the natural (C) and an altered (M) peptide ligand for the P14 TCR transgenic system. One hundred cognate DCs (a and b) or 300 cognate DCs (c and d) are analyzed.

The results displayed in Figure 2.3b and 2.3d make direct the connection with the experimental observations of Henrickson et al.(18). They observed the T cell migration patterns in LNs containing adoptively transferred DCs pulsed with various antigenic peptides *ex vivo*. Henrickson et al. define the time corresponding to the transition from phase one to phase two as that at which some large fraction (e.g., 50% of the T cells) are no longer motile (i.e. the median times of interaction between antigen-specific T cells and peptide pulsed DCs are greater than 30 minutes in a 60-minute observation period). T

cells do not transition to phase two in a synchronous manner. The duration of phase one type behavior for individual T cells in each of our *in silico* trajectories varies widely (from minutes to hours), especially at the threshold concentration of pMHCs required to induce a transition to phase two. In experiments too, different T cells stop at different times. Similarly, because of the stochastic nature of this process, the duration of phase one observed by Henrickson et al. also differs from one experimental realization to another, fluctuating around some average value. Similar behavior is also captured in our simulations. In both our simulations and in the experiments, an average value of the time at which a large fraction of T cells are arrested is reported. This time is representative of the behavior of the population of T cells, but does not imply synchronous behavior for every T cell.

Figure 2.3b and 2.d show how the average time at which 50% of the T cells are arrested depends on the initial value of antigen concentration on DC surfaces and the density of cognate DCs (e.g. 300 vs. 100 cognate DCs per LN). The shape of these curves is strikingly similar to that reported by Henrickson et al. for the dependence of the time of a transition from phase one to phase two on the peptide concentration used to pulse DCs *ex vivo*. Besides the two values of DC loadings displayed in Figure 3, several other values were also tested and led to no qualitative difference (see discussion in Appendix).

One of the pMHC ligands studied by Henrickson et al. (18) is called the "M-peptide". This is an altered peptide ligand for the P14 TCR transgenic system, wherein T cells recognize a peptide from lymphochoriomeningitis virus (LCMV, KAVYNFATC is the natural peptide and KAVYNFATM is the "M-peptide"). They report that for DCs pulsed with 100pM of M-peptide, a transition to phase two was not observed. Pulsing concentrations of 200pM resulted in phase-two-type behavior after 6-8 hours, and all higher pulsing concentrations led to a phase one that lasted 2-4 hours (18). Thus, this experimental data seems to exhibit the thresholding (with 200 pM as the threshold) and asymptotic behavior observed in our simulation results. The thresholding behavior results from the nature of the dose-response curve characterizing T cells signaling (Figure 2.2).

The stability of pMHC determines the amount of cognate pMHC left on the DC surface at various times after adoptive transfer. Consequently, the time-scale τ characterizing pMHC dissociation influences T cell migration and activation by affecting how the probability of productive signaling (k) varies over time. Two values of τ differing approximately by a factor of 2 (3.4 and 8.7 hours, respectively) are considered in Figure 2.3. These values were chosen because they correspond to the stability characteristics of the M- and C-peptide in the experimental studies of Henrickson et al.(18). We also explored a range of τ values between 100 to 800 min, the qualitative behavior parallels those shown in Figure 2.3 (see discussion in Appendix). Our results show that, while keeping all other parameters the same, values of τ that differ by a factor of 2 can result in a substantial difference in the fraction of T cells arrested before the exit time has elapsed (Figure 2.3a and 2.3c). Equivalently, the less stable peptide requires a longer time to transition into phase two. Ligand concentrations that result in a transition to phase two for the M-peptide would not lead to such a transition for the C-peptide, as observed in experiments (18).

However, there are some subtleties. For example, at the threshold concentration required to observe a transition to phase two, the duration of phase one obtained from simulations is roughly the same for the M- and C-peptide (note, however, this threshold concentration is much higher for the C-peptide), if TCR binds both pMHC with the same affinity. In reality, however, the C-peptide could bind TCR slightly more weakly compared to the M-peptide. This can be modeled by moving the threshold in the relationship between k and antigen concentration to higher concentrations. We could establish that while such changes do not alter our conclusions in qualitative ways, the results do change quantitatively (see discussion in Table 2). For example, shifting this threshold by a factor of 1.5 results in transition times around 9 hours (ranging from 6 to 12 hours) for the C-peptide, which is consistent with experimental observations (18).

Finally, these results suggest a rough bound on the number of pMHC complex needed to activate T cells in vivo. Previously, it has been shown in vitro that 1 cognate pMHC can stimulate Ca2+ flux in a T cell, and ~10 pMHC complexes can trigger the formation of

synapse between a T cell and an APC (43). The requirement in vivo remains unclear. Henrickson et al. observed that 10μM C-peptide is the minimum pulsing concentration that could elicit a transition from phase one to phase two (1). Furthermore, a pulsing concentration of10μM is high enough to replace almost all endogenous peptides in the MHC grooves of the DCs, thus the initial pMHC loading is roughly 4000 per cell. At 24 h post-injection (approximately when the transition takes place), there remain about 60 pMHC complexes per cell (pMHC for C-peptide has a half life about 2.36h). Henrickson et al. also observed that 200pM M-peptide and 10μM C-peptide are both threshold dosages required to elicit a transition from phase one to phase two. Therefore, one can assume that by the time the transition takes place, the number of M-peptide-pMHC and C-peptide-pMHC remaining on the surface of DCs should be comparable (~60 pMHC). A reasonable estimate for the size of a T cell – DC contact zone is about 50μm2, or 10% of the total DC surface area. This implies that ~6 pMHC complexes can elicit the transition from phase one to phase two in vivo. In other words, with a pulsing concentration of 200pM, at the time of injection, there are approximately 480 pMHC complexes per cell (pMHC presenting the M-peptide has a half life about 6h). Other factors likely further increases the probability of peptide loss from the time of DC injection to the transition from phase one to phase two, therefore this initial pMHC loading is very likely an overestimate. This simple numerical analysis highlights that the number of cognate pMHC complexes needed to activate T cells in vivo is very low.

The results shown in Figure 2.3 and corresponding experimental observations (18) show that antigen quality and quantity determine the duration of phase one.

2.3.2 A consolidated measure of antigen quality and quantity

A common conceptual framework that reveals how antigen dose and type influence the duration of phase one is obtained by recognizing that the pertinent stochastic processes are described by distinct average time-scales.

One potentially important time-scale is the length of time required for T cells to encounter cognate DCs, by effectively random processes. This time, τ_e (the subscript "e"

denotes "encounter"), scales as $\frac{1}{\rho^{2/3}D}$, where ρ is the density of cognate DCs in the LN, and D is the T cell motility coefficient which is calculated from experimental results (4, 9-11). Experimental values of D, ρ, and the duration of phase one, make clear that τ_e is much smaller than the duration of phase one. In other words, prior to exiting the LN T cells have ample opportunities to encounter cognate DCs. This is consistent with Bousso and Robey's findings that DCs scan at least 500 T cells per hour in the absence of antigen (6), and other previous studies (10, 19, 25, 44). Similarly our simulations are carried out for a range of conditions wherein τ_e (the time required to encounter DCs) is not limiting.

Since different peptides are lost from the DC surface at different rates over time, another time-scale, the characteristic time for peptide loss (τ) discussed earlier, is an important measure of the quality of antigen. However, how different values of τ affect the duration of phase one will depend on other key variables. For example, if the half-life of the pMHC complex is shorter (smaller τ, less stable pMHC), the effect on the duration of phase one will depend on the prevailing antigen dose. This is because a higher antigen dose could compensate for a less stable pMHC. How do we properly compare the effect of a change in antigen dose (units of molarity) with a change in the peptide half-life (units of time)? A systematic method to compare the relative impact of changing different measures of antigen quantity and type (each measured in different units) would be extremely useful for interpreting and designing experiments.

Assessing the impact of changing the value of one variable while taking into account the context (values of other pertinent variables measured in different units) is facilitated by grouping (e.g., as products or ratios) the relevant variables to obtain non-dimensional quantities (45). The change in the value of such a non-dimensional quantity upon altering a particular variable properly reflects the relative effect of manipulating this variable. Our goal is to compare the effect of a change in the stability of the pMHC (a time-scale) with changes in other measures of antigen type and dose such as TCR-pMHC binding characteristics, pMHC dose, and number of cognate DCs. To do this, we need to relate

measures of the latter quantities to a time-scale pertinent to the process of T cell – DC interaction.

As T cells migrate through the lymph node, the number of encounters with DCs (or time) required to receive a stop signal should depend on the number of cognate DCs, pMHC per DC, and the TCR-pMHC binding characteristics (represented by the pMHC-to-k mapping in our model). For example, small values of antigen concentration, cognate DC number, or half-life of the TCR–pMHC interaction will result in a longer phase one. In other words, the time required to receive a stop signal (τ_s) is determined by k and ρ (the number of cognate DCs in the LN). Thus, the effect of changing k or ρ is contained in one single variable: the time-scale τ_s.

The non-dimensional grouping τ/τ_s allows for an "apples to apples" comparison of the effects of antigen dose and TCR-pMHC binding characteristics with the half-life of the pMHC complex. If this hypothesis is correct, data obtained from varying diverse measures of antigen quantity and quality should collapse onto one consolidated master curve if graphed against the ratio, τ/τ_s. How can the value of this ratio be obtained in terms of the individual measures of antigen quantity and quality?

Our computer simulations naturally include stochastic fluctuations which are normal for all biological systems. Stochastic effects can be important for many phenomena in molecular immunology (e.g.,(36, 37)). The importance of stochastic effects for the transition from phase one to phase two behavior is highlighted by the fact that, for identical conditions, in our computer simulations the duration of phase one varies widely (over a range of 2 to 3 hours) from one simulation to another. Experiments also show such variability (18). This is not surprising as for a related problem in physics (survival probability of particles diffusing in a medium composed of randomly placed sites that can trap the particles with some probability) the importance of stochastic fluctuations has been proven in a mathematically rigorous manner (46, 47). Also, the importance of stochastic effects has been noted by Preston et al. (48) in the context of T cell migration in lymphoid tissue. Therefore, a computational treatment that *a priori* assumes that every T cell undergoes a transition from phase one to phase two behavior at precisely the same

time (the average value of the duration of phase one) is over-simplified. However, such a mathematical description can be useful in identifying how quantities (such as our time-scale ratio τ/τ_s) depend upon other parameters, and may be satisfactory for obtaining the mean values of certain quantities.

In such treatment, one writes down a differential equation for the spatio-temporal evolution of the concentration of the T cells that have not received a stop signal (denoted as T):

$$\frac{\partial T}{\partial t} = D\nabla^2 T - k\rho T \qquad \text{Eq. 2. 2}$$
$$T(t=0) = T_0 \quad T(t,\pm\infty) = 0$$

The spatially averaged solution has the form $T/T_0 = \exp\left(-\rho\int_0^t k(t')dt'\right)$. In other words, the number of T cells that have received a stop signal depends only on $\rho\int_0^t k(t')dt'$, which equals τ/τ_s.

We have carried out computer simulations wherein diverse measures of antigen quantity and quality are varied to examine whether all the resulting data collapse onto one consolidated master curve when graphed against τ/τ_s (given by the last formula).

Figure 2.4 shows that all our simulation results (varying initial antigen concentration, half-life of pMHC complex, fraction of cognate DCs, etc.) collapse onto one consolidated master curve when the fraction of T cells arrested is plotted against this scaling variable. This result demonstrates that, since the time required for T cells to traverse the LN is not limiting, antigen quality and quantity determine the time to transition from phase one to phase two via an interplay between the time-scales necessary for a productive T cell-DC encounter (τ_s) and the time-scale describing the loss of peptides from DCs (τ). The smaller the value of the ratio of these two time-scales (τ/τ_s), the longer the time required for a transition to take place (or equivalently, the lower the fraction of T cells arrested prior to exit).

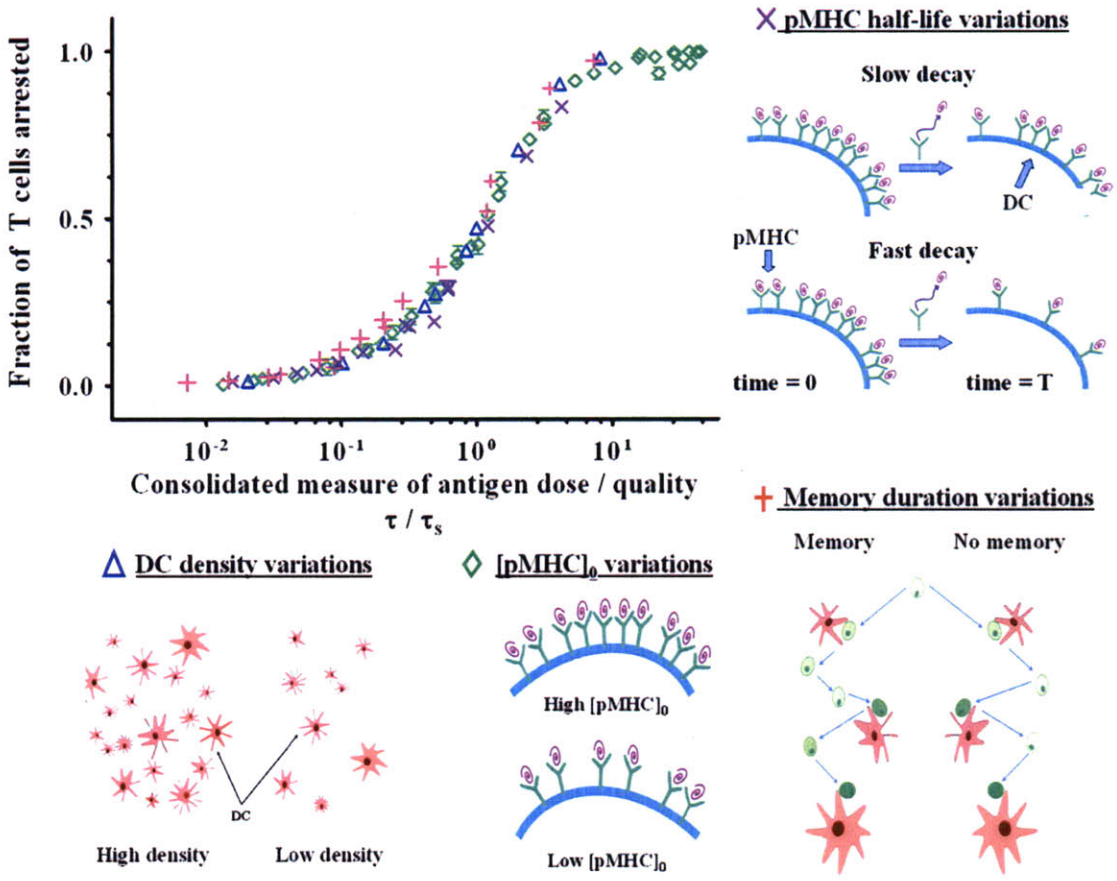

Figure 2. 4: Unifying conceptual framework describing how antigen dose and quality determine the transition from phase-one- to phase-two-type behavior. Results obtained upon varying diverse quantities (green diamonds, initial pMHC concentration on DCs prior to adoptive transfer and TCR-pMHC binding characteristics; blue triangles, the number of cognate DCs; purple x's, stability of pMHC complexes) all fall on the same consolidated curve when graphed against the consolidated measure of antigen dose/quality. The latter is calculated as the ratio of two time-scales, namely the time-scale of pMHC loss from the cognate DC surface (τ) and the time-scale for a productive T-cell-DC encounter to take place (τ_s) (see the text for derivation). Results of simulations carried out with or without the "memory effect" (the ability to integrate signals from serial T-cell-DC encounters) also fall on the same curve (red crosses). Variations of one parameter and simultaneous variation of two parameters are considered. The number of cognate DCs is varied from 50 to 500; the initial pMHC concentration is varied from 3 to 160,000; the half-life of pMHC is varied from 40 min to 16 h; the memory time-scale, τ_m, is varied from 0 to 6 h. Increasing the number of DCs, pMHC pulsing concentration, or stability, as well as the memory time-scale, all lead to a larger fraction of T cells arrested prior to the exit time (24 h). We also applied modifications to the scheme of T-cell activation upon cognate encounter. Specifically, in alternative scheme 1, instead of being able to receive a stop signal during the entire scanning period (three steps), the T cell can only receive a stop signal during the first waiting step, i.e., immediately after the encounter happens. In the second alternative scheme, the T cell can receive a stop signal throughout the scanning period but peptide loss is allowed during this time, leading to progressively smaller values of k. We were able to reproduce the master curve for each modified scheme similar to the one shown here.

Henrickson et al (18) observed that a 2-fold decrease in pMHC per DC cannot be compensated by a 10-fold increase in the number of cognate DCs. Our analyses and results suggest that this is because the impact of changes in pMHC per DC on τ/τ_s exhibits a threshold, which is because the relationship between signaling efficiency and pMHC concentration is not linear as discussed earlier (Figure 2.2). On the other hand, the number of cognate DCs, ρ, affects this ratio in a linear fashion, as the relationship $\tau/\tau_s = \rho\int_0^t k(t')dt'$ implies. Therefore, a 2-fold decrease in initial pMHC concentration leads to a much greater reduction in $\rho\int_0^t k(t')dt'$ which can only be compensated by a significantly larger increase in cognate DC number.

We have also studied situations where there is no antigen loss with time, since peptide half-lives in MHC class II systems can be very long. Furthermore, in some settings, DCs could continuously synthesize new pMHC molecules from an intracellular pathogen or self antigen. In these cases, there is only one relevant time-scale, τ_s, and it equals $1/(k\times\rho)$ (note that k, the probability of receiving a stop signal, does not change with time in this case). Indeed, for these cases, our simulation results obtained from varying the concentration of pMHC ligands or cognate DC numbers collapse to one consolidated master curve when time is scaled (divided) by τ_s (data not shown).

2.3.3 Signal integration

The need for signal integration

The fact that the diffusion time is short implies that T cells can efficiently scan many DCs (6, 10, 19, 25, 44) in a period shorter than the time at which the transition from phase one to phase two occurs. Previous studies (e.g., Bousso and Robey (6), Miller et al. (10) and Beltman et al. (19)) show that DCs scan many T cells in a time-scale shorter than the duration of phase one. However, the transition from phase one to phase two type behavior requires 6 to 10 hours for the C-peptide (18) and (9). Given that the time required to encounter a cognate DC is relatively short, why does this transition not occur at earlier times when antigen dose is higher as fewer peptides have dissociated from DC

surfaces? This is likely because the propensity for generating a stop signal is low from the very beginning in these systems. This, in turn, suggests that T cells may be integrating signals from multiple sequential interactions with DCs because of a "memory" that is intrinsic to the topology of the signaling network. In light of this, we explored the consequences of such a phenomenon in our computer simulations.

The effects of signal integration

The T cell signaling network has many features that could potentially enable signal integration. For example, disassembly of membrane-proximal signaling complexes formed upon interactions with TCR will occur some time after the initial stimulus is removed. Many feedback loops have also been identified in TCR signaling, including those involved in membrane-proximal signaling that may be relevant for early events that result in a stop signal (37, 40, 49). These feedback loops could potentially provide additional mechanisms for signal integration. Moreover, recent imaging experiments have examined the ability of T cells to integrate signals derived from successive encounters (15, 17) and biochemical experiments have suggested the existence of memory in T cell signaling (29). Finally, while endogenous pMHC are not explicitly considered in our model, T cell encounters with DCs displaying endogenous pMHC may also contribute to a "memory", as such interactions could help sustain the effects of encounters with cognate ligands.

In future modeling and experimental efforts, molecular details of signaling and migration must be examined simultaneously in order to understand the origin and effects of memory in detail. At present, however, we adopt a minimalist approach by postulating that the T cell signaling network has a "memory" of previous encounters with DCs, which decays with a characteristic time-scale, τ_m. τ_m is determined by the molecular details of the signaling network, although, currently the precise origin and values of this time-scale are unknown.

Specifically, we use the following protocol to simulate signal integration from serial T cell-cognate DC encounters. A "memory", M (initially equals zero), is associated with each T cell. Upon the first T cell – cognate DC encounter, k is evaluated using the same

procedure as in the case without memory. Should this encounter be unproductive, the T cell leaves with a memory of $M = k(t)$, where t is the time for the first encounter with cognate DC for this T cell. Prior to the next encounter with a cognate DC at some later time t', the memory decays with some time-scale, τ_m. Thus $M(t') = M(t)\exp\left(-\frac{t'-t}{\tau_m}\right)$. At the second cognate DC encounter, the total propensity to receive a stop signal is $k_{tot}(t')=k(t')+M(t')$ or 1, whichever is smaller. If the T cell does not receive a stop signal, the value of k_{total} is added to its "memory". In this manner, the "memory", M, of previous encounters may enhance the propensity of a stop signal. This process is repeated upon subsequent encounters. Since values of τ_m that are significantly shorter than the time-scale between successive encounters of a T cell with a cognate DC would have little effect, and values comparable to the exit time are unlikely, we focused our studies on values of τ_m which are on the order of diffusion time-scale.

Our computer simulations show that initial pMHC concentrations on DCs that would otherwise not result in a transition to phase two may stimulate sustained contacts when signal integration is incorporated (Figure 2.5). These results suggest that, even if pMHC concentrations on DCs in the LN are so low that a single T cell-DC encounter cannot be productive, integration of signals from serial encounters can result in extended T cell-DC contacts. This concurs with experimental findings by Henrickson et al. (18) which show a transition to phase two type behavior under conditions where the antigen density on any particular DC must be quite small. Figure 5 shows that the effects of signal integration are more pronounced for less stable pMHC ligands (e.g., the C-peptide in Henrickson et al.). With the same degree of signal integration (i.e. same decay rate of the signal, τ_m = 160 minutes), the threshold concentration of pMHC required to induce a transition to phase two is reduced by 52% for the M-peptide and 58% for the C-peptide. This is because, given the same initial antigen density loaded on to DCs *ex vivo*, DCs will display fewer of the less stable pMHC ligands in the LN. The ability to integrate signals from serial encounters therefore becomes more important for the less stable pMHC antigen. This is also true for the other values of τ_m we had examined using computer simulation. With a

larger τ_m (more persistent "memory"), the threshold concentration required to induce a transition to phase two can be reduced until a maximum enhancement is reached, beyond which larger τ_m no longer reduces the threshold concentration (see Appendix).

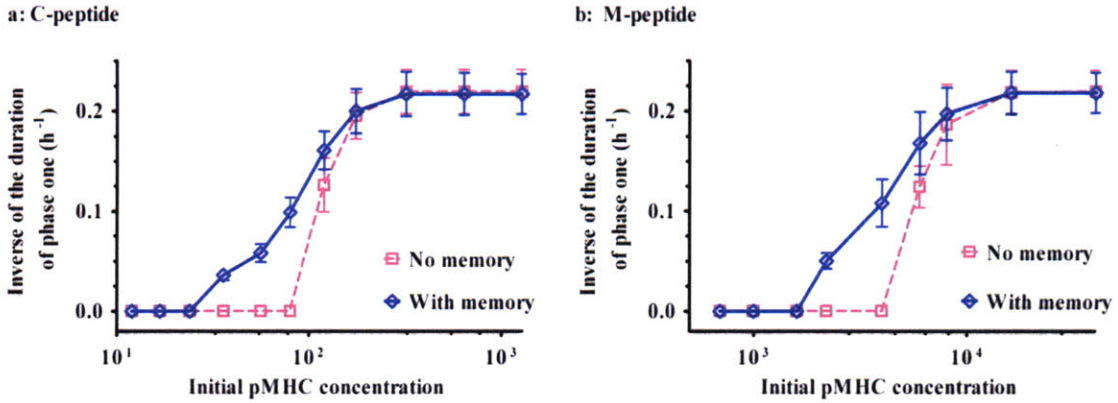

Figure 2. 5: The ability to integrate signals from serial T-cell-DC encounters lowers the antigen dose required to enable a T cell to transition from phase-one- to phase-two-type behavior. The inverse of the mean duration of phase one is plotted as a function of the initial pMHC concentration on DCs after pulsing prior to adoptive transfer. The duration of phase one is defined as the time required for 50% of the T cells to make sustained contacts with DCs, as described in the text. The way in which signal integration (memory) is incorporated is described in the text. The time-scale for memory decay is 160 MC steps (or minutes). (a) The half-life of the pMHC ligand is 2.35 h (corresponds to the C peptide in experiments reported in reference 22). (b) The half-life of the pMHC ligand is 6 h (corresponds to the M peptide in experiments reported in reference 22). For the results in both panels, 100 cognate DCs were simulated. The effects of memory are more pronounced for the less-stable pMHC ligand (a). For example, there is a 58% reduction in the dose required for a transition to phase-two-type behavior in panel a upon incorporation of memory and a 52% reduction in panel b. These specific values depend upon the number of cognate DCs, TCR-pMHC binding characteristics, and other relevant parameters. However, they are almost independent of the time-scale characterizing memory (see the text) if this quantity exceeds a threshold value.

Note, however, that the shapes of the curves in Figure 2.5 are not altered by incorporating signal integration. Signal integration simply reduces the time-scale required for a productive T cell-DC encounter (τ_s) if a T cell has previously encountered cognate DCs, and in so doing increases the fraction of arrested T cells. In other words, signal integration increases the average probability for a stop signal (i.e. the mean value of k) during the process, as the loss of cognate ligands from the DC surface is ameliorated. This makes the effective value of τ/τ_s smaller. Figure 4 makes this point strikingly as all the simulation results, with and without signal integration, exhibit the same scaling behavior with respect to the interplay of the important time-scales identified earlier. As

we note in the next section, the same would be true if memory was conferred by DCs changing pMHC presentation efficiency upon repeated encounters with cognate T cells.

2.4 Discussions

Understanding the behavior of T cells in lymphoid tissue as they begin to be primed by APCs is very important as it is a key stage that leads to the detection of antigen and the mounting of an immune response. Progress in this regard has been aided by the recent application of multiphoton microscopy technology (50, 51) to immunological questions as it has enabled spatially resolved *in vivo* imaging of T cells in real time (3-17). Among the earliest findings from these studies was that the migratory pattern of T cells (on large length and time-scales) exhibited the statistical features characteristic of a random walk (4, 10). Subsequent computer simulations have suggested that this enables efficient scanning of DCs in LNs (19). Furthermore, recent experiments suggest that the apparently random (or diffusive) motion may be because T cells follow "tracks" made up of reticular fibers which span the LN in a statistically random manner, and T cells can choose different tracks at the intersections (13, 22). Other important findings are that chemokines can influence the details of T cell motility patterns (52-55), and that T cells can organize into dynamic "streams" (19).

The dynamic characteristics of T cell migration in LNs varies over time (8, 9, 11, 14, 15). In CD8+ T cells, the first stage (phase one) of rapid scanning (characterized by random walk statistics) is followed by a second phase wherein T cells make extended contacts with DCs. In this second phase, presumably, T cells are making sustained contacts with DCs that are known to be necessary *in vitro* for full commitment to activation (e.g. (28)). Therefore, a mechanistic understanding of which factors determine the transition into phase two, and how they regulate this decision is crucial. Such an understanding was not available, which was the impetus for this study.

We reasoned that the transition from phase one to phase two results from T cell signaling stimulated by encounters with cognate DCs. This, in turn, suggested that this transition is strongly influenced by the quantity and quality of antigen. We have studied this hypothesis extensively *in silico* by systematically varying conditions that determine

antigen quantity and quality. Our results are qualitatively consistent with experimental observations (18), and they provide a mechanistic framework that describes how antigen dose and type impact the ability of T cells to detect antigen and "decide" to make extended contacts with DCs.

Increasing the initial concentration of cognate ligands loaded on DCs or increasing the fraction of cognate DCs reduces the duration of phase one, because both actions lead to a higher propensity for a productive T cell–DC encounter. If antigen concentration on DCs and/or density of cognate DCs exceeds a threshold value, the transition from phase one to phase two occurs very rapidly. This may explain why it is difficult to observe phase one type behavior in a system characterized by high doses of high affinity antigen on essentially all endogenous LN DCs (12).

Stability of the pMHC complex itself is also an important variable, with more stably bound peptides resulting in a shorter phase one. This is because, unlike *in vitro* experiments with multiple or single cells or lipid bilayers, a T cell might encounter a DC in the LN several hours after antigen loading (as in the experiments reported in (4, 8-11, 14)). During this time, peptides are lost from the DC surfaces. The less stable pMHC complex will thus display lower amounts of cognate ligand, thereby decreasing the probability of productive T cell-DC encounters.

The power of our theoretical analysis is that it shows that these seemingly unrelated findings emerge from a single conceptual framework. We have identified three important time-scales. The first is the characteristic time for T cells to find DCs bearing cognate ligands, which is rather short for conditions that have been studied previously (6, 8, 10, 44) and by us. Therefore, it is not as important a determinant for the transition from phase one to phase two behavior. It is worth remarking, however, that in the early stages of a real infection, the number of DCs bearing cognate ligand may be smaller than that in *in vivo* imaging experiments (e.g., ~100 - 300 cognate antigen bearing DCs are in the draining LN at the time of T cell adoptive transfer in the experiments of Henrickson, et al,(18)), and this time-scale may become important. It may also become important if antigen dose is un-physiologically high, in which case the T cells would receive a

sufficiently high stimulus from the first cognate DC they encounter. As a result the time it takes to encounter the first cognate DC dictates the duration of phase one.

An important time-scale is the time required for a productive T cell-DC encounter to occur (τ_s). Using a mean-field approach, we derived how this time-scale is determined by various measures of antigen dose and type. Specifically, we identified the non-dimensional ratio of τ_s and the half-life of the pMHC complex as the composite variable, which controls the behavior of the system. Our simulation results for a wide range of values of diverse quantities that reflect antigen dose and quality all collapse onto one master curve when plotted against this ratio. For systems where antigen loss due to peptide dissociation is not important, diverse results scale with τ_s alone as it is the only relevant time-scale.

These results show that differences in T cell migratory patterns observed upon manipulating different variables (antigen dose, density of DCs bearing cognate ligands, peptide stability, TCR-pMHC binding, etc.) result from how this particular change, combined with all other prevailing conditions, affects the ratio τ/τ_s. Changing each of these variables changes the balance between two relevant time-scales, thereby influencing the way in which migrating T cells interact with and respond to DCs. We hope that these implications of the conceptual framework revealed by our study will help guide future experimentation.

Our computer simulations and experiments reported by Henrickson et al. (18) both highlight the existence of a sharp threshold in the antigen dose on DCs, beyond which the T cell's ability to transition to phase two drastically improves. The value of this threshold concentration is higher for less stable pMHC ligands and weaker TCR-pMHC binding characteristics (also observed *in vitro* (15)). The existence of a threshold is predicated by the fact that dose-response curves characterizing T cell signaling exhibit a threshold (36, 41).

The time-scale associated with T cell-DC encounters is much shorter than the times at which a transition from phase one to phase two type behavior is observed in the experimental study by Henrickson et al.(18). This observation, combined with the fact

that there is a higher amount of pMHC ligands on cognate DCs at shorter times, led us to suggest that T cells may be able to integrate signals from multiple serial encounters with DCs. This aspect of our study differs from previous studies such as a recent study by Preston et al. (48), in which the detection of antigen and activation of T cells are viewed as a transport-limited process, i.e., the T cells commit to activation upon their first encounter with cognate DCs. Signal integration could result from various aspects of the T cell signaling network that may confer memory. Our calculations show that such memory effects would enable a transition from phase one to phase two type behavior when it otherwise may not have occurred because of too low an antigen dose on DCs. We believe that *in vivo*, productive T cell – cognate DC interactions are stochastic events. The ability to integrate signals from sequential T cell-DC encounters enhances the sensitivity with which T cells can detect antigen. Furthermore, it may also narrow the distribution of stochastic times at which individual T cells stop, thereby making the transition to phase two type behavior appear to be more sharply defined.

It has been suggested that DCs may alter the presentation of pMHC ligands upon serial encounters with T cells, which provides the source of such "memory" (8). In our current model, this would simply result in a different type of variation of the propensity of a productive T cell-DC encounter (k) with time. Thus, it will result in a different value for the ratio of the two important time-scales we have identified. Nevertheless, as noted earlier, the results will still depend only on this ratio, and simulations carried out with DCs as the source of memory will also collapse onto the consolidated master curve shown in Figure 4. To resolve whether the origin of "memory" lies in the T cell signaling network and/or pMHC presentation on DCs requires the integration of molecular signaling models with migration simulations and concomitant experiments. It is expected that the details of the temporal migratory patterns should be different in the two cases since the dynamical behavior of the T cell signaling network and enhanced pMHC presentation on DCs (e.g., by clustering ligands) should be very different. Experiments aimed towards resolving this are reported by Henrickson et al. (18).

The close connection between T cell signaling and migration revealed by our studies highlights the need for experimental and computational studies that connect molecular

scale signaling processes to migratory patterns in detail. Multi-scale computational models that seamlessly integrate molecular signaling events with T cell motion are required. Furthermore, the development of efficient computer simulation methods that do not employ a lattice representation of space and can simultaneously incorporate the complexity of signaling are required, if all non-cognate T cells and DCs are to be included in order to generate models that are quantitatively accurate. Similarly, experimental technologies that can combine the tracking of T cell motion with the imaging of signaling molecules (as is currently possible *in vitro*) must be developed. Synergy between such experiments and computational studies will help elucidate how T cells are activated in lymphoid tissues.

2.A Appendix for Chapter 2

2.A.1 Scaling the measured T cell motility coefficient to Lattice units.

Previous imaging work has suggested that the motility coefficient of T cells during phase one is on the order of 10~20 μm^2/min (9-11). Since one lattice spacing and one elementary step correspond to 10μm and 1 minute, respectively, the motility coefficient for the simulated migration needs to be approximately 0.1~0.2LS^2/MCS (LS = lattice spacing, MCS = elementary MC step) to match the experimentally measured value of 10~20μm^2/min. As T cells scan both cognate and non-cognate DCs for antigen, a larger number of DCs will result in a lower motility coefficient. Thus, one can adjust the number of noncognate DCs to obtain the experimentally measured motility coefficient. Many simulations were performed with only non-cognate DCs present in the lattice to determine the appropriate number of non-cognate DCs. It was found that a loading of 3,000 non-cognate DCs results in a motility coefficient of approximately 0.1LS^2 / MCS, i.e. 11 μm^2/min. The relevant simulation result is shown in Figure 2.A.1 in which the mean square displacement $\langle R^2 \rangle$ averaged over 500 trajectories is plotted against time. The linear dependence of $\langle R^2 \rangle$ on time attests to the diffusive nature of the simulated T cell motion. Furthermore, in the case of diffusive migration in 3D, the slope of $\langle R^2 \rangle$ vs. time equals $6D$, where D is the motility coefficient (56). Simulation with 3,000 non-cognate APCs results in a slope of 6D = 0.681LS^2/MCS, which corresponds to the aforementioned motility coefficient of 0.11LS^2/MCS.

Since in most simulations performed, the number of cognate DCs is at least one order of magnitude smaller than 3,000, the motility coefficient does not change significantly during simulations where cognate DCs are present. Therefore, 3,000 non-cognate DCs were used in all simulations.

2.A.2 Estimating the appropriate number of cognate DCs for the simulations.

The number of cognate DCs in the lymph node is estimated to be on the order of 300 per lymph node by Henrickson et al. using their experimental protocol (1). The total volume of an inflamed lymph node typically imaged by Henrickson et al. is approximately 1 mm^3. As frequently observed in imaging experiments, DCs are concentrated near the high endothelial venules (HEV) via which T cells enter the lymph node. Therefore, the pertinent number is most likely the number of cognate DCs in the volume surrounding HEVs. Assuming that this volume is about 5-10% of the entire lymph node, and that the 300 cognate DCs are all distributed therein, the density of cognate DCs is approximately

3000-6000 DC per 1 mm^3. The volume of the lattice used in the simulations is 0.027 mm^3. Therefore, the number of cognate DCs in the lattice should be on the order of 100 DCs. We have varied the number of cognate DCs between 100 and 1000 in our computer simulations.

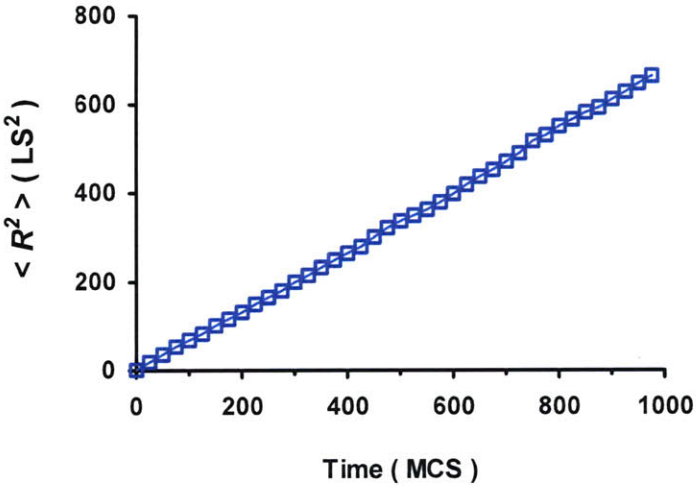

Figure 2.A 1: Mean square displacement vs. time in units of lattice spacing and elementary MC steps, respectively, with 3,000 non-cognate DCs on the lattice. The slope is approximately $0.68LS^2/MCS$.

2.A.3 Justifications for treating DCs as stationary

Diffusive motion can be described using the Langevin equation as $\frac{d\mathbf{r}}{dt} = f(t)$ where $\mathbf{r}$ is a vector that describes the position of the particle, which is subject to a random force f(t). The random force is characterized by $\langle f(t) \rangle = 0$ and $\langle f(t) f(0) \rangle = 6Dt$, where D is the diffusivity or motility coefficient (56). Consider a pair of such random walkers (e.g. a motile T cell and a motile DC) whose motions are uncorrelated on time scales longer than some short time scale present in the problem (such as the time over which a T cell and a DC are in contact). On time scales longer than such short times, the motions of these particles satisfy the Langevin equation, namely $\frac{d\mathbf{r}_1}{dt} = f_1(t)$ and $\frac{d\mathbf{r}_2}{dt} = f_2(t)$. Since their motions are uncorrelated, $\langle f_1(t) f_2(t') \rangle = 0 \forall t, t'$. An encounter occurs when $\mathbf{r}_1 = \mathbf{r}_2$.

As the Langevin equation is linear, the separation between the two random walkers can be written as $\frac{d(\mathbf{r}_1 - \mathbf{r}_2)}{dt} = f_1(t) - f_2(t)$. Therefore, the original two-body problem can be re-written as a problem with one random walker and one stationary object. Define

$\mathbf{r}' = \mathbf{r}_1 - \mathbf{r}_2$ and $f'(t) = f_1(t) - f_2(t)$, then an encounter occurs when $\mathbf{r}' = \mathbf{0}$. The diffusivity D in this case is

$$\frac{\langle f'(t)f'(0)\rangle}{6t} = \frac{\langle f_1(t)f_1(0) - f_1(t)f_2(0) - f_2(t)f_1(0) + f_2(t)f_2(0)\rangle}{6t}$$

and since there are no cross correlations,

$$\frac{\langle f'(t)f'(0)\rangle}{6t} = \frac{\langle f_1(t)f_1(0)\rangle}{6t} + \frac{\langle f_2(t)f_2(0)\rangle}{6t} = D_1 + D_2$$

Consequently, keeping the DCs fixed (as in our simulations) is equivalent to allowing both DCs and T cells to move as long as the T cell motility coefficient is taken to be the sum of the T cell motility coefficient and that of the DC. As the DC motility coefficient is much smaller than that of T cells, ignoring the motility coefficient of the DCs does not alter any of our qualitative conclusions.

2.A.4 Sensitivity to variations in the number of cognate DCs.

Good estimates for the number and distribution of cognate DCs in the lymph node remain difficult to obtain. While the experimental protocol employed by Henrickson et al.. yielded approximately 300 DCs per LN (1) a loading of DCs up to 10^4 DCs per LN have been reported previously (6). Simulations were carried out with a wide range of numbers of cognate DCs. Figure 2.A.2 shows that the qualitative behavior remains the same as that shown in Fig. 2 of the main text, as the number of cognate DCs is varied. For reasons described in the main text, larger numbers of cognate DCs result in a lower threshold concentration of pMHC ligands for a transition to phase two-type behavior.

2.A.5 Sensitivity to variations in the number of cognate T cells

In the model developed for this work, T cells are not permitted to co-occupy the same lattice site. Such mutual exclusion may potentially affect the results in qualitative ways only if the number of T cells is very high, i.e. crowding becomes significant. This scenario, however, is not physiologically relevant. The simulation results reported in the main text are for 500 cognate T cells, which occupy approximately 1.9% of the total number of available sites. At such low occupancy, T cells are very unlikely to run into each other. As demonstrated in Figure 2.A.3 for cognate T cell numbers 50% above or below 500, there is little discernable difference in the fraction of T cells arrested upon exit. This would be predicted by the mean-field analysis as the initial number of cognate T cells appears only as a scale factor. Similarly, there is very little difference in the duration of phase one.

Finally, the model does not explicitly consider the presence of non-specific T cells, whose presence will mostly affect the motility coefficient of the specific T cells in situations relevant to this study. Therefore, the influence of non-specific T cells can be incorporated by adjusting the motility coefficient.

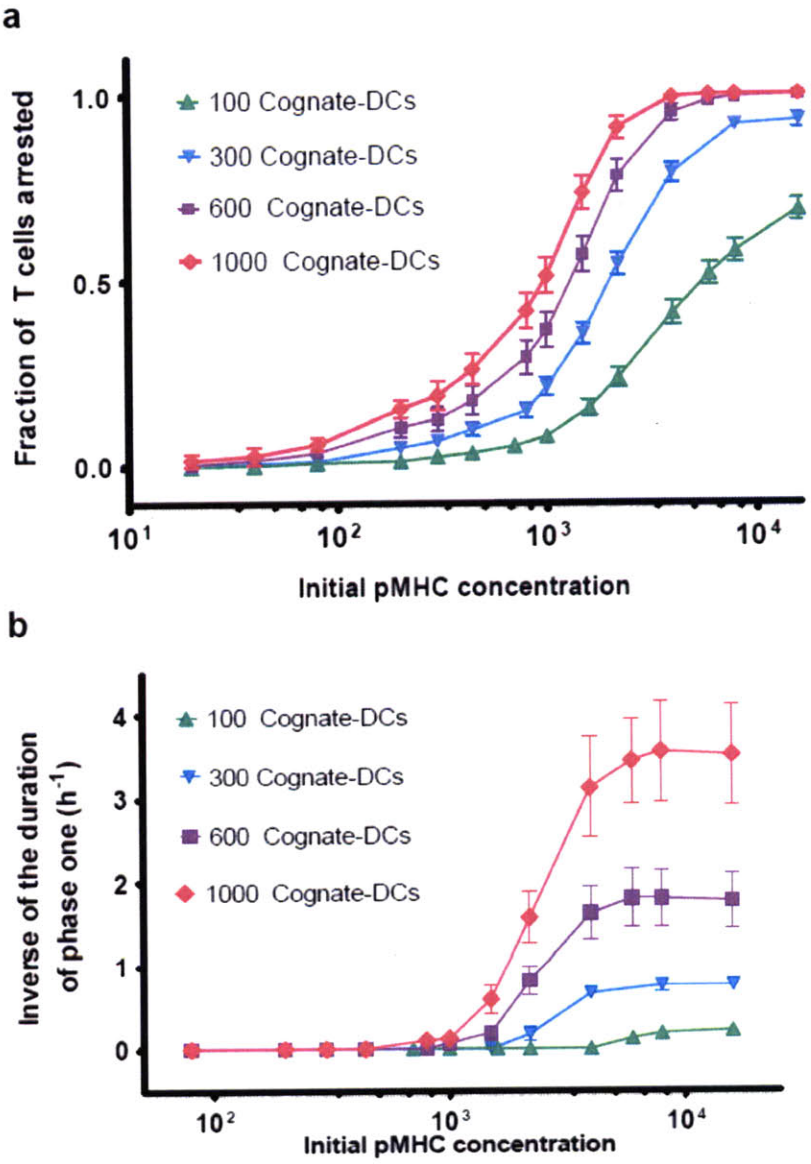

Figure 2.A 2: Variations in the number of cognate DCs do not lead to qualitatively different conclusions. Fraction of T cells arrested and inverse phase one duration is plotted against the initial concentration of pMHC on DCs prior to adoptive transfer, at various numbers of cognate DCs. There is no memory and the rate of loss of peptides is that characteristic of the C-peptide in companion study by Henrickson et al.(1).

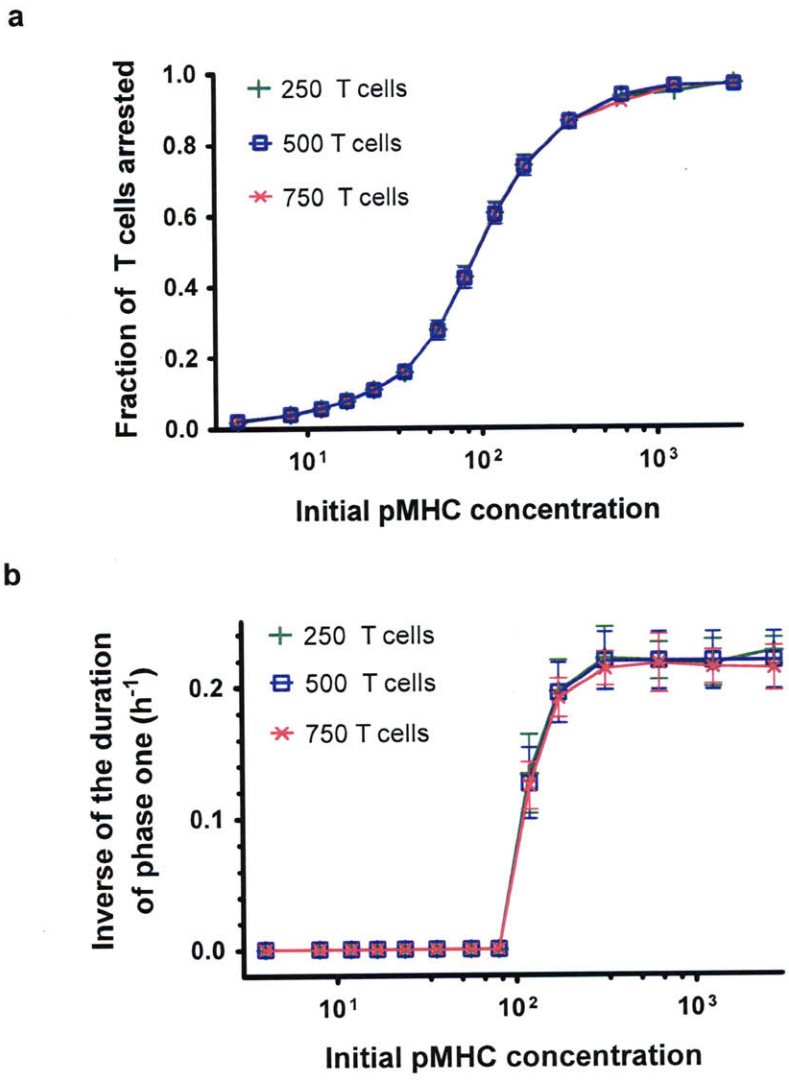

Figure 2.A 3: Changing the number of cognate T cells results in little change in the fraction of T cells arrested, and only small quantitative differences in the duration of phase one. Fraction of T cells arrested upon exit (a) and the inverse duration of phase one; (b) are plotted against the initial concentration of pMHC on DCs prior to adoptive transfer. The peptide has characteristics similar to the M-peptide in Henrickson et al.(1). Results for 3 different numbers of cognate T cells are shown. There are 100 cognate DCs. The results in (b) point to the importance of fluctuations in this problem.

2.A.6 Sensitivity to variations in the scanning time upon a T cell – DC encounter.

The scanning time, τ_w, has two opposing effects on how effectively a T cell receives a stop signal upon encountering a DC, as well as the duration of phase one. Increasing τ_w slows down the migration of T cells, thus the frequency of T cell – DC encounters decreases. On the other hand, with prolonged scanning, the probability of a productive encounter

increases. The relative strengths of these two effects determine whether increasing τ_w leads to a higher arrest fraction and shorter phase one. The increase in encounter frequency upon decreasing scanning time only affects the duration of phase one at high antigen loading (Figure 2.A.4). Figure 2.A.4a shows a more subtle effect. At low pMHC concentration, increasing τ_w does not change the propensity of receiving a stop signal from a given encounter. Thus the decreased frequency of encounters leads to a small reduction in the fraction of arrested T cells. At high pMHC concentration, a longer scanning time increases the propensity of a given T cell – cognate DC encounter to be productive.

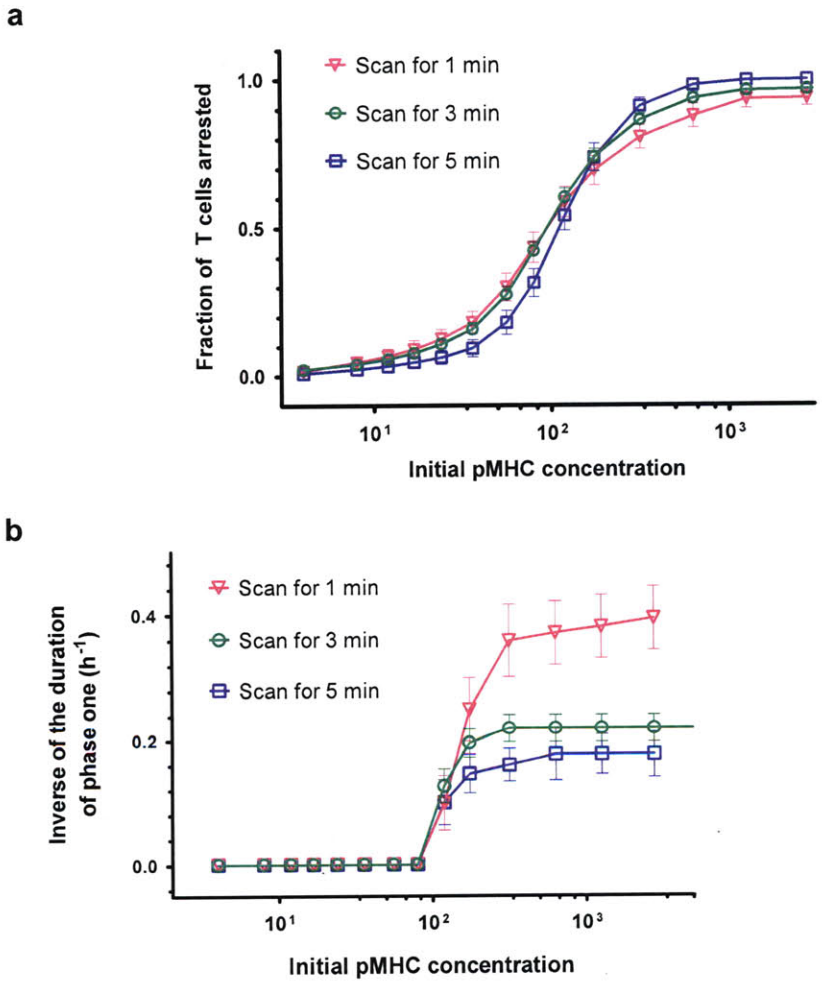

Figure 2.A 4: Fraction of T cells arrested and the duration of phase one plotted against the initial concentration of pMHCs on DCs prior to adoptive transfer, for different values of the scanning time. 100 DCs and 500 T cells are present on the lattice. No memory is implemented for these results. Results are shown for a value of the characteristic time for peptide dissociation that is representative of the M-peptide in companion work by Henrickson et al.(1).

2.A.7 Relationship between pMHC concentrations and probability of a stop signal, *k*.

As discussed in the main text, when a T cell contacts a cognate DC, it can receive a stop signal with a probability *k*. *k* is determined by the concentration of cognate pMHC ligands, their TCR binding characteristics, and the types and numbers of displayed endogenous ligands. Various experimental studies have demonstrated a sigmoidal dependence of markers of T cell activation on the dose of cognate pMHC ligands (e.g. (36, 41)). The threshold concentration described by such a sigmoidal function depends upon TCR-pMHC binding characteristics. In principle, detailed signaling models can provide a mapping between TCR-pMHC binding characteristics, ligand density, and activation probability. In the present study, we consider a general treatment and adopt a sigmoidal function, which is empirical and not derived from detailed molecular considerations. In addition, we also investigate different sigmoidal functions in order to examine the sensitivity of our results to such variations. For the results shown in the main text, the sigmoidal function is represented by the following piecewise-continuous function:

$$k_1(t) = \begin{cases} 4\times10^{-3}\,p(t), & p(t) \le 3 \\ \dfrac{1.2218p(t)^2 - 1.9878p(t)}{734.118 - 19.7905p(t) + p(t)^2}, & 3 < p(t) < 30 \\ 1, & p(t) \ge 30 \end{cases} \qquad \text{Eq. 2.A.1}$$

where *p(t)* is the concentration of pMHC ligands on a DC at time *t*. Note that in the above expressions, the time, *t*, refers to the time after the DCs have arrived in the lymph node, i.e. 18 hours or so after pulsing with peptides and injection (Figure 2.A.5). To trace back to the pre-injection pMHC loading on DC surfaces, $[\text{pMHC}]_0$, one needs to account for the loss of pMHC during the 18 hours, which can be estimated as $[pMHC]_0 = p_{18}\exp(18/\tau)$, where τ is the time scale of pMHC loss in units of hours, which take the values of 8.7 and 3.4 hours (corresponding to half-lives of 6 and 2.35 hours) for the M- and C-peptides in the experimental studies of Henrickson et al. (1)and most of our simulations..

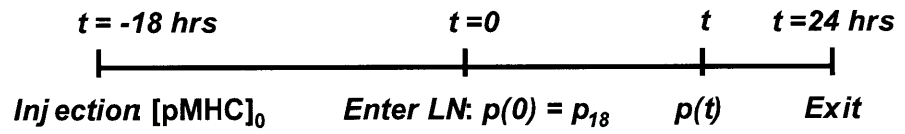

Figure 2.A 5: A schematic timeline showing the sequence of events.

We have explored the dependence of our simulation results on TCR-pMHC binding characteristics by using other forms of the sigmoidal function. While keeping the asymptotic limits for *k* fixed on both ends, one can alter the sigmoidal function to change

the location of the threshold, as well as the sharpness of the "switch" portion (the sharp increase from 0 to the upper plateau). Simulations were performed using the following alternative representations (also shown in Figure 2.A.6

- Alternative 1 (threshold moved to the right compared to Eq.2.A.1)

$$k_1(t) = \begin{cases} 8\times10^{-3}\,p(t), & p(t) \le 12 \\ \dfrac{0.5356p(t)^2 - 4.9397p(t)}{395.5824 - 31.9878p(t) + p(t)^2}, & 12 < p(t) < 31 \\ 1, & p(t) \ge 31 \end{cases} \qquad \text{Eq. 2.A.2}$$

- Alternative 2 (sharpness reduced compared to Eq. 2.A.2)

$$k_1(t) = \begin{cases} 3\times10^{-3}\,p(t), & p(t) \le 3 \\ \dfrac{0.6612p(t)^2 - 2.5683p(t)}{222.1416 - 19.9089p(t) + p(t)^2}, & 3 < p(t) < 27 \\ 1, & p(t) \ge 27 \end{cases} \qquad \text{Eq. 2.A.3}$$

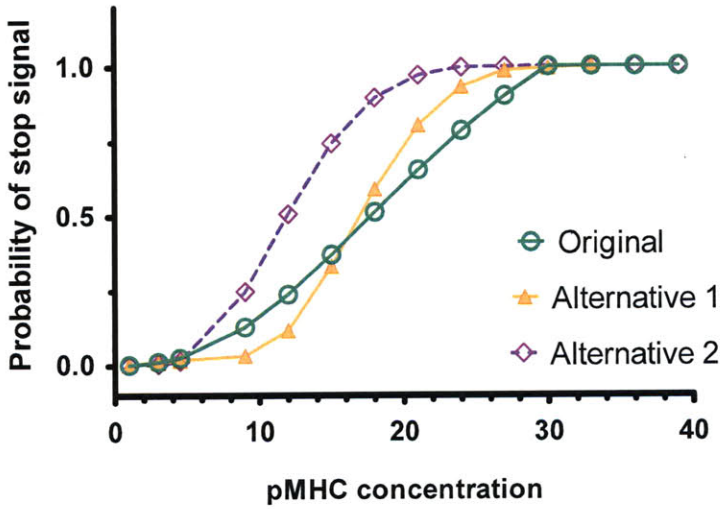

Figure 2.A 6: Probability for T cells to receive a stop signal upon encountering a cognate-DC (k) plotted against the concentration of pMHC on DCs after pulsing with the M-peptide, prior to adoptive transfer. Alternative 1 is the original mapping with the pMHC threshold moved to the right (so a higher initial value is needed for the same probability of stopping), while alternative 2 maintains the original threshold location, but exhibits a sharper response. As a consequence, k increases more sharply as initial pMHC concentration is increased.

Results presented in Figure 2.A.6 illustrate that these alternative mappings only lead to quantitative differences. Larger shifts of the threshold (e.g., of several logs) would result in substantial changes in the ligand concentration required for a transition to phase two

type behavior. Nonetheless, the qualitative shapes of the results shown in Figs. 2-4 in the main text will not be altered. In other words, the conclusions drawn from those results are robust to changes in the threshold location and sharpness, or alternatively parameters that are determined by TCR – pMHC binding characteristics.

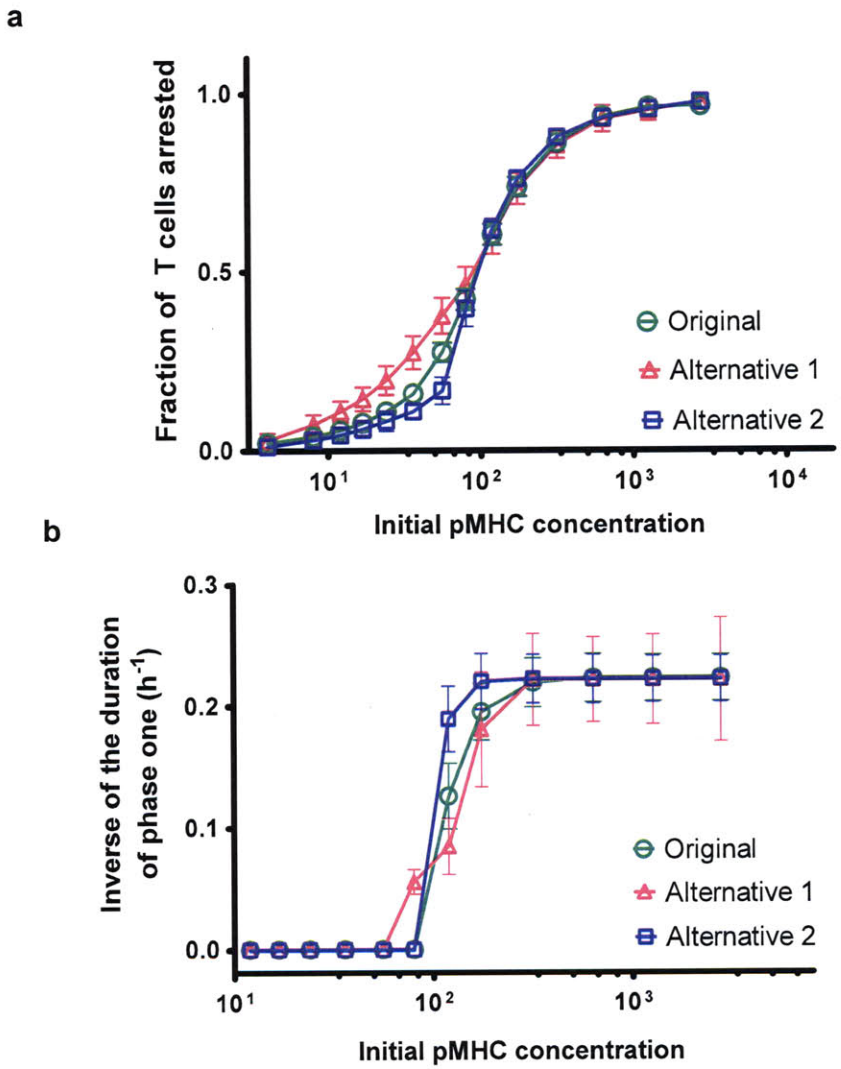

Figure 2.A 7: Altering the detailed relationship between the concentration of initial pMHC on DCs and the probability to receive a stop signal does not lead to qualitative changes in the results. Fraction of T cells arrested (a) and the inverse duration of phase one (b) are plotted against the concentration of pMHCs on DCs after pulsing, prior to adoptive transfer. 500 T cells and 100 DCs are present in the lattice. pMHC are lost with a characteristic time scale that represents the M-peptide used by Henrickson et al.(1). No memory effect is incorporated in these results.

2.A.8 Sensitivity to variations in the exit time.

For all simulations discussed in the main text, the exit time has been set to 24 hours (23), or 1440 elementary MC steps, according to the conversion rule that 1 MCS = 1 minute. If

there was no peptide loss with time, the fraction of T cells making sustained contacts with DCs would increase monotonically with the exit time. If peptide loss is included in the simulations (corresponding to the experimental situation by Henrickson et al.), the fraction of arrested T cells saturates to a constant value if the exit time exceeds the time beyond which most pMHCs are lost from DC surfaces (data not shown). As the exit time is far longer than other pertinent time scales, as shown in Figure 2.A.8, the fraction of arrested T cells is not sensitive to three-fold changes in the value of the exit time. The only exception is when the exit time is reduced by an order of magnitude, and it becomes of the same order as the other time scales. Based on experimental results, such scenarios are not physiologically relevant.

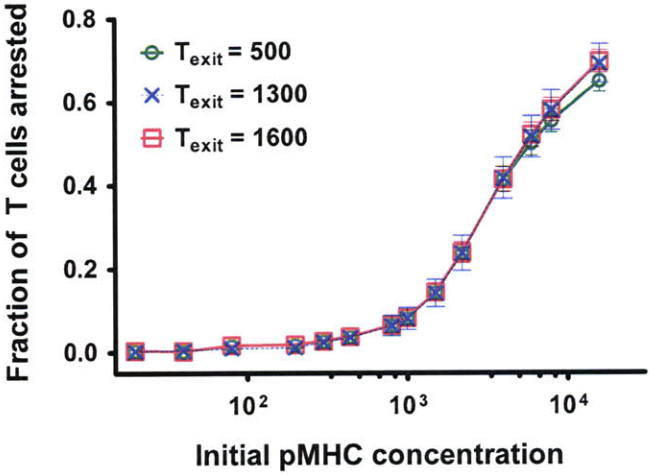

Figure 2.A 8: Fraction of T cells arrested as a function of the initial pMHC concentration on DCs prior to adoptive transfer for different values of the exit time. 500 T cells and 100 cognate DCs are present. The dissociation of pMHC molecules is characterized by a time scale representative of the M-peptide in companion study by Henrickson et al.

2.A.9 Sensitivity to alternative simulation protocols for signaling.

The simulation results shown in the main text are for cases where T cells can receive a stop signal at any time during the scanning period, and there is no peptide loss during this time. This seems to be the most reasonable scenario. However, we have examined the sensitivity of our results to two alternative schemes. In the first scenario, instead of being able to receive a stop signal during the entire scanning period (3 steps), the T cell can only receive a stop signal during the first waiting step, i.e. immediately after the encounter happens. In the second case, the T cell can receive a stop signal at all times during the scanning period, but peptide loss is allowed during this time, leading to smaller values of k. As Figure 2.A.9 shows, the original scheme used to obtain the results in the main text and these alternatives result in very similar fraction of arrest and the duration of phase

one. In scheme 2, where the T cells have only one chance of receiving a stop signal, the fraction arrested is slightly lower. In scheme 3, even though *k* decays during the scanning period due to peptide loss (rather than staying constant as in the original scheme), the fraction arrested and the duration of phase one is not significantly different because, based on experimental values (1) and ((6)), $\tau_w << \tau$.

More importantly, the key mechanistic principle revealed by our study, the interplay between relevant time scales, remains unchanged by changing the simulation protocol during the scanning time. Regardless of the scheme that we choose, all simulation results collapse onto the consolidated master curve described in the main text, as shown by Figure 2.A.10.

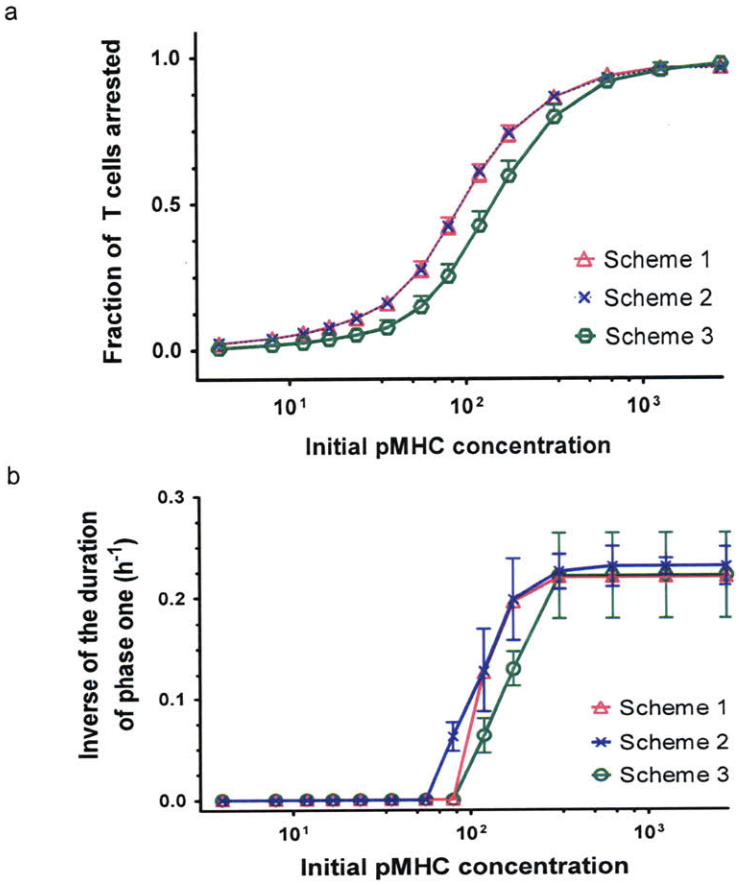

Figure 2.A 9: Fraction of T cells arrested and the inverse duration of phase one vs. the initial pMHC concentration on DCs prior to adoptive transfer for 3 different simulation protocols described above; scheme 1 is the one used to obtain results in the main text, and schemes 2 and 3 are described above. 100 DCs and 500 T cells are present on the lattice. Memory effect is not incorporated for these results. Results are shown for a peptide dissociation time scale that is representative of the M-peptide in companion study by Henrickson et al (1).

a: Scheme 2

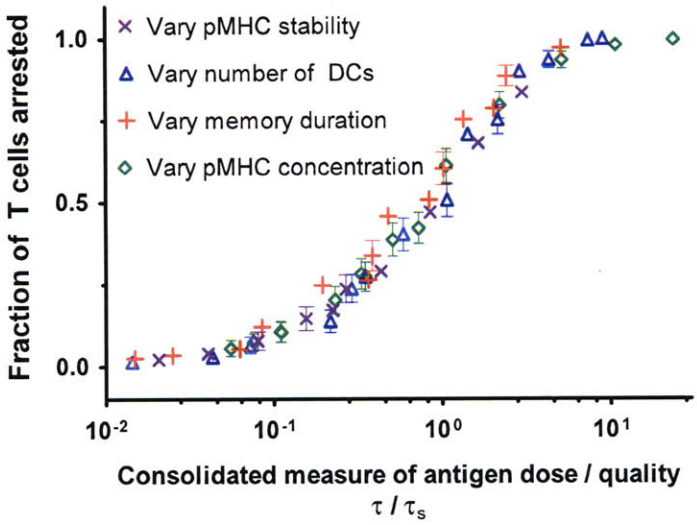

b: Scheme 3

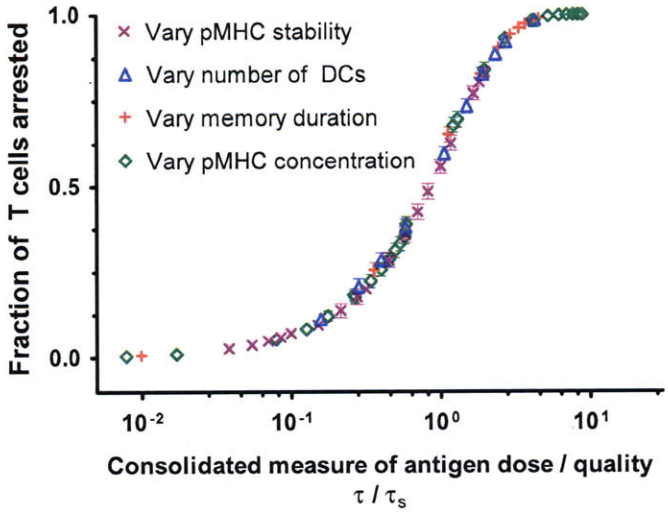

Figure 2.A 10: All schemes for describing events during T cell-cognate DC contacts result in collapse of all simulation results on to a single consolidated master curve. The result for Scheme 1 is Fig.3 in the main text. Scheme 2 and 3 (a and b) are shown here. The four categories of variations in conditions that were simulated are the same as those in Fig. 3 of the main text.

2.A.10 Sensitivity to variations in the time scale (τ) over which peptide dissociation occurs.

As illustrated by the comparisons between the M-and C-peptide presented in the main text, the value of τaffects the time to transition from phase one to phase two. The slower the decay is, the higher the activation probability at a given time is. In addition, when DC homing is taken into consideration, the effect of pMHC stability is further magnified. When DCs pick up foreign antigens at the site of infection, it typically takes hours before

they home to the lymph nodes. Consequently, by the time DCs enter the lymph node, there would be fewer cognate ligands remaining on the surface of DCs for a less stable antigen, which further limits the probability of antigen detection. To examine these two effects, simulations were performed with a range of different values of τ (i.e. a range of pMHC stability), while keeping a constant loading of 100 cognate DCs in the lattice and a simulation period of 24 hours. As shown in Figure 2.A.11, increasing τ (and thus increasing the pMHC half-life) greatly enhances the fraction of arrested T cells for low and intermediate initial pMHC loadings. When the pMHC loading becomes excessive, the loss of pMHC no longer has any effect, as reflected by the upper asymptotic limit seen in most curves. Such high values of cognate ligand density on a DC are unlikely to be physiologically relevant. Higher values of τ also shift the curves further to the left, because more stable pMHCs suffer less loss during DC homing (fixed at 18 hours for all simulations following Henrickson et al. (1). The duration of phase one (defined as the time required to arrest 50% of the total T cells) is approximately the same for all cases when the concentration of cognate ligands is sufficiently high (Figure 2.A.10b). This is because at high pMHC concentrations the activation propensity is large enough to stop T cells upon the first encounter with a DC. Under such circumstances, the duration of phase one is more strongly dependent on the diffusion time scale (Figure 2.A.2).

a

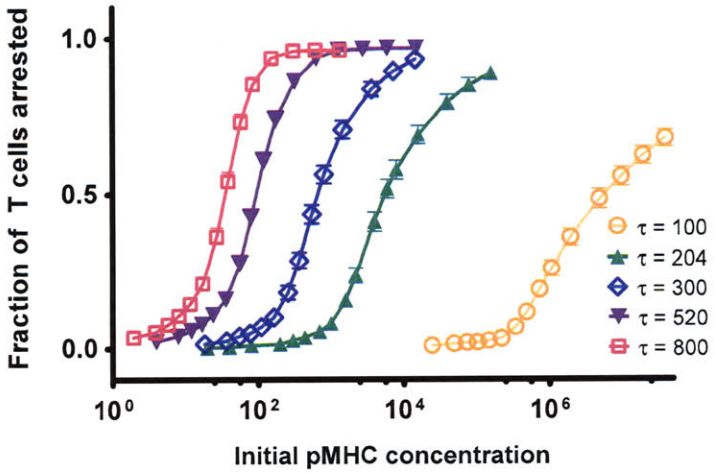

b

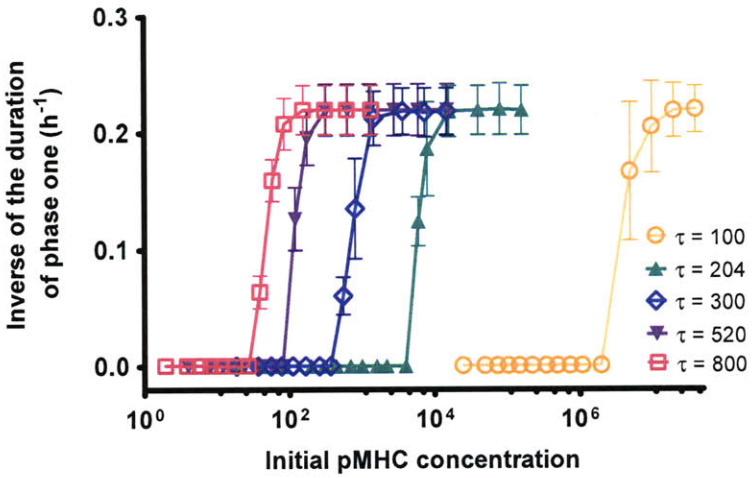

Figure 2.A 11: Fraction of T cells arrested and inverse of the duration of phase one plotted against the initial concentration of pMHC on DCs prior to adoptive transfer, for various pMHC decay time scales (τ). No memory effect is incorporated for these results. 100 DCs are present on the lattice.

2.A.11 Sensitivity to variations in the characteristic time scale over which memory is manifested (τ_m).

As mentioned in the main text, incorporating memory from past T cell-DC encounters into the model does not alter the results qualitatively. We have carried out simulations over t_m that range from 0 to 4 hours to demonstrate this (data not shown). With a more persistent memory (a larger value of t_m), the decline in the probability for T cells to receive a stop signal can be better ameliorated. By incorporating the possible effect of memory, the threshold pMHC concentration required to induce a transition to phase two can be reduced. Such a reduction can be used as a measure of the enhancement due to memory (Figure 2.A.12).

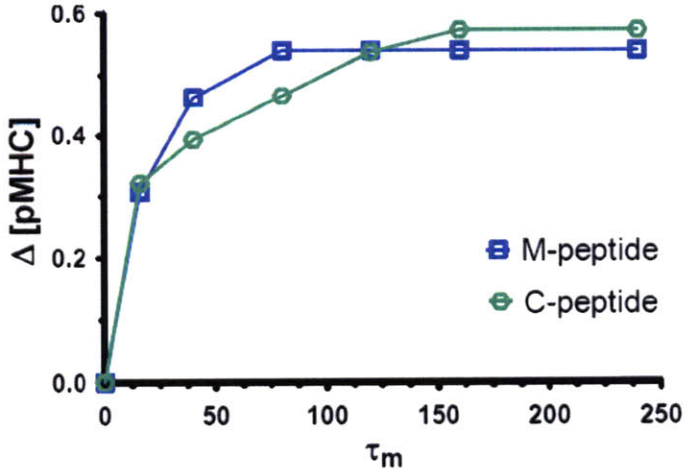

Figure 2.A 12: The decrease in the threshold concentration of pMHC required for a transition to phase two type behavior upon increasing t_m vs. length of memory time scale. D[pMHC] is defined as

$\frac{[pMHC]_c - [pMHC]_c'}{[pMHC]_c}$ where $[pMHC]_c'$ and $[pMHC]_c$ are the required threshold concentrations with and without memory, respectively. Simulation results are shown for cases corresponding to pMHC stabilities representative of the M- and C-peptide used in the companion work by Henrickson et al.

2.A.12 The mean-field treatment and solution

The differential equation describing the number of T cells that have not received a stop signal (T), has the following general form:

$$\frac{\partial T}{\partial t} = D\nabla^2 T - k\rho T$$
$$T(t=0) = T_0 \quad T(t, \pm\infty) = 0 \qquad \text{Eq. 2.A.4}$$

where the value of k typically varies over time as $k(t)$ in some complicated way, as dictated by the exponential decay of pMHC concentration, and the sigmoidal mapping between pMHC concentration and k, as described previously. In this case, the analytical solution is not generally available. The analytical solution for two simplified cases, however, can be easily obtained.

- No pMHC loss over time: $k(t) = k_0$

First, the equation can be non-dimensionalized by scaling the pertinent quantities using T_0 ,τ_e and L, where T_0 is the total number of cognate T cells (also the initial number of *motile* T cells), τ_e is the diffusion time scale and L is the average distance between two cognate DCs ($\sim 1/\rho^{2/3}$). Then one obtains the following:

$$\frac{\partial \bar{T}}{\partial \bar{t}} = \bar{\nabla}^2 \bar{T} - \tau_e k_0 \rho \bar{T}$$
$$\bar{T} = T/T_0 \qquad \bar{\nabla}^2 = \nabla^2 / L^2 \qquad \text{Eq. 2.A.5}$$
$$\bar{t} = t/\tau_e \qquad \tau_e = L^2/D$$
$$\bar{T}(\bar{t}=0) = 1 \quad \bar{T}(\bar{t}, \pm\infty) = 0$$

Then one can define $\tau_s = \frac{1}{k_0 \rho}$, which is the time scale for a productive T cell – DC encounter. Transforming to Fourier variables conjugate to space, one obtains $\frac{d\bar{T}}{d\bar{t}} = -\kappa^2 \bar{T} - \frac{\tau_e}{\tau_s}\bar{T}$, where κ is the Fourier variable. The solution of this equation is $\bar{T}(\bar{t}) = \exp\left[-\left(\kappa^2 + \frac{\tau_e}{\tau_s}\right)\bar{t}\right]$. To examine only the spatially averaged solution, we set κ = 0 and arrive at $\bar{T}(\bar{t}) = \exp\left[-\frac{\tau_e}{\tau_s}\bar{t}\right]$ or $T(t) = \exp\left[-\frac{t}{\tau_s}\right]$ in terms of dimensional variables.

Therefore, the fraction of T cells arrested in this context is simply $f = \exp(-t/\tau_s) = \exp(-k_0 \rho t)$. Notice that the integral $\rho \int_0^t k(t')dt' = \rho k_0 t$ in this case.

- pMHC decays exponentially

In this case, the equation becomes

$$\frac{\partial T}{\partial t} = D\nabla^2 T - k_0 \exp(-t/\tau)\rho T \qquad \text{Eq. 2.A.6}$$
$$T(t=0) = T_0 \quad T(t, \pm\infty) = 0$$

Similar to the treatment in the first case, one can obtain the dimensionless form:

$$\frac{\partial \bar{T}}{\partial \bar{t}} = \bar{\nabla}^2 \bar{T} - \tau_e k_0 \rho \exp(-\tau_e \bar{t}/\tau)\bar{T}$$
$$\bar{T} = T/T_0 \qquad \bar{\nabla}^2 = \nabla^2 / L^2 \qquad \text{Eq. 2.A.7}$$
$$\bar{t} = t/\tau_e \qquad \tau_e = L^2/D$$
$$\bar{T}(\bar{t}=0) = 1 \quad \bar{T}(\bar{t}, \pm\infty) = 0$$

The spatially Fourier-transformed form is $\frac{d\bar{T}}{d\bar{t}} = -\kappa^2 \bar{T} - \tau_e k_0 \rho \exp(-\tau_e \bar{t}/\tau)\bar{T}$, whose solution is $T = \exp\left[-\kappa^2 \bar{t} - \tau k_1^0 \rho(1 - \exp(-\tau_d \bar{t}/\tau))\right]$ The spatial average of the solution, corresponding to the case with κ = 0, is $T = \exp\left[-\tau k_1^0 \rho(1 - \exp(-\tau_d \bar{t}/\tau))\right]$which is $T = \exp\left[-\tau k_1^0 \rho(1 - \exp(-t/\tau))\right]$in dimensional variables. Since the exit time is typically much longer than the time scale of pMHC loss, the asymptotic limit of T is $T_{t>>\tau} \to \exp\left[-\rho k_0 \tau\right]$.

The mean value of $\frac{\tau}{\tau_s}$ is the integral defined in the text because $\rho \int_0^t k_1(t')dt' = \rho k_1^0 \int_0^t e^{-t'/\tau} dt' = \rho k_1^0 (1 - e^{-t/\tau})$ One can observe that in the limit of $t \gg \tau$, this integral converges to $\rho k_0 \tau$. Therefore, again the fraction of T cells arrested after the exit time has elapsed converges to $f_{t>>\tau} \to \exp(-\tau/\tau_s)$.

References

1. Henrickson, S. E., T. R. Mempel, I. B. Mazo, B. Liu, M. N. Artyomov, H. Zheng, A. Peixoto, M. P. Flynn, B. Senman, T. Junt, H. C. Wong, A. K. Chakraborty, and U. H. von Andrian. 2008. T cell sensing of antigen dose governs interactive behavior with dendritic cells and sets a threshold for T cell activation. *Nat. Immunol* 9:282-291.
2. Zheng, H., B. Jin, S. E. Henrickson, A. S. Perelson, U. H. von Andrian, and A. K. Chakraborty. 2008. How Antigen Quantity and Quality Determine T-Cell Decisions in Lymphoid Tissue *Mol. Cell. Biol.* 28:4040-4051.
3. Bousso, P., N. R. Bhakta, R. S. Lewis, and E. Robey. 2002. Dynamics of thymocyte-stromal cell interactions visualized by two-photon microscopy. *Science* 296:1876-1880.
4. Miller, M. J., S. H. Wei, I. Parker, and M. D. Cahalan. 2002. Two-photon imaging of lymphocyte motility and antigen response in intact lymph node. *Science* 296:1869-1873.
5. Stoll, S., J. Delon, T. M. Brotz, and R. N. Germain. 2002. Dynamic imaging of T cell-dendritic cell interactions in lymph nodes. *Science* 296:1873-1876.
6. Bousso, P., and E. Robey. 2003. Dynamics of CD8(+) T cell priming by dendritic cells in intact lymph nodes. *Nature Immunology* 4:579-585.
7. Bousso, P., and E. A. Robey. 2004. Dynamic behavior of T cells and thymocytes in lymphoid organs as revealed by two-photon microscopy. *Immunity* 21:349-355.
8. Hugues, S., L. Fetler, L. Bonifaz, J. Helft, F. Amblard, and S. Amigorena. 2004. Distinct T cell dynamics in lymph nodes during the induction of tolerance and immunity. *Nature Immunology* 5:1235-1242.
9. Mempel, T. R., S. E. Henrickson, and U. H. von Andrian. 2004. T-cell priming by dendritic cells in lymph nodes occurs in three distinct phases. *Nature* 427:154-159.
10. Miller, M. J., A. S. Hejazi, S. H. Wei, M. D. Cahalan, and I. Parker. 2004. T cell repertoire scanning is promoted by dynamic dendritic cell behavior and random T cell motility in the lymph node. *Proceedings of the National Academy of Sciences of the United States of America* 101:998-1003.
11. Miller, M. J., O. Safrina, I. Parker, and M. D. Cahalan. 2004. Imaging the single cell dynamics of CD4(+) T cell activation by dendritic cells in lymph nodes. *Journal of Experimental Medicine* 200:847-856.
12. Shakhar, G., R. L. Lindquist, D. Skokos, D. Dudziak, J. H. Huang, M. C. Nussenzweig, and M. L. Dustin. 2005. Stable T cell-dendritic cell interactions precede the development of both tolerance and immunity in vivo. *Nature Immunology* 6:707-714.
13. Bajenoff, M., J. G. Egen, L. Y. Koo, J. P. Laugier, F. Brau, N. Glaichenhaus, and R. N. Germain. 2006. Stromal cell networks regulate lymphocyte entry, migration, and territoriality in lymph nodes. *Immunity* 25:989-1001.
14. Schneider, H., J. Downey, A. Smith, B. H. Zinselmeyer, C. Rush, J. M. Brewer, B. Wei, N. Hogg, P. Garside, and C. E. Rudd. 2006. Reversal of the TCR Stop Signal by CTLA-4. *Science* 313:1972-1975.

15. Skokos, D., G. Shakhar, R. Varma, J. C. Waite, T. O. Cameron, R. L. Lindquist, T. Schwickert, M. C. Nussenzweig, and M. L. Dustin. 2007. Peptide-MHC potency governs dynamic interactions between T cells and dendritic cells in lymph nodes. *Nature Immunology* 8:835-844.
16. Wei, S. H., O. Safrina, Y. Yu, K. R. Garrod, M. D. Cahalan, and I. Parker. 2007. Ca2+ signals in CD4+ T cells during early contacts with antigen-bearing dendritic cells in lymph node. *Journal of Immunology* 179:1586-1594.
17. Celli, S., Z. Garcia, and P. Bousso. 2005. CD4 T cells integrate signals delivered during successive DC encounters in vivo. *Journal of Experimental Medicine* 202:1271-1278.
18. Henrickson, S. E., T. R. Mempel, I. B. Mazo, B. Liu, M. N. Artyomov, H. Zheng, A. Peixoto, M. P. Flynn, B. Senman, T. Junt, H. C. Wong, A. K. Chakraborty, and U. H. von Andrian. 2008. T cell sensing of antigen dose governs interactive behavior with dendritic cells and sets a threshold for T cell activation. *Nature Immunology* 9:282-291.
19. Beltman, J. B., A. F. M. Maree, J. N. Lynch, M. J. Miller, and R. J. de Boer. 2007. Lymph node topology dictates T cell migration behavior. *Journal of Experimental Medicine* 204:771-780.
20. Beltman, J. B., A. F. M. Maree, and R. J. de Boer. 2007. Spatial modelling of brief and long interactions between T cells and dendritic cells. *Immunology and Cell Biology* 85:306-314.
21. Freed, K. F. 1987. *Renormalization group theory of macromolecules.* J. Wiley, New York.
22. Beauchemin, C., N. M. Dixit, and A. S. Perelson. 2007. Characterizing T Cell Movement within Lymph Nodes in the Absence of Antigen. *J Immunol* 178:5505-5512.
23. Halin, C., M. L. Scimone, R. Bonasio, J.-M. Gauguet, T. R. Mempel, E. Quackenbush, R. L. Proia, S. Mandala, and U. H. von Andrian. 2005. The S1P-analog FTY720 differentially modulates T-cell homing via HEV: T-cell-expressed S1P1 amplifies integrin activation in peripheral lymph nodes but not in Peyer patches. *Blood* 106:1314-1322.
24. Shiow, L. R., D. B. Rosen, N. Brdickova, Y. Xu, J. P. An, L. L. Lanier, J. G. Cyster, and M. Matloubian. 2006. CD69 acts downstream of interferon-alpha/beta to inhibit S1P(1) and lymphocyte egress from lymphoid organs. *Nature* 440:540-544.
25. Catron, D. M., A. A. Itano, K. A. Pape, D. L. Mueller, and M. K. Jenkins. 2004. Visualizing the first 50 Hr of the primary immune response to a soluble antigen. *Immunity* 21:341-347.
26. Young, A. J. 1999. The physiology of lymphocyte migration through the single lymph node in vivo. *Seminars in Immunology* 11:73-83.
27. Gunzer, M., A. Schafer, S. Borgmann, S. Grabbe, K. S. Zanker, E. B. Brocker, E. Kampgen, and P. Friedl. 2000. Antigen presentation in extracellular matrix: Interactions of T cells with dendritic cells are dynamic, short lived, and sequential. *Immunity* 13:323-332.

28. Huppa, J. B., M. Gleimer, C. Sumen, and M. M. Davis. 2003. Continuous T cell receptor signaling required for synapse maintenance and full effector potential. *Nature Immunology* 4:749-755.
29. Faroudi, M., R. Zaru, P. Paulet, S. Muller, and S. Valitutti. 2003. Cutting edge: T lymphocyte activation by repeated immunological synapse formation and intermittent signaling. *Journal of Immunology* 171:1128-1132.
30. van Stipdonk, M. J. B., G. Hardenberg, M. S. Bijker, E. E. Lemmens, N. M. Droin, D. R. Green, and S. P. Schoenberger. 2003. Dynamic programming of CD8+ T lymphocyte responses. *Nature Immunology* 4:361-365.
31. van Stipdonk, M. J. B., E. E. Lemmens, and S. P. Schoenberger. 2001. Naive CTLs require a single brief period of antigenic stimulation for clonal expansion and differentiation. *Nature Immunology* 2:423-429.
32. Mercado, R., S. Vijh, S. E. Allen, K. Kerksiek, I. M. Pilip, and E. G. Pamer. 2000. Early Programming of T Cell Populations Responding to Bacterial Infection. *Journal of Immunology* 165:6833-6839.
33. Kaech, S. M., and R. Ahmed. 2001. Memory CD8+ T cell differentiation: initial antigen encounter triggers a developmental program in naive cells. *Nature Immunology* 2:415-422.
34. Dustin, M. L., S. K. Bromley, Z. Y. Kan, D. A. Peterson, and E. R. Unanue. 1997. Antigen receptor engagement delivers a stop signal to migrating T lymphocytes. *Proceedings of the National Academy of Sciences of the United States of America* 94:3909-3913.
35. Lee, K. H., A. R. Dinner, C. Tu, G. Campi, S. Raychaudhuri, R. Varma, T. N. Sims, W. R. Burack, H. Wu, O. Kanagawa, M. Markiewicz, P. M. Allen, M. L. Dustin, A. K. Chakraborty, and A. S. Shaw. 2003. The immunological synapse balances T cell receptor signaling and degradation. *Science* 302:1218-1222.
36. Li, Q. J., A. R. Dinner, S. Y. Qi, D. J. Irvine, J. B. Huppa, M. M. Davis, and A. K. Chakraborty. 2004. CD4 enhances T cell sensitivity to antigen by coordinating Lck accumulation at the immunological synapse. *Nature Immunology* 5:791-799.
37. Wylie, D. C., J. Das, and A. K. Chakraborty. 2007. Sensitivity of T cells to antigen and antagonism emerges from differential regulation of the same molecular signaling module. *Proceedings of the National Academy of Sciences of the United States of America* 104:5533-5538.
38. Goldstein, B., J. R. Faeder, and W. S. Hlavacek. 2004. Mathematical and computational models of immune-receptor signalling. *Nature Reviews Immunology* 4:445-456.
39. Cemerski, S., J. Das, J. Locasale, P. Arnold, E. Giurisato, M. A. Markiewicz, D. Fremont, P. M. Allen, A. K. Chakraborty, and A. S. Shaw. 2007. The stimulatory potency of T cell antigens is influenced by the formation of the immunological synapse. *Immunity* 26:345-355.
40. Altan-Bonnet, G., and R. N. Germain. 2005. Modeling T cell antigen discrimination based on feedback control of digital ERK responses. *Plos Biology* 3:1925-1938.
41. Sykulev, Y., A. Brunmark, M. Jackson, R. J. Cohen, P. A. Peterson, and H. N. Eisen. 1994. Kinetics and affinity of reactions between an antigen-specific T cell receptor and peptide-MHC complexes. *Immunity* 1:15-22.

42. Frenkel, D., and B. Smit. 2001. *Understanding Molecular Simulation.* Academic Press, Inc., Orlando, FL.
43. Purbhoo, M. A., D. J. Irvine, J. B. Huppa, and M. M. Davis. 2004. T cell killing does not require the formation of a stable mature immunological synapse. *Nat. Immunol.* 5:524-530.
44. Slifka, M. K., R. Antia, J. K. Whitmire, and R. Ahmed. 1998. Humoral immunity due to long-lived plasma cells. *Immunity* 8:363-372.
45. de Gennes, P.-G. 1985. *Scaling concepts in polymer physics.* Cornell University Press, Ithaca, NY.
46. Kayser, R. F., and J. B. Hubbard. 1983. Diffusion in a medium with a random distribution of static traps. *Physical Review Letters* 51:79-82.
47. Kayser, R. F., and J. B. Hubbard. 1984. Reaction diffusion in a medium containing a random distribution of nonoverlapping traps. *Journal of Chemical Physics* 80:1127-1130.
48. Preston, S. P., S. L. Waters, O. E. Jensen, P. R. Heaton, and a. D. I. Pritchard. 2006. T-cell motility in the early stages of the immune response modeled as a random walk amongst targets. *Physical Review E: Statistical, Nonlinear, and Soft Matter Physics* 74:011910.
49. Reth, M., and T. Brummer. 2004. Feedback regulation of lymphocyte signalling. *Nature Reviews Immunology* 4:269-277.
50. Zipfel, W. R., R. M. Williams, and W. W. Webb. 2003. Nonlinear magic: multiphoton microscopy in the biosciences. *Nature Biotechnology* 21:1368-1376.
51. Zipfel, W. R., R. M. Williams, R. Christie, A. Y. Nikitin, B. T. Hyman, and W. W. Webb. 2003. Live tissue intrinsic emission microscopy using multiphoton-excited native fluorescence and second harmonic generation. *Proceedings of the National Academy of Sciences of the United States of America* 100:7075-7080.
52. Castellino, F., A. Y. Huang, G. Altan-Bonnet, S. Stoll, C. Scheinecker, and R. N. Germain. 2006. Chemokines enhance immunity by guiding naive CD8+ T cells to sites of CD4+ T cell-dendritic cell interaction. *Nature* 440:890-895.
53. Guarda, G., M. Hons, S. F. Soriano, A. Y. Huang, R. Polley, A. Martin-Fontecha, J. V. Stein, R. N. Germain, A. Lanzavecchia, and F. Sallusto. 2007. L-selectin-negative CCR7- effector and memory CD8+ T cells enter reactive lymph nodes and kill dendritic cells. *Nature Immunology* 8:743-752.
54. Worbs, T., T. R. Mempel, J. Bolter, U. H. von Andrian, and R. Forster. 2007. CCR7 ligands stimulate the intranodal motility of T lymphocytes in vivo. *Journal of Experimental Medicine* 204:489-495.
55. Stachowiak, A. N., Y. Wang, Y. C. Huang, and D. J. Irvine. 2006. Homeostatic lymphoid chemokines synergize with adhesion ligands to trigger T and B lymphocyte chemokinesis. *Journal of Immunology* 177:2340-2348.
56. Doi, M., and S. F. Edwards. 1988. *The Theory of Polymer Dynamics.* Clarendon, Oxford.

Chapter 3

A computational method for simulating T cell migration and signaling in lymphoid tissues predicts possible mechanisms for signal integration

3.1 Introduction

The detection of invading antigen (Ag) by circulating T cells and the subsequent activation of adaptive immune defense mainly take place in secondary lymphoid tissues such as the lymph node (LN) and spleen, where professional Ag presenting cells (APCs), chiefly dendritic cells (DCs), present Ag fragments on their surfaces. The molecular signatures of Ag are peptide-major histocompatibility complexes (pMHC), where the peptides are derived from foreign proteins. While the mechanisms via which Ag is recognized in vivo by T cells remain to be fully uncovered, much new data has been obtained in recent years thanks to the advent of sophisticated in vivo multiphoton and two photon microscopy techniques (1-29). In vivo imaging of T cell triggering in LN showed that both CD4+ and CD8+ T cells exhibit motility changes over time. For example, Mempel et al. showed that, upon entering the LN, naïve CD8+ T cells move rapidly and change directions randomly. Their contacts with DCs, regardless of whether cognate Ag is presented, only last for a few minutes. The time period characterized by such motility features has been termed "phase one" (1, 2). If cognate Ag is present, however, Ag-specific T cells may terminate phase one-type behavior and engage in stable contacts with cognate-DCs, thus entering a "phase two" type of motility behavior. More specifically, phase two is defined to be when a large fraction of the cognate T cells (e.g. 50%) have switched their motility characteristics (1, 2). Similar trends have been observed for CD4+ T cells (3-6).

As many such experiments were performed using different types of Ag at vastly different doses, contradictory motility behaviors were reported, and questions arose regarding whether phase one-type behavior was necessary for T cell activation (7). Along with experimental collaborators, we have previously demonstrated, via experimental, computational and theoretical analyses, that whether and when T cells transition from

phase one to phase two-type behavior is determined by the quantity and quality of cognate Ag in the LN (2, 8). The interdependence between T cell motility features and its activation via TCR-pMHC interactions has also been shown for CD4+ T cells recently (9).

Nevertheless, while establishing this conclusion, a new puzzle emerged. One metric for Ag "quality" is the stability of the Ag-derived pMHCs. Henrickson et al. (10) showed that Ag peptides dissociate from the MHC groove over time in an apparently exponential manner. In other words, T cells are exposed to a higher dose of pMHC earlier during phase one, before significant pMHC dissociation has occurred. If the probability for activation is determined by the dose and strength of pMHC a T cell sees on one single DC, then the T cells are more likely to become activated earlier on. However, Henrickson et al. also observed that given a low initial loading of a fast-dissociating pMHC on DCs, the T cells spent a longer time (an additional 1~2 hours) in phase one. This result presents a paradox; namely, why does this transition not occur at earlier times when the Ag dose is higher prior to significant pMHC dissociation? One possible answer is that T cells are hunting for rare DCs that present unusually large doses of pMHC. Data presented by Henrickson et al (10) argues against this possibility, as T cells appeared to distribute uniformly in space, similar to situations where Ag quantity and/or quality were high. Why, then, does T cell activation require a larger number of transient contacts with cognate DCs at a relatively low dose of stimulation?

We hypothesized that since the initial pMHC dose per DC was too low to elicit a stop signal with high probability, the T cells that eventually stopped may have achieved a stop signal by integrating signals from multiple interrupted sequential interactions with APCs bearing cognate Ag. Such a possibility has been suggested by several other experimental studies (35, 37-40). Moreover, it is likely that the full activation of T cell signaling requires the TCR membrane proximal signal to sustain beyond some critical duration (11), and integration of sequential signals may help achieve this. Nonetheless, the molecular mechanism that might enable integration of membrane-proximal TCR signal (i.e. a short-term "memory" of previous encounters with DC-presented Ag) is not known.

Das et al. recently reported an intrinsic hysteresis in the TCR membrane-proximal signaling network resulting from a positive feedback loop in the conversion of RasGDP to

RasGTP mediated by two different guanine nucleotide exchange factors (GEFs): RasGRP and SOS (12). Specifically, Ras activation via RasGRP happens in a graduated manner with respect to stimulus strength (analog), whereas the SOS-mediated pathway exhibits digital signaling upon priming with RasGRP-mediated RasGTP production. After RasGDP molecules are phosphorylated into RasGTP, they can bind to an allosteric pocket in SOS, which drastically increases SOS' catalytic activity for producing RasGTP (13). Since the dissociation of RasGTP from the allosteric pockets occurs over a finite period of time, after the removal of stimulus from a strongly stimulated T cell, many SOS molecules still hold RasGTP in their allosteric pockets and remain highly active for some time. Computational and experimental analyses by Das and coworkers have demonstrated that, within a certain time window, a stimulus ordinarily insufficient to elicit strong RasGTP response may quickly trigger a fast rise in RasGTP, if the cells have been recently stimulated. This will not occur if long enough time has elapsed such that the dissociation of RasGTP from the SOS allosteric pockets has proceeded beyond a critical level. This threshold value of RasGTP that allows rapid Ras activation by a weak re-stimulation is called the separatrix (Figure 3.3.1). Das et al. showed that such "short term memory" (or hysteresis) requires SOS, as a SOS-/- mutation abrogates hysteresis.

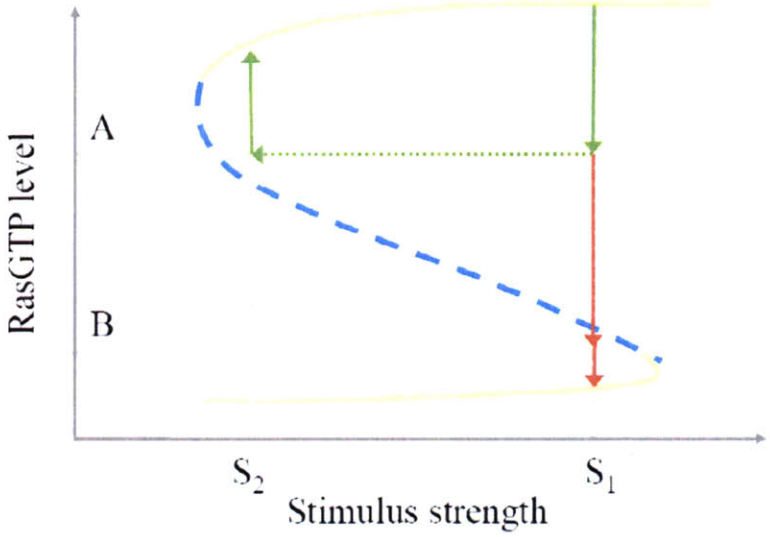

Figure 3.3.1: A schematic showing the hysterisis in RasGTP production due to a positive feedback in the TCR membrane proximal signaling network. The middle branch (dashed line) represents the unstable steady states, while the top and bottom branches represent the stable

steady states. A first strong stimulus S_1 stimulated high RasGTP production, then the stimulus is removed. As long as RasGTP has not decayed below the unstable steady states corresponding to the second weak stimulus (S_2), e.g. point A, RasGTP level rapidly returns to the upper branch. If RasGTP decays below the separatrix, e.g. point B, then RasGTP will continue to decline, and the T cell will not respond to the second weak stimulus.

This result led us to postulate a mechanism for signal integration during T cell migration in vivo. Suppose via a brief contact with a cognate DC, a T cell experiences a sharp rise in RasGTP. The T cell disengages and migrates until it encounters another DC, which likely presents a weak stimulus since during the disease outset the dose of Ag is relatively low. As shown in several microscopy studies, the interval between two consecutive encounters with DCs is very short (14, 15). Thus RasGTP levels in the T cell may remain above the separatrix corresponding to the weak stimulus presented by the DC encountered next. Due to the phenomenon described above, the T cell can quickly recover a high level of RasGTP. By constructing and analyzing an in silico model, we show that signal integration enabled by this mechanism is indeed feasible for T cells in LN and leads to significant enhancement in T cell sensitivity for invading Ag. Note that we make no attempt to establish this as the only mechanism for signal integration, as other mechanisms likely exist to achieve similar functionality, and collectively enhance detection sensitivity of T cells in vivo.

For example, an alternative mechanism for signal integration has been suggested; namely that DCs may alter the presentation of pMHC ligands upon serial encounters with T cells (16). One possible molecular basis for such "modification" might be that after a transient T cell-DC encounter, the pMHC complexes become locally concentrated for a finite period of time. If a cognate T cell arrives and interacts with the locally concentrated pMHCs, the likelihood for a productive contact may increase. To explore this possibility and the differences between these two mechanisms that can potentially be tested experimentally, we adapted our model to carry out a computational study. The results showed that this DC-based mechanism requires the enhanced pMHC concentration to persist for a long time on a large number of cognate DCs. This seems unlikely under physiological conditions.

To explore the mechanistic questions we raised, we also tackled a daunting computational challenge that has not been addressed. Our studies require the development of a simulation method that combines T cell migration with molecular signaling, whenever a T cell-DC contact happens. The difficulty here is how to efficiently simulate the migration of individual cells on the time scale of minutes and hours, and length scale of microns, simultaneously with intracellular signaling events that operate on much smaller scale. We were able to enhance our previous lattice-based migration model to allow for off-lattice migration of the cells, while also performing fast molecular signaling simulations using a method called Stochastic Simulator Compiler (SSC) developed by Lis et al (17). Besides the unique advantage of combining dynamics of disparate time and length scales while maintaining computational feasibility, this computational platform is readily adaptable to study various other biological systems that require simulations of cell migration subject to signaling events due to cell-cell interactions.

3.2 Methods

Several published in silico studies have examined the migration and activation of naive T cells in LN in the past few years(8, 18-20). The rich motility data generated by microscopy experiments have also been subjected to sophisticated statistical analyses (21). As the LN is densely packed with large numbers of different cells, one of the challenges for in silico studies is how to capture the relevant biology while maintaining computational tractability. Beltman et al. constructed a computational framework based on the Cellular Potts Model (CPM), which was able to recapitulate many experimentally measured T cell motility data. They demonstrated that the motility changes exhibited by T cells, including velocity variations and stoppage, are not dictated by some internal program in T cells, but instead are dependent on the LN environment T cells are exposed to (18, 19). In a subsequent study, Beltman et al. also developed a method to estimate the true distribution of T cell - DC contact time given the experimental measurements, which are typically not comprehensive due to the very limited length of the imaging period (21). This methodology and the knowledge of true contact time distribution may become very

useful as signal duration has been identified to have a major impact on T cell activation. Bogle et al. developed an agent-based simulation framework, in which the space is discretized into a 3D lattice and packed with over 1 million cells. The high packing density in LN is faithfully mimicked while the computation remains efficient (20).

Rather than stressing quantitative recapitulation of known experimental facts regarding T cell motility, we aimed at obtaining qualitative mechanistic insight that may assist in the design and interpretation of analogous experimental studies. To determine whether phase one occurs and its duration, we previously developed a lattice-based representation of the space corresponding to the LN with periodic boundary conditions (i.e. the edges of the box such as the left and right or top and bottom are pasted together) in which T cells perform isotropic hopping between grid points. We also devised a simple and ad hoc, yet mechanistically motivated, scheme to allow T cell activation in a dose-responsive manner as they encounter DCs displaying Ag of different doses and types. This model allowed us to derive some mechanistic insights (2, 8).

We first extended this simulation method to use a continuous representation of the LN and avoided a lattice representation, as the former better reflects physical reality. Periodic boundary conditions were retained to permit the simulation of large spatial extent.

As shown in our earlier work, the explicit inclusion of non-cognate T cells does not alter the results qualitatively but drives up the computational cost drastically (8). Thus only Ag-specific T cells are explicitly considered here. T cells and DCs are randomly placed into the simulation box initially as spheres with different radii. The DCs remain stationary throughout the simulation while T cells perform random walk-like motion. As shown by intravital microscopy, T cells typically move in a directed fashion over distances of the order of 10μm over 1 min before changing direction randomly. To simulate such motion in free space, a random step size is drawn from a Gaussian distribution centered upon 10μm with a standard deviation of ~2.5μm (16). A sphere with this step size as radius and centered at the T cell can then be specified. A uniform random number is drawn to select a point on the surface of this sphere for the T cell's new center coordinates. Microscopy experiments have also shown that T cells can squeeze past each

other when they come into close contact, thus we define a minimal length of separation between the centers of two T cells, which is set to be 2μm. If a proposed move leads to a center-to-center distance smaller than this threshold value, the move is rejected. DCs, on the other hand, are characterized by multiple long dendrites that sweep the surrounding space and a highly non-spherical cell shape. However, if we consider the time average of an "effective scanning volume" around a DC swept out by these dendrites, a sphere with a radius approximately equal to the average dendrite length is an appropriate representation. This radius is set to be uniformly 15μm. Care is taken so that in the initial placement the DCs' "scanning volumes" do not overlap. Similar to the case of two T cells, the minimal separation of 2 DCs is set to be 7μm, and the minimal T cell – DC separation is 5μm. In subsequent steps, any proposed move for a T cell is rejected if the relevant separation constraints are violated. On the other hand, if the center of the T cell falls inside a DC's "scanning volume" without violating the exclusion constraint, then the T cell is considered to be "scanning" the DC. Very rarely would a T cell be inside the "scanning volume" of more than one DC. Should this happen, the interaction with only one DC (randomly chosen) is considered. The simulation period of 1440 elementary steps corresponds to a 24-hour residence period of T cells in the LN.

Before implementing explicitly a population of DCs, let's consider the main task at hand; namely, how to establish, with maximal computational efficiency, whether hysteresis in the T cell signaling network can enable signal integration. The hallmark event of such signal integration takes place when a recently stimulated T cell quickly upregulates RasGTP as it encounters a subsequent weak stimulus. In other words, we look for a "chain" of T cell – DC contacts with high RasGTP output, among which the first contact most likely happens on a DC bearing strong stimulus, while the subsequent ones occur on DCs presenting weak stimuli. Also, removal of SOS should prevent such events. Thus, there need to be at least two types of DCs: the strongly stimulating ones which can elicit a transient RasGTP rise in a T cell with basal RasGTP, and another group of DCs bearing significantly weaker stimulus (i.e. fewer and / or lower-affinity pMHCs), which may only trigger a high level of RasGTP if the T cell encountering it has a RasGTP level

above a threshold (i.e. the separatrix, see Figure 3.3.1). We will refer to the two types of DCs as S-DCs (strong) and W-DCs (weak), respectively. Note that the strength of stimulus on a particular DC is dictated by 2 factors: the binding characteristics (K_d) between TCR and pMHC, and the concentration of pMHCs. In this work the "strong" and "weak" DCs are differentiated based on the off-rate of their pMHCs with respect to TCR. Specifically, the two types of DCs bear pMHCs of the same k_{on} for the TCR, but with k_{off} values differing 10^4-fold. Note, however, that generalizing this to concentration differences is straightforward. Moreover, effects due to concentration differences and k_{off} differences can be related (8).

During phase one T cells typically interact with each DC for just a few minutes. Thus, when a T cell comes into contact with a DC, it "scans" the DC for 3min for Ag, and the relevant stochastic molecular signaling network is simulated using a fast implementation of the Gillespie algorithm recently developed by Lis et al (17). This new method also allows rule-based specification of signaling in spatially inhomogeneous environments. This simulation method adapted to our problem takes as input the number and binding affinity of pMHC molecules on this particular DC being scanned, as well as the number of any residual RasGTP that may have remained from a previous productive encounter with a DC. The output is the number of RasGTPs after the "scanning time". If a T cell has not previously contacted any DC, or if previously activated RasGTPs have been dephosphorylated almost entirely, then a basal number of RasGTP is used. Other details of the signaling network can be found in Das et al (12). If the RasGTP output exceeds a high threshold, a productive encounter is recorded. To implement the duration requirement for a "sustained high RasGTP", the criterion for stopping a T cell for full activation is set to be n consecutive productive encounters with DCs within a time window ΔT. If a T cells has accrued n productive encounters within ΔT, it is considered to have met the stopping requirements and will transition into phase two-type behavior and no longer migrates. Otherwise, the T cell disengages from the DC and continues to migrate until the next encounter. In between two consecutive encounters with DCs, the RasGTP that may have formed in the first encounter decays in an exponential manner with a characteristic time scale of 10 min until it reaches the basal level. The remaining

RasGTP at the time of the next encounter serves as an input to the signaling network simulation. While the lack of experimental measurements prevents us from specifying the values of n and ΔT, we have varied these numbers and observed no qualitative changes in our conclusions.

The results shown here are produced by simulating 500 T cells, 3000-7000 DCs with various S-DC versus W-DC ratios. The size of the simulation box is 300μm×300μm×300μm, thus the maximum cell-occupied volume is under 50% of the total simulation box. Each set of conditions is simulated 60 times to obtain the statistics shown in the Results section.

3.3 Results

Hysteresis due to positive feedback regulation allows weak stimuli to activate high level of RasGTP production in T cells following a single productive encounter with a cognate DC. .

As discussed previously, the hallmark event of the signal integration scheme under investigation is the fast upregulation of RasGTP in T cells upon encountering a DC presenting weak stimulus. We denote this type of event as W_H, i.e. an interaction with a W-DC that yields a high RasGTP level after "scanning". The presence or absence of such events would provide a measure for whether signal integration happens and its relative importance. On the other hand, the nature of the separatrix predicates that unless a T cell has recently been stimulated strongly and still holds enough residual RasGTP (i.e. above separatrix), the chances for a fast rise in RasGTP upon encountering a W-DC is negligible. Our simulation results confirmed this expectation.

In a series of simulations, we maintained a fixed number of weakly stimulating pMHCs on the W-DCs, while the number of strongly-stimulating pMHCs on the S- DCs is varied from low to high. The number of weakly binding pMHCs per W-DC is chosen such that the RasGTP outcome bifurcates depending on whether the T cell arrives at the W-DC with RasGTP level above the separatrix or not. The frequencies of different types of events were counted (see **Table I** for complete listing). Experimentally, the RasGTP hysteresis disappears in the SOS-/- mutants (12). Therefore we also performed simulations with an

identical signaling network with zero SOS molecules to mimic the SOS-/- mutants. In the simplest case, we considered the activation criteria that a T cell needs to acquire two consecutive high RasGTP-inducing contacts within a window of 25 min, i.e. $n = 2$, $\Delta T = 25$. If n > 2, the results are qualitatively similar.

Figure 3.3.2 shows the fraction of W_H-type events among all T cell – DC encounters as the pMHC loadings on the S-DCs are varied. The ratios between W- and S-DCs (N_W/N_S), and the total population of DCs (N_{tot}) were varied to obtain the different curves shown in Figure 3.3.2. In T cells capable of feedback regulation (containing SOS), above some threshold pMHC loading, the fraction of W_H-type events becomes positive. As the pMHC loading increases further, this fraction decreases sharply by a small amount and reaches a plateau value. On the other hand, in SOS-/- T cells, the number of W_H-type events is zero regardless of pMHC loading on S-DCs. Loss of Ras-SOS-dependent hysteresis abrogates the T cells' ability to integrate signals, as expected.

There are some interesting features in the shape of the graphs for W_H. For example, the common threshold pMHC loading defining the onset of conditions that enable signal integration for all variations in DC population and composition, as well as the plateau value of W_H. How may one rationalize the shape of these curves? Let's first consider how may a W_H-type event occur, and then analyze how the pMHC loading on S-DCs affects these processes.

First of all, a W_H-type event requires a T cell to have been strongly stimulated in the recent past. This requires a recent encounter with an S-DC bearing a sufficient number of high-affinity pMHC, because W-DCs are not able to stimulate naïve T cells with basal RasGTP levels. The probability of this happening is either close to 1 or nearly 0, depending on whether the pMHC loading on S-DC is above or below a threshold, which is entirely dictated by TCR-pMHC binding characteristics. Therefore, so long as the TCR-pMHC binding characteristics stay constant, the location of this threshold remains unchanged, as seen in Figure 3.3.2. Below this threshold, the S-DCs are not sufficiently stimulatory and W_H-event cannot occur, hence its absence for stimulus levels below the threshold. At the threshold pMHC concentration, this fraction reaches its peak, i.e. signaling integration's enhancing effect is the most prominent. Above this pMHC loading

on S-DCs, due to increasing pMHC loading on S-DCs, their ability to activate T cells quickly reaches 100%. Thus, more S-DCs lead to high RasGTP levels, making the relative contribution of W-DCs to the total number of productive encounters smaller. Thus the fraction of W_H-type events decreases slightly.

Figure 3.3.2 shows that when the number of high affinity-pMHCs on S-DC is high (i.e. high stimulus levels), W_H reaches different plateau heights depending on the composition of the DC population. The plateau heights can be calculated using a set of probabilistic arguments. After a productive encounter with an S-DC, a T cell departs with a high level of RasGTP and soon arrives at a second DC. Several outcomes are possible depending on whether this T cell subsequently reaches an S- or W-DC, and whether its active RasGTP level has decayed to a level below the separatrix value, denoted as R^* in Table I. These scenarios can be explained as the interplay of competing time-scales. Thus, before we calculate the probability for each possible scenario, we need to first identify some important time scales.

The total number of DCs loaded into the simulation box determines the average time it takes for a T cell to migrate from one DC to the next. This average time between 2 consecutive T cell – DC encounters is denoted as τ_e^T. It scales with the motility coefficient of T cells, D, and the density of all DCs, ρ, as $\tau_e^T \sim \frac{1}{\rho^{2/3} D}$. At the parameters used in our simulation, this time ranges from 4 to 6min, depending on the number of DCs (i.e. ρ) in the simulation box. The statistics gathered from simulations are consistent with this estimate. Another important time-scale is the characteristic time for RasGTP decay, which we will be denoted as $\tau^T{}_d$. As Das et al. have shown, the ability to integrate signal conferred by the Ras-SOS feedback loop lasts for at least 10 min.

Since the arrival at a DC and the decay of RasGTP during migration are two independent processes, their probabilities are independent. In our simulations, the T cells perform isotropic random walks while the DCs are randomly placed according to a uniform distribution. Thus, the probability that the next encounter happens on a W- DC as opposed to an S-DC, denoted as f, is simply the fraction of W-type DCs, $\frac{N_W}{N_W + N_S}$, where

N_W and N_S denote the number of W- and S-DCs, respectively. On the other hand, since the migration of T cells and the dephosphorylation of RasGTP to RasGDP are both first order events, the probability that the former event occurs before the latter is simply $\frac{\tau_e^T}{\tau_e^T + \tau_d^T}$, which we denote as x. Using x and f, we can calculate the probability of each possible type of event (**Table I**). The frequency of W_H events is the product fx. Given the DC population makeup, f can be calculated. The average time between two consecutive T cell – DC encounters can be estimated from either the DC densities or from encounter time statistics gathered from the simulations (4~6min, as mentioned above). **Table II** lists the percent discrepancy between the predicted probability of occurrence of W_H-type events (related to the plateau value in Figure 3.3.2), using this argument and the simulation results. There is overall a good agreement between them.

Code	DC type	Residual RasGTP	RasGTP output	Probability
W/L/L	W	$< R^*$	Low	$f(1\text{-}x)$
W/L/H	W	$< R^*$	High	0
W/H/L	W	$> R^*$	Low	0
W/H/H	W	$> R^*$	High	fx
S/L/L	S	$< R^*$	Low	0
S/L/H	S	$< R^*$	High	$(1\text{-}f)(1\text{-}x)$
S/H/L	S	$> R^*$	Low	0
S/H/H	S	$> R^*$	High	$(1\text{-}f)x$

Table I: In the $n = 2$ case, all possible scenarios for T cell – DC encounters subsequent to a productive T cell – S-DC encounter are listed here, followed by their probability. W and S stand for the "Weak" and "Strong" DCs. The first letter denotes either weak (W) or strong (S) pMHC stimulus presented by the DC in contact. The second letter stands for high (H) or low (L) residual RasGTP upon T cell arrival. More specifically, "high" and "low" are distinguished by whether the RasGTP level remains above the separatrix or has decayed below it. The third letter stands for high (H) or low (L) RasGTP output from the current encounter after "scanning". Here, "high" and "low" refer to the upper and lower steady states (see Figure 3.3.1 in main text for more details).

DC population makeup N_w/N_s	% error
1500 / 1500	4%

3500 / 1500	4%
2500 / 2500	0
1500 / 3500	-2%
3500 / 3500	6%
2100 / 4900	3%
6300 / 700	5%

Table II: The frequency of W_H events in T cell – DC encounter subsequent to a first productive encounter using the probabilistic arguments described in the text, and directly estimated from simulation results. Total DC number ranged from 3000 to 7000, and percentage of "W"-DC from 30% to 90%. The % deviation of the probabilistic calculation from simulation results are denoted as % error.

To summarize, hysteresis resulting from the Ras-SOS feedback regulation does indeed confer T cells the ability to integrate signals from sequential encounters with DCs. The degree to which such signal integration enhances the activation of T cells is dependent on the TCR-pMHC binding characteristics and the composition of the DC population. At the threshold level of pMHC stimulus, the enhancement in T cell activation due to signal integration is the highest. Under physiological conditions, the pMHC stimulation during the onset of a disease may be near such threshold levels. Therefore, signal integration may play an important role in improving the detection sensitivity of T cells.

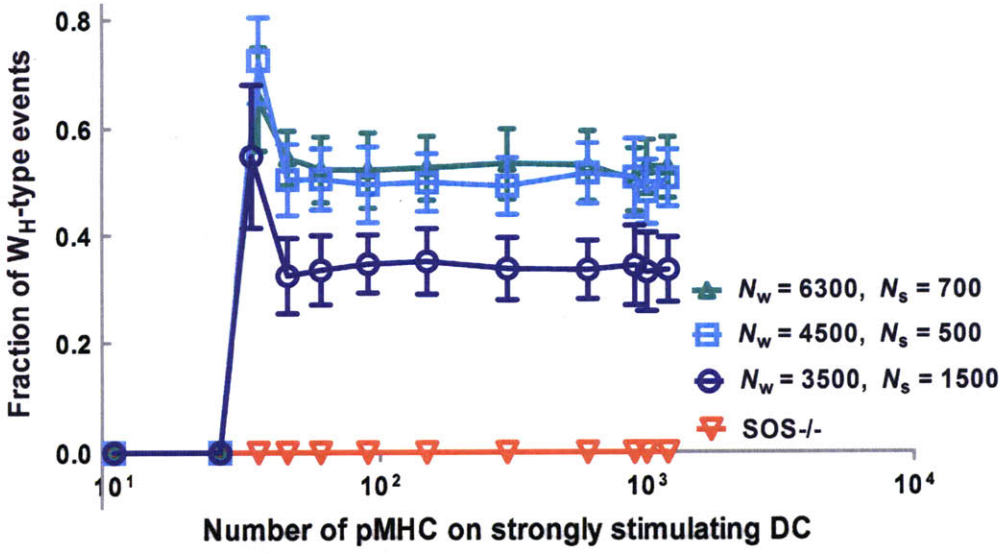

Figure 3.3.2: Fraction of W_H-type events among all productive encounters subsequent to a "chain initiating" S/L/H event (see Table I). Simulations were carried out with 3 different DC population compositions with total DCs numbering 5000 or 7000, and with either 90% or 30% of all DCs bearing high k_{off} pMHCs ("W"-DC). SOS-/- T cells are simulated with 4500 "W"-DCs and 1500 S-DCs.

Signal integration is unnecessary when there are abundant and potent pMHC stimuli.

In Figure 3.3, the fraction of T cells arrested given different numbers of "W" and S- DCs is plotted against the number of pMHCs on S-DC on a log scale. To see how the composition of the DC population affects the activation of T cells, the total number of DCs and the ratio between "W"- and S-DCs, N_W/N_S are varied.

First, a common feature among them is that when the pMHC loading on S-DCs becomes very large, SOS-/- T cells can compensate for their inability to integrate signals to varying degrees and achieve variable sizes of activated T cell population. The degree of such improvement is dependent on the DC population. If the total number of DCs is increased from 5000 to 7000 while keeping N_W/N_S constant at 9:1 (i.e. $x = 0.9$), then the plateau rises as f reduces. On the other hand, if N_W/N_S is reduced from 9 to 1, due to the greatly increased presence of S-DCs, x decreases from 0.9 to 0.5, the fraction of T cell arrested also increases. In fact, with a high enough loading of S-DC, there is no longer any difference between WT and SOS-/- T cells in their abilities to activate T cells. Thus, the contribution to T cell arrest from signal integration decreases as the relative abundance and potency of S-DCs increases. In experiments where large numbers of potently loaded DCs are used to present Ag to the T cells, f is nearly zero, since $N_W << N_S$. Consequently, signal integration does not play a significant role. Our results (Figure 3.3) may explain why in some experiments, phase one-type behaviors were not observed (7). Note that this is not expected to represent physiological conditions during the onset of a real infection. In those cases, cognate and potent DCs are relatively scarce.

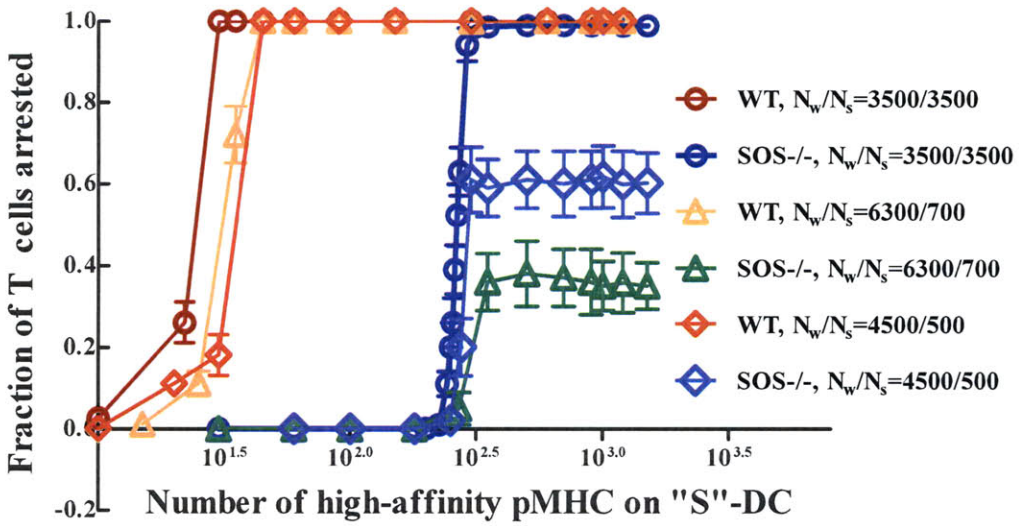

Figure 3.3: Fraction of T cells arrested after the total simulation time has elapsed in WT T cells capable of Ras-SOS digital signalings and SOS-/- T cells. Two values of the total number of DCs and 2 values for the ratio of N_w/N_s are comapred. The 3 different sets of DC compositions are i) N_{tot} = 7000, N_w/N_s= 3500/3500=1; ii) N_{tot} = 7000, N_w/N_s=6300/700=9; iii) N_{tot} = 5000, N_w/N_s= 4500/500=9.

DC-mediated signal integration exhibits distinctly different dependence on DC numbers and other system parameters.

The ability to integrate signals may not only reside on the T cells. In fact, certain characteristics of DCs also affect the duration and quality of a cognate DC-T cell engagement. Experimentally, it has been shown that the maturation state of DCs may dictate whether DCs can form stable and long-lasting conjugation with T cells (16, 22). The authors suggested that maturation allows for surface modifications that enhance adhesion of mature DCs to T cells, and that such a stabilizing effect is Ag-independent. While no molecular mechanism was proposed for these results, they do prompt us to consider an alternative signal integration mechanism due to modification to DC surfaces. Additionally, it provides an opportunity to demonstrate that the computational platform we have constructed is indeed versatile enough to be readily adapted to study diverse situations.

Specifically, we consider the following scenario. As a T cell leaves the surface of a cognate DC after a brief contact, there may be a locally enhanced concentration of pMHCs, as pMHCs may have gathered in the contact zone. Such locally enhanced pMHC presentation may persist for some finite time. Meanwhile, if another T cell interacts with this DC before such locally enhanced pMHC presentation fully dissolves. The likelihood of a productive interaction may increase. Our in silico model can easily be adapted to examine such "DC-mediated signal integration", and compare it with the previously described T cell-mediated scheme to suggest ways to differentiate between the two schemes.

To simulate this situation, first the "T cell signal integration" is turned off by using a population of SOS-/- T cells. Most other parameters, procedures and activation criterion remain the same, and all DCs present a default baseline pMHC concentration. Then as encounters with T cells happen, the pMHC concentration on DCs undergo changes as follows:

1) If the DC interacts with a T cell at the baseline pMHC concentration, denoted as $[\text{pMHC}]_0$, after the T cell disengages, its pMHC concentration is increased by some fraction f_+, i.e. $[\text{pMHC}]=(1+f_+)[\text{pMHC}]_0$ to represent a "clustering" effect.
2) As time progresses in the simulation, this "enhancement" in pMHC presentation decays exponentially with some time scale, τ_d^{DC} (different from the decay time scale, τ_d^T, in the "T cell signal integration" case).
3) If a DC encounters another T cell while its [pMHC] is elevated, we simulate the T cell signaling network with [pMHC] at the time of encounter. And if the T cell leaves, this DC's [pMHC] returns to the fully enhanced level, i.e. $(1+f_+)[\text{pMHC}]_0$. This is based on the consideration that during a T cell-DC conjugation, pMHC molecules may migrate towards the contact zone, and thus become further concentrated.
4) Should a DC simultaneously engage several T cells, one may expect some competition for pMHC among different contact zones. As the total number of pMHC is conserved, these T-DC contact zones may not all experience equally elevated pMHC concentration at the same time. To simplify the simulation, we do

not currently consider such conservation of total pMHC. This approximation provides an upper bound for the increased activation propensity due to enhanced pMHC presentation, as in reality, some T cell interacting with a single DC may not benefit from enhanced pMHC presentation.

Due to the speculative nature of this scheme for signal integration, relevant parameters also need to be postulated. However, by performing a time scale analysis similar to what was done for the "T cell signal integration", we can examine the functional dependence of simulation results on these parameters. Then some simulation results using parameters informed by time scale analysis will be discussed.

The activation criterion stipulates that an encounter leading to RasGTP signal above some threshold is productive, and that a T cell must receive 2 such successive productive encounters to become arrested within a time window, ΔT. As discussed earlier, the time between 2 consecutive contacts with DCs by a certain T cell has an exponential distribution, with an average value denoted as $\tau^{\mathrm{T}}_{\mathrm{e}}$. A superscript of "T" is used to differentiate from an analogous quantity defined for DCs. The probability that a T cell arrives at a DC before ΔT elapses is the cumulative probability $1-\exp(-\Delta T/\tau_e^T)$.

Switching to the DC side, what's the probability that when this encounter happens, there remains sufficient pMHC enhancement to facilitate a productive conjugation? Encounters with such DC likely will be productive only if the enhanced concentration has not decayed below some threshold. Suppose this duration of "effective enhancement" is T_m. Then for a T cell to benefit from such enhancement, it must arrive at the DC within T_m time steps after the previous T cell's departure. What is the time for a second T cell to arrive at a DC after the previous one has left? Similar to the characteristic time for a T cell to reach a DC, $\tau^{\mathrm{T}}_{\mathrm{e}}$, this is also an exponential random variable. Denote this time as τ_e^{DC}. Its value is related to the density of T cells, ρ_{T}, as $\tau_e^{DC} \sim \frac{1}{\rho_T^{2/3} D}$. Since exp(-3)= 5% (i.e. 95% loss), within $2\sim3\,\tau_d^{DC}$, this enhancement will dissipate entirely. Thus T_m can be maximally $1\sim2\ \tau_e^{DC}$. At the time of T cell – DC encounter, if we know whether this DC has waited

more than T_m since the last visit of a T cell, then the probability calculation is complete. The time that its last encounter was no more than T_m ago is simply $1-e^{-T_m/\tau_e^{DC}}$.

Taking advantage of the fact that the encounters between different T cells and DCs are largely independent, the overall probability for a T cell to encounter a DC while they are both able to potentially produce a productive contact is $(1-e^{-\Delta T/\tau_e^T})(1-e^{-T_m/\tau_e^{DC}})$.

This expression can be simplified further. First consider the case that $\tau_e^{DC} >> T_m$, or $\frac{T_m}{\tau_e^{DC}} << 1$. Under physiological conditions, this may be true as the number of naïve T cells of a particular specificity is very small, thus ρ_T is small. As a consequence, τ_e^{DC} is large. For a DC to consecutively encounter 2 cognate T cells, the time interval will be very long. Then via series expansion and retaining the first term, $1-e^{-T_m/\tau_e^{DC}} \approx \frac{T_m}{\tau_e^{DC}}$. Thus this probability scales as $P \sim \frac{T_m(1-e^{-\Delta T/\tau_e^T})}{\tau_e^{DC}}$. Note that since $1-e^{\Delta T/\tau_e^T} < 1$, and $\frac{T_m}{\tau_e^{DC}} << 1$, this probability is typically low. Simulation results corroborated this point, as shown by a comparison in Figure 3.4a. If the enhancement factor, f_+, is 1 (pMHCs are twice as concentrated after encountering with a T cell), and if the time scale of decay. As τ_d^{DC} = 20min (comparable to ΔT, moderate rate of decay), there is no visible enhancement in T cell arrest due to the presence of such DC-mediated signal integration. With a higher enhancement factor, $f_+ = 3$, the improvement is still moderate (Figure 3.4b).

Alternatively, if $\frac{T_m}{\tau_e^{DC}} \gg 1$, then $P \sim (1-e^{\Delta T/\tau_e^T})$. As discussed previously, $\Delta T/\tau_e^T$ is of order 1 or larger, which implies that the probability P is close to 1. In other words, if the enhancement of pMHC presentation on DC persists for long time (much longer than the time for 2 T cells to hit the same DC, or $\frac{T_m}{\tau_e^{DC}} \gg 1$), then such DC-mediated signal integration can lead to significantly greater likelihood for productive encounter with T cells. Hugues et al. and Benvenuti et al. showed that the period when matured DCs are able to engagement T cells with improved stability is on the order of 10 hours (16, 22).

Though the mechanism considered here is different, it also requires a modification to DC surface that persists for a very long time to be effective. This is shown in Figure 3.4b. Increasing the decay time scale, τ_d^{DC}, by a factor of 2 from 20min to 40min, the threshold dose of pMHC required to arrest T cells drastically is reduced by a factor of about 1.9, consistent with the linear dependence of T_m.

Next we will use this probability expression to see how the DC loading may influence DC-mediated and T cell-mediated signal integration in different ways. Recall that in the T cell-mediated case scenario discussed above, the probability of a second productive encounter due to signal integration is $1 - f + fx$ (see Table I for full details), or $1-\frac{N_S}{N_S+N_W}\frac{1}{1+\tau_d^T/\tau_e^T}$. Increasing the number of DCs leads to a smaller τ^T_e. The second term is small, thus the probability is close to 1. In other words, if T cells encounter DCs more frequently, a larger fraction of the productive encounters that took place were results of signal integration via T cell-mediated signal integration. As seen in Figure 3.3, with progressively higher DC density and S-DC fraction, the threshold concentration of pMHC required for T cells to be arrested reduces. However reducing τ^T_e does not lead to the same improvement in DC-mediated signal integration. For example, if τ^T_e is reduced by a factor of 2, then the improvement in activation probability is only $\frac{(1-e^{-25/3})}{(1-e^{-25/6})}-1\approx 0.016$. Simulation results concur with this estimate. We increased the number of DCs by a factor of 2.8 to reduce τ^T_e by a factor of 2, the improvement is very small (Figure 3.4a). Finally, note that in order to isolate the effect of enhanced pMHC presentation of DC, the Ras-SOS feedback loop was disabled in the T cells simulated. These simulated SOS-/- T cells are less sensitive to pMHC stimulation than WT T cells, which is partially the reason that the threshold pMHC dose to trigger T-cell-mediated signal integration is orders of magnitude lower than the DC-mediated case (Figure 3.4b).

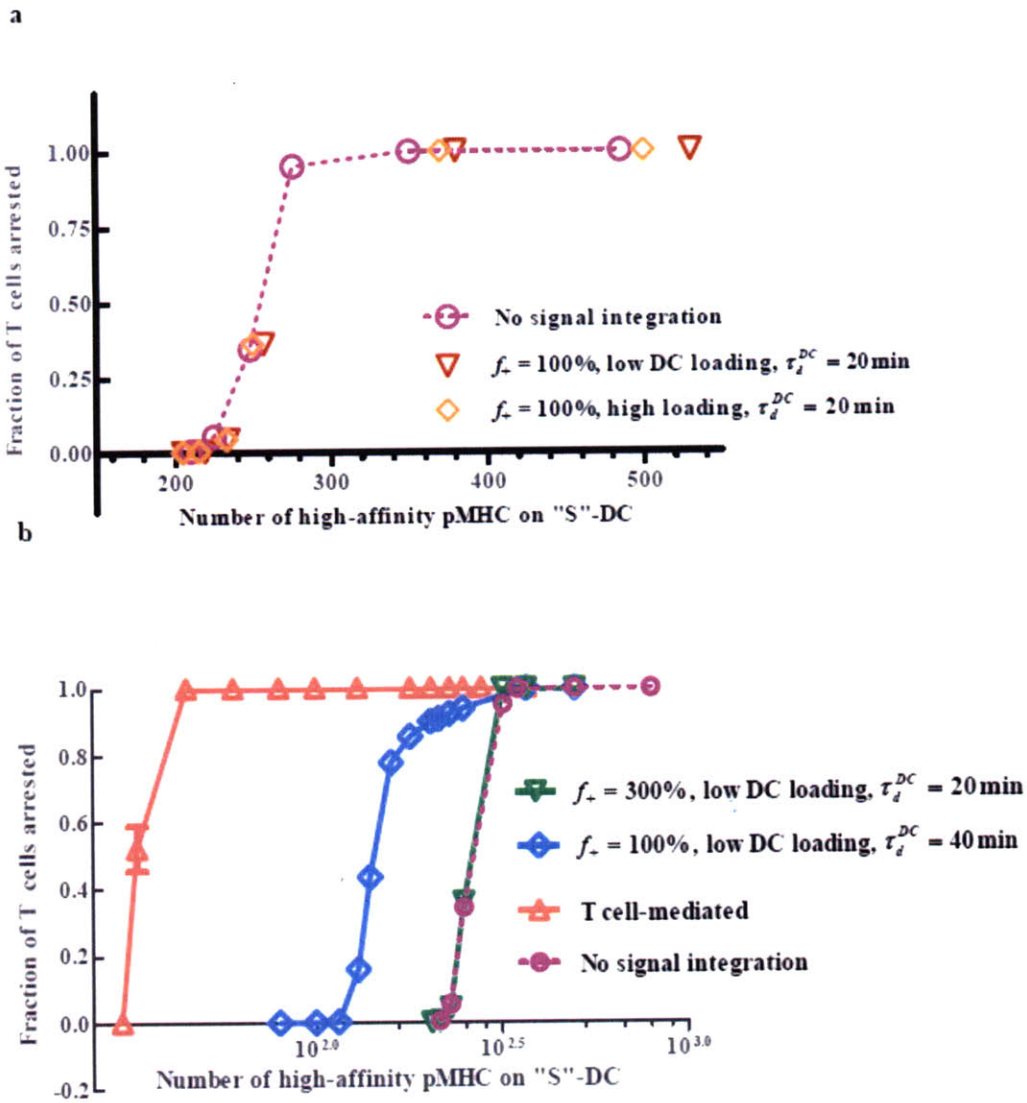

Figure 3.4: The effect of DC-mediated signal integration. 500 T cells and 500 S-DCs are placed in a simulation space 135mm×135mm×135mm in size. The degree of pMHC "clustering" is represented as the increase in [pMHC], or f_+. The time scale over which such enhanced [pMHC] persists is either 20min or 40min. Figure 3.4.a and b both contain the case without either T cell-mediated or DC-mediated signal integration (purple circles). Results with T cell-mediated signal integration while holding all other parameters the same are shown in b (red triangles).

3.4 Discussion

T cells are known for their remarkable sensitivity in detecting invading Ag in secondary lymphoid tissues, even during disease onset when only a few cells among hundreds of millions of DCs are presenting Ag, and the Ag-presenting pMHC per DC may also be relatively low (23). In recent years, intravital microscopy techniques have provided an

effective means to help understand the initiation of T cell activation in vivo. Among the first discoveries is that the T cells exhibit a type of motility behavior characterized by random walk-like motion upon entering the LN, and transient engagement with either cognate or non-cognate DCs along the way (1, 14). In the presence of Ag, some T cells stop on the surface of cognate DCs for stable conjugations that last for hours (1-5, 7, 14-16, 24-27). In our previous work, we showed that whether and when the T cells transition from phase one to phase two depends on the quality and quantity of Ag in the environment (2, 8). Observations from experiments also suggested that the T cells may integrate sequential sub-optimal signals derived from transient interrupted encounters with DCs to achieve activation, in the absence of DCs bearing potently high concentrations of pMHCs (28). Such enhancement in detection sensitivity was further corroborated by our simulations (2, 8). However, the molecular origin of this ability to integrate signals from multiple interrupted encounters was unclear.

A recent finding suggests that the TCR membrane proximal signaling network exhibits hysteresis due to positive feedback regulation of Ras activation by SOS. This is a plausible mechanism for signal integration. In order to explore whether hysteresis in the membrane proximal signaling network can lead to signal integration, we carried out a computational study. Carrying out this study required the development of a computational algorithm that could simultaneously simulate T cell migration and stochastic intracellular signaling. We have developed such a hybrid computational method. The migration of T cells is simulated in continuous space by a Monte-Carlo algorithm, and every time a T cell encounters an APC, a stochastic Gillespie simulation of the signaling network is carried out on the fly (12, 13). Our method is very general, and can be applied to a variety of different biological systems where both cell migration and signaling occur simultaneously. Our computational framework decouples the implementation of migration and cell contact from intracellular molecular signaling networks. Therefore, one could implement an alternative signaling scheme without having to alter the migration simulation.

Our results enable us to assess the feasibility of our signal integration hypothesis. The results suggest that hysteresis due to positive feedback regulation can indeed provide a

mechanism for a "short term molecular memory" in vivo. The contribution to the total number of productive T cell – DC encounters due to signal integration is particularly prominent when the number of potently stimulatory DCs is low. Loss of SOS abrogates the ability to integrate signals via this mechanism.

Conceptually, experimental verification of these results can be straightforward, should it be possible to experimentally monitor the level of RasGTP or other related signaling products in real time as T cells migrate. First of all, many model antigens have altered peptide ligands (APLs) with greatly different affinities for the same TCR. Thus the S- and W-DCs in our model can be implemented experimentally. By titrating the pMHC loading per DC and the total loading of cognate DCs into the LN, then tracking signaling dynamics paralleled with T cell migration, signal integration and its dependence on various parameters can be studied. Finally, similar experiments with SOS-/- T cells can serve to examine its role in enabling signal integration. SOS-/- T cells should lose the ability to integrate signal unless a much higher pMHC dosage is used. The primary barrier to carrying out such experiments is to simultaneously image migrating T cells and signaling molecules within them. A recently developed mouse model that enables imaging of calcium signals while carrying out intravital microscopy experiments seems promising in this regard (8).

We also explored the possibility of DC-mediated signal integration, based on the speculation that transient contact with T cells may alter the pMHC presentation on DCs in ways that favor T cell activation. The computational platform we have constructed was readily converted to address this problem. We found that in reasonable parameter ranges, the probability of such DC-mediated signal integration is low, and its contribution to T cell activation is minimal. The bottleneck lies in the requirement for large number of cognate T cells, which is not likely under normal physiological conditions.

References

1. Mempel, T. R., S. E. Henrickson, and U. H. von Andrian. 2004. T-cell priming by dendritic cells in lymph nodes occurs in three distinct phases. *Nature* 427:154-159.
2. Henrickson, S. E., T. R. Mempel, I. B. Mazo, B. Liu, M. N. Artyomov, H. Zheng, A. Peixoto, M. P. Flynn, B. Senman, T. Junt, H. C. Wong, A. K. Chakraborty, and U. H. von Andrian. 2008. T cell sensing of antigen dose governs interactive behavior with dendritic cells and sets a threshold for T cell activation. *Nat. Immunol* 9:282-291.
3. Wei, S. H., O. Safrina, Y. Yu, K. R. Garrod, M. D. Cahalan, and I. Parker. 2007. Ca2+ signals in CD4+ T cells during early contacts with antigen-bearing dendritic cells in lymph node. *Journal of Immunology* 179:1586-1594.
4. Miller, M. J., O. Safrina, I. Parker, and M. D. Cahalan. 2004. Imaging the single cell dynamics of CD4(+) T cell activation by dendritic cells in lymph nodes. *Journal of Experimental Medicine* 200:847-856.
5. Zinselmeyer, B. H., J. Dempster, A. M. Gurney, D. Wokosin, M. Miller, H. Ho, O. R. Millington, K. M. Smith, C. M. Rush, I. Parker, M. Cahalan, J. M. Brewer, and P. Garside. 2005. In situ characterization of CD4+ T cell behavior in mucosal and systemic lymphoid tissues during the induction of oral priming and tolerance. *J. Exp. Med.* 201:1815-1823.
6. Celli, S., Z. Garcia, and P. Bousso. 2005. CD4 T cells integrate signals delivered during successive DC encounters in vivo. *Journal of Experimental Medicine* 202:1271-1278.
7. Shakhar, G., R. L. Lindquist, D. Skokos, D. Dudziak, J. H. Huang, M. C. Nussenzweig, and M. L. Dustin. 2005. Stable T cell-dendritic cell interactions precede the development of both tolerance and immunity in vivo. *Nat. Immunol.* 6:707-714.
8. Zheng, H., B. Jin, S. E. Henrickson, A. S. Perelson, U. H. von Andrian, and A. K. Chakraborty. 2008. How Antigen Quantity and Quality Determine T-Cell Decisions in Lymphoid Tissue *Mol. Cell. Biol.* 28:4040-4051.
9. Celli, S., F. Lemaître, and P. Bousso. 2007. Real-Time Manipulation of T Cell-Dendritic Cell Interactions In Vivo Reveals the Importance of Prolonged Contacts for CD4+ T Cell Activation. *Immunity* 27:625-634.
10. Henrickson, S. E., T. R. Mempel, I. B. Mazo, B. Liu, M. N. Artyomov, H. Zheng, A. Peixoto, M. P. Flynn, B. Senman, T. Junt, H. C. Wong, A. K. Chakraborty, and U. H. von Andrian. 2008. T cell sensing of antigen dose governs interactive behavior with dendritic cells and sets a threshold for T cell activation. *Nature Immunology* 9:282-291.
11. Davis, D. M. 2009. Mechanisms and functions for the duration of intercellular contacts made by lymphocytes. *Nat. Rev. Immunol.* 9:543-555.
12. Das, J., M. Ho, J. Zikherman, C. Govern, M. Yang, A. Weiss, A. K. Chakraborty, and J. P. Roose. 2009. Digital Signaling and Hysteresis Characterize Ras Activation in Lymphoid Cells. *Cell* 136:337-351.
13. Margarit, S. M., H. Sondermann, B. E. Hall, B. Nagar, A. Hoelz, M. Pirruccello, D. Bar-Sagi, and J. Kuriyan.
14. Miller, M. J., A. S. Hejazi, S. H. Wei, M. D. Cahalan, and I. Parker. 2004. T cell repertoire scanning is promoted by dynamic dendritic cell behavior and random T cell motility in the lymph node. *Proceedings of the National Academy of Sciences of the United States of America* 101:998-1003.

15. Bousso, P., and E. Robey. 2003. Dynamics of CD8(+) T cell priming by dendritic cells in intact lymph nodes. *Nature Immunology* 4:579-585.
16. Hugues, S., L. Fetler, L. Bonifaz, J. Helft, F. Amblard, and S. Amigorena. 2004. Distinct T cell dynamics in lymph nodes during the induction of tolerance and immunity. *Nature Immunology* 5:1235-1242.
17. Lis, M., M. N. Artyomov, S. Devadas, and A. K. Chakraborty. 2009. Efficient stochastic simulation of reaction-diffusion processes via direct compilation. *Bioinformatics* 25:2289-2291.
18. Beltman, J. B., A. F. M. Maree, and R. J. de Boer. 2007. Spatial modelling of brief and long interactions between T cells and dendritic cells. *Immunol. and Cell Bio.* 85:306-314.
19. Beltman, J. B., A. F. M. Maree, J. N. Lynch, M. J. Miller, and R. J. de Boer. 2007. Lymph node topology dictates T cell migration behavior. *J. Exp. Med.* 204:771-780.
20. Bogle, G., and P. R. Dunbar. 2009. Agent-based simulation of T-cell activation and proliferation within a lymph node. *Immunol. and Cell Bio.*
21. Beltman, J. B., S. E. Henrickson, U. H. von Andrian, R. J. de Boer, and A. F. M. Marée. 2009. Towards estimating the true duration of dendritic cell interactions with T cells. *J. Immunol. Methods* 347:54-69.
22. Benvenuti, F., C. Lagaudriere-Gesbert, I. Grandjean, C. Jancic, C. Hivroz, A. Trautmann, O. Lantz, and S. Amigorena. 2004. Dendritic Cell Maturation Controls Adhesion, Synapse Formation, and the Duration of the Interactions with Naive T Lymphocytes. *J Immunol* 172:292-301.
23. Purbhoo, M. A., D. J. Irvine, J. B. Huppa, and M. M. Davis. 2004. T cell killing does not require the formation of a stable mature immunological synapse. *Nat. Immunol.* 5:524-530.
24. Bousso, P., and E. A. Robey. 2004. Dynamic behavior of T cells and thymocytes in lymphoid organs as revealed by two-photon microscopy. *Immunity* 21:349-355.
25. Catron, D. M., A. A. Itano, K. A. Pape, D. L. Mueller, and M. K. Jenkins. 2004. Visualizing the first 50 Hr of the primary immune response to a soluble antigen. *Immunity* 21:341-347.
26. Skokos, D., G. Shakhar, R. Varma, J. C. Waite, T. O. Cameron, R. L. Lindquist, T. Schwickert, M. C. Nussenzweig, and M. L. Dustin. 2007. Peptide-MHC potency governs dynamic interactions between T cells and dendritic cells in lymph nodes. *Nat. Immunol.* 8:835-844.
27. Stoll, S., J. Delon, T. M. Brotz, and R. N. Germain. 2002. Dynamic imaging of T cell-dendritic cell interactions in lymph nodes. *Science* 296:1873-1876.
28. Zaru, R., T. O. Cameron, L. J. Stern, S. Muller, and S. Valitutti. 2002. Cutting Edge: TCR Engagement and Triggering in the Absence of Large-Scale Molecular Segregation at the T Cell-APC Contact Site. *J Immunol* 168:4287-4291.

Chapter 4

Summary and future steps

4.1 A summary of completed studies

The overarching theme of this thesis is to develop efficient computational models for studying the triggering of T cells *in vivo*. More specifically, the models were designed to capture pertinent key features of the corresponding physical reality while maintaining computational feasibility. All modeling efforts were in close synergy with experimental investigations. Specifically, I postulated mechanisms based on experimental observations, especially ones that are counter-intuitive. Then the mechanisms were implemented as computer programs and simulated to obtain numerical results. Different analytical tools including PDEs, ODEs, and Markovian probability were also employed to help derive mechanistic insights from simulation results. The results of these efforts finally fed back to the experimental investigations by 1) providing explanations for puzzling results; 2) suggesting new experiments for the testing of proposed mechanisms.

In Chapter 2, with experimental collaborators Sarah E. Henrickson and Uli von Andrian, I investigated how the quantity and quality of Ag in the LN may affect T cells' decision to stop migration and engage cognate DCs in stable conjugation. In the microscopy experiments by Henrickson et al., it was observed that class-I restricted P14 T cells first perform rapid diffusive motion and transiently engage DCs upon encountering them. After several hours of such phase one type behaviors, should the DCs bear appropriate type and amounts of Ag, the T cells will cease migration and engage a cognate DC for long periods of time, after which they become activated T cells and begin to proliferate (1). The controversy we wanted to address was whether the stopping of T cells was dictated by a predetermined developmental program internal to the T cells and independent of the LN milieu. We hypothesized that the decision to stop was a response to the Ag presence in LN, rather than an internal program. The testing of this hypothesis requires a model to track a large number of T cells individually as they migrate randomly in LN and interact with DCs. Upon an encounter, the model also needs to stochastically determine whether

the T cell would enter phase two-type behavior based on the type and the number of pMHC present on this particular DC. In short, the objectives posed a multi-scale challenge.

The solution was as follows. I developed a model of random walk on a cubic lattice to simulate the migration of T cells during phase one, with relevant migration parameters matched to those measured or estimated for the experimental analogue of Henrickson et al. A probability for T cell stopping upon encountering a cognate DC was drawn from a dose response curve, each time a T cell – DC encounter occurs. Drawing this propensity from a postulated dose-responsive curve of the correct qualitative shape allowed us to bypass simulating the T cell signaling network every time a T cell encounters a DC. A sensitivity analysis on the dose-response curve further showed that the simulation results do not vary qualitatively so long as the dose-response curve retains its shape (2).

Together with our experimental collaborators, we showed that whether and when a T cell may stop the random migration and perform stable conjugation with a DC depends on the dose and type of Ag being presented by these DCs. Our theoretical analysis further revealed a single parameter dictating the duration of phase one. Using this parameter, the results from varying a diverse set of parameters all fall onto one consolidated curve. With the help of this consolidated master curve, I was able to explain a previously puzzling experimental observation by Henrickson et al. Specifically, varying the number of cognate DCs in LN has a linear effect on the probability of T cell stoppage, whereas increasing the number of pMHCs initially loaded onto individual DCs improves this probability in a super-linear fashion. Therefore they are not interchangeable (1, 2).

Another puzzling observation from this set of experiments initiated the investigation covered in Chapter 3. As shown in Chapter 2 and corresponding publications, pMHC dissociates over time, resulting in a progressively lower dose of Ag stimulation. At the threshold dose of pMHC required to elicit a phase two-type behavior, T cells spent more time in phase one before the transition into phase two. This is counter-intuitive because prior to significant pMHC dissociation, the Ag stimulation was stronger and more favorable for activation. T cells should have stopped migration earlier rather than later. One possible explanation is that T cells are able to integrate sub-optimal signals derived

from several successive encounters with DCs. To test this hypothesis, a molecular mechanism to enable "signal integration" is required.

By taking advantage of a newly discovered, bi-stable signaling module in the TCR signaling network (3), I was able to formulate such a mechanism. In lymphocytes, the catalytic conversion of signaling molecule RasGDP to its active GTP form by SOS exhibits bi-stable behavior due to the positive feedback regulation in this process. Because of the associated hysteresis, a recently stimulated cell with residual active RasGTP can quickly return to a high RasGTP-state after a weak stimulation. This does not happen in T cells that have not recently been stimulated (3).

I postulated that T cells require several consecutive "productive" encounters (high RasGTP-producing) with DCs to fully stop. During the migration period between 2 consecutive encounters, the previously converted RasGTP gradually decays back into its GDP form. If a subsequent encounter with a DC occurs before RasGTP level has decayed beyond a critical level, a subsequent weak stimulus cannot trigger T cell (details see Chapter 3 and (3)). The computational model described in Chapter 2 was adapted to incorporate signaling and T cell migration simultaneously. A fast implementation of the TCR membrane-proximal signaling network was developed separately to simulate the reactions from TCR-pMHC engagement to RasGTP production. Then this simulation was integrated with a simulation of T cell migration in free space. The resulted *in silico* model encompasses dynamics that occur within microseconds inside a cell, as well as those which occur over many hours, at the cell population level. The full history for each cell could be recorded for analyses.

The results showed that the bi-stability inherent in the Ras-SOS feedback loop does enable T cell to integrate signals. With signal integration, T cells are arrested by cognate DCs at much lower doses of Ag stimulation than otherwise. Thus, signal integration may be physiologically important as it enhances the detection sensitivity for Ag. These results have motivated the design of new experiments.

Finally, besides being fast and robust, the computational framework can be easily adapted for other possible mechanisms of signal integration, or other problems in biological systems that require an understanding of the interplay between signaling and

cell migration. I included two such examples in Chapter 3. First, a DC-based signal integration scheme was investigated. It has been proposed that DCs may undergo surface modifications that render them more effective at stimulating T cells (4). In other words, the ability for "signal integration" may instead reside on the DCs. I modified the in silico model to test out such a possibility. I discussed the difference between the two alternatives and possible experimental tests. The other example is the infection of liver cells (hepatocytes) by the hepatitis C virus (HCV). Though the problems of T cell triggering and HCV infection may appear disparate, our computational framework was poised to address the multi-scale nature of the HCV problem.

4.2 The next step: T cell proliferation in vivo

Encouraged by the progress in studying T cell triggering, I became interested in the dynamics on greater scales. This entails a further expansion in the time- and length-scale one must consider. In this section I will first motivate the approach I selected for studying T cell proliferation *in vivo*. Then I will briefly discuss an experimental study based on which a well-defined question was formulated. These will prepare us for the discussion on the initial modeling efforts in section 4.3.

4.2.1 Motivation

As complex as it is, the arrest of a naïve T cell on the surface of a cognate DC only marks the beginning of a series of complex downstream activities, which not only lead to immediate immune defense actions targeting the ongoing infection, but also create an "immune memory" that persists for years to come.

Following TCR-pMHC engagement, a plethora of intracellular molecular reactions ensue within the T cell. Expression of new surface proteins and cytokines can begin within minutes. Activated T cells soon begin to proliferate over the next few hours, up to several days, greatly increasing the number of T cells of this particular clone. Some time during this proliferation phase, activated T cells update their surface adhesion properties and begin to gradually exit from secondary lymphoid organs. They travel via blood circulation and enter peripheral tissues, where they carry out effector functions. After the primary response, most of the activated T cells die during a contraction phase, while a

small fraction persists throughout the organism's lifetime to maintain an immune memory. This memory response is also often referred to as the secondary or recall response.

Many experimental studies have shown that the effectiveness in both the primary and the recall response are dependent on the binding of TCR to pMHC. This implies that the knowledge of TCR-pMHC binding characteristics is extremely important for the prediction of dynamics of both primary and secondary responses. Compared to their *in vivo* counterparts, *in vitro* studies of TCR-pMHC binding and their impact on the primary and recall functions are much easier to conduct, and have generated a far greater wealth of data. Thus the central question becomes how can we use these *in vitro* measurements to glean some insights on the *in vivo* dynamics, which are far more functionally relevant?

To translate *in vitro* measurement into *in vivo* predictions is no trivial task. Despite the great necessity for such knowledge and the tremendous efforts devoted to studying this question, the answers remain shrouded in mystery. The first step toward mapping the *in vitro* measurements to their counterparts *in vivo* is to identify the factors that cause the in vivo observations or measurements to differ from those in vitro, and find out how these factors operate in both cases.

A major drawback of *in vitro* setups is that they lack the plurality of interacting cells and biochemical messengers abundant in the *in vivo* environment. Furthermore, the immune system is cohesively regulated at the level of the entire organism. *In vitro* studies, on the other hand, cannot reproduce such aspects. Therefore these are the areas on which efforts should be focused.

One faces several hefty obstacles were one to investigate these areas using a modeling approach. Earlier we have seen how the mingling of different time- and length-scales may pose great challenge to any modeling effort. Here, consideration of the dynamics at the organism level entails treatment of even longer time- and length-scales. Secondly, we are still constrained by the lack of understanding at the molecular level, similar to the previous studies but to a more severe degree. Constructing an informative model from the limited knowledge available without adding too many hypothetical elements that dilute the model's biological relevance is great challenge.

To cope with these difficulties, a more realistic approach is to define a very specific question, which focuses on a small subset of the areas of *in vitro-in vivo* divergence mentioned above. One can then identify the most relevant subset of dynamical events at different levels, and reduce the number of different time-scales we need to simultaneously consider. This choice must be motivated by the available experimental data.

Experimentally, the main measurable quantities of the primary response include the proliferation kinetics and the size of peak T cell population. They are relatively straightforward to monitor both *in vitro* and *in vivo*, and have been shown to strongly correlate with TCR-pMHC binding affinity. We also need to ponder how to incorporate elements from the vast array of cell types and signaling molecules involved: enzymes, cytokines, receptors, etc. The choice will again be dictated by available experimental data. In the next section, I will describe an experimental study, in preparation for the discussion of a hypothesis and model built upon the data and observations from this study.

4.2.2 CD8+ T cell proliferation in vivo: some puzzling observations

In a recent study, Zehn et al. studied how TCR-pMHC binding affinity affects the primary and secondary functions of activated T cells *in vivo* (5). The T cells used were OT-I CD8+ T cells bearing transgenic TCRs that bind to ovalbumin (OVA) epitope with high affinity. Recombinant *Listeria monocytogenes* were engineered to express ovalbumin (OVA). To focus on the effect of different binding affinities, altered peptide ligands (APLs) of the wild type (WT) epitope N4 were derived by mutating one amino acid in the WT sequence. The APLs all form pMHC complexes with H-2K^b equally well but differ significantly in their ability to stimulate OT-I cells to produce IFN-γ *in vitro*.

For the in vivo experiments, 3000 OT-I cells were transferred into each mouse. This low number of adoptive transfer more closely mimics the physiological frequency of T cell precursors. After the adoptive transfer of these OT-I cells, the mice were infected with recombinant Listeria. The OVA epitopes are presented by a type of class-I-restricted MHC, H-2K^b. Though endogenous T cells in these mice also respond to OVA, within 4

days, OT-I T cells have outgrown the endogenous population by at least 30-fold, which implies that clonal competition from the endogenous T cells was insignificant. Zehn et al. found that despite significant difference in their avidity, pMHCs of different APLs stimulated comparable T cell division through the first 4 days. Afterward, the OT-I cells activated by higher-affinity APLs continue to proliferate for 2-3 days, reaching their peak expansion and began to contract. Meanwhile, OT-I cells stimulated with lower affinity-APLs reached peak expansion earlier at a lower peak population, and began to contract much earlier. On the other hand, their exit into the blood appeared earlier than those OT-I cells stimulated by higher-affinity APLs.

Various phenotype markers were also assayed in these experiments. During the initial 4 days when T cells stimulated by different APLs exhibited comparable proliferation, the T cell surface markers were also found to be comparable, with the only exceptions of CD25 and C-C chemokine receptor 7 (CCR7). CD25 is the α-subunit of the interleukin-2 (IL-2) receptor (IL-2R), while CCR7 is involved in T cell homeostasis. Their biology will be discussed in further details later on. In T cells activated by lower-affinity APLs, these two markers were also lower on day 4. Aided by microscopy data, the authors pointed out that this earlier down-regulation of CCR7 is consistent with the earlier egress of T cells from LN.

In addition to measuring the primary response, Zehn et al. also studied the secondary recall response by these T cells. This is beyond the scope of the question we are trying to define, thus its discussion is omitted here.

Finally, I'd like to comment on the CD4+ T cells in these mice experiments. Another important parameter in this study is the extent of CD4+ T cell response. As we discussed earlier, much of complexity *in vivo* is due to the interactions between different cell types. CD4+ T cells are known to "help" the CD8+ T cell response in several ways. Since only the class-I-restricted epitope was mutated, we can fairly safely assume that the class-II-restricted epitopes presented by Listeria remain un-altered. This implies that the CD4+ T cell response in mice infected with different APLs had comparable CD4+ T cell response. In other words, though CD8+ proliferated to different extents, they may have received comparable amount of "help" from CD4+ T cells.

4.2.3 A task defined

The study by Zehn et al. is a particularly good case study for modeling consideration, because many variables associated with an *in vivo* setting have been well controlled. These include the stable presentation of epitopes by *Listeria monocytogenes*, comparable binding affinity of APLs to MHC, and most importantly, a relatively uniform CD4+ T cell response. They recorded proliferation amount and surface marker expression over the entire course of primary proliferation, which are the type of data we seek. Finally, some counter-intuitive trends in their observations present a great opportunity to utilize modeling and simulation.

The modeling goal is to construct a mechanism for CD8+ T cell proliferation *in vivo*, which is capable of reproducing the following behaviors qualitatively: 1) a lower-affinity APL may induce CD8+ T cell proliferation comparable to that of a higher-affinity APL during the initial proliferation; 2) lower-affinity APL stimulated T cells exit LN slightly earlier; 3) the peak in proliferation occurs earlier for T cells stimulated with lower-affinity APLs and at a lower peak size. In addition, the model must account for CD4+ "help" at least in a coarse-grained manner. This model must be able to explain why CD8+ T cell response *in vivo* is a "dampened" version of what happens in vitro. If a model can achieve these goals, it can make predictions regarding the mechanisms underlying the phenomena described above and suggest additional experimental tests. Such iterations between experiments and model refinement can then help provide mechanistic underpinning to the puzzling observations.

4.3 How CD4+ T cells help CD8+ T cell response

In this section I will provide some necessary background information on the two main venues for CD4+ T cells to provide help to CD8+ T cells during primary response: licensing of immature DCs and secretion of interleukin-2 (IL-2).

4.3.1 The "licensing" of DCs for more effective Ag presentation

In order for either CD4+ or CD8+ T cells to detect the invasion by their cognate Ag, APCs must first process and present this Ag in the form of class-II or class-I MHC, respectively. Again, most often these APCs are DCs, which we will limit our attention to in the following

discussion. Immature DCs have low expression of MHC and costimulatory molecules such as CD40 and CD80. The capture of Ag-derived signal and interactions with CD4+ T cells may drive them through a maturation process, which enhances the expression of MHC and costimulatory molecules and readies DCs for T cell engagement. Detailed characterization of this process and of the different maturation states of DCs are subjects of intense research efforts. Some features of DC maturation are necessary for the model we're building, though caution must be taken to avoid introducing an excess of irrelevant complications.

Mechanism of DC maturation and CD4+ T cell help

Consolidating the findings of several pertinent experimental studies, it appears that Ag-derived signal may come in several different incarnations, including fragments of necrotic or apoptotic cells, toll-like receptor (TLR) ligands, and inflammatory cytokines (6). Exposure to one of them or a combination of several leads to the maturation of DCs. There is ongoing debate regarding how different maturation signals may lead to different DC maturation outcome. For example, some believe that inflammatory cytokine-driven maturation, in the absence of TLR, leads to a kind of "unlicensed maturation" which ultimately results in a tolerance response, rather than effector response (7). As far as our modeling task is concerned, it is sufficient to know that some pathogen-derived signal is needed to "prime" the DCs, and an important outcome of such priming is the up-regulation of MHC-II, which would enable DCs to more readily interact with CD4+ T cells. In other words, inflammation can help to enhance class-II pMHC presentation to CD4+ T cells.

These CD4+ T cells are then able to "license" DCs for better class-I MHC presentation. Specifically, researchers found that without CD4+ T cells, naïve CD8+ T cells do not develop into cytotoxic T lymphocytes (CTLs) when stimulated *in vitro* (8, 9). It was proposed that after interaction with mature DCs presenting cognate class-II MHC, CD4+ T cells upregulate CD40, which then bind to CD40 ligands (CD40L or CD154) on the DC surface, causing DCs to process MHC-I epitopes to be recognizable by CD8+ T cells (8, 9). An alternative explanation involving CD40-CD40L interactions stipulates that upregulated

CD40Ls on DC surface bind to the CD40 on CD8+ T cells to facilitate CD8+ T cell and DC conjugation, although this route has been shown to make a relatively small contribution (10-12). Given the present state of mechanistic understanding, we need to be extra cautious if a molecular signaling model was to be constructed. But from these limited experimental observations, it appears that the activation of CD4+ T cells precedes that of CD8+ T cells.

Functional consequence of CD4-help in vivo

Initially, it was largely believed that without the licensing of DCs by CD4+ T cells, only the long-term memory function suffers and the effector functions of CD8+ T cells are not affected. For example, Sun and Bevan showed that in a CD4+ T cell-deficient mouse, memory function is impaired, and the CD4+ help is provided in an Ag-independent manner (11). In other words, the CD8+ T cells are still able to proliferate vigorously and perform cytotoxic killing in the primary response.

Meanwhile, Shedlock and Shen, as well as Janssen et al. argued the exact opposite, namely, CD4-help is required for priming but not so much for maintenance of memory function (13, 14). More recently, Smith et al. found that in the case of HSV infection, CD4+ T cell help is required for primary cytotoxic functions (15). Moreover, the "help" is provided in an Ag-specific manner. Specifically, CD4+ and CD8+ T cells must engage the same cognate DC to become activated, because in chimeric mice whose DCs either express MHC-I or MHC-II but not both, the immune response to an HSV infection is poor.

The modeling implication here is that linking CD4-help to any specific functional outcome requires caution, because this relationship remains largely unclear and likely highly dependent on what type of Ag and TCRs are used for experiments. Before more definitive results emerge, model implementation should strive for high flexibility, so as to accommodate different licensing—function relationships.

Interchangeability between inflammation and CD4-licensing in DC maturation

There also appears to be a degree of redundancy between licensing delivered by helper (CD4+) T cells and licensing via inflammatory signals, especially during acute infections. Depending on the offending pathogen, the degree of inflammatory response may differ.

With severe inflammation (e.g. *Listeria monocytogenes* (11)) , which typically occurs *in vivo* during acute viral or bacterial infections, the need for CD4+ help may be bypassed (15, 16). Several other infectious agents, including ectromelia, vesicular stomatitis virus, human immunodeficiency virus, Epstein-Barr virus, influenza, and cytomegalovirus have been shown to bypass at least partially CD4 help (17-20). One possible mechanism, as investigated by Johnson et al. in a 2009 publication implicates these infectious agents' ability to directly induce CD40L expression on DC, thus stimulate helper-independent licensing of DCs (21).

Modeling implications

Presently no definitive conclusion can be made about how, under different infection conditions, DC licensing takes place and how it affects either primary or secondary immune response. However, the diverse opinions and findings reviewed here seem to agree that 1) some form of "help" is needed to activate DCs; 2) the degree of "licensing" has several levels, rather than a binary "on"-"off" switch; 3) there likely exist multiple mechanisms, and the relationship between them may be relatively fluid to ensure rapid and efficient Ag presentation and immune response. While our model must account for the DC licensing, we do not have comprehensive knowledge regarding this matter to opt for one detailed mechanism over another. We must develop a model with a high degree of flexibility that allows for 1) easy conversion between different mechanisms for "licensing"; 2) straightforward incorporation of new experimental findings.

4.3.2 IL-2 biology

Another important type of "help" provided by activated CD4+ T cells for CD8+ T cells is the secretion of IL-2. In this sub-section, I will review the current understanding on the production, consumption and functions of both IL-2 and IL-2 receptors (IL-2R).

First isolated in early 1980s, IL-2 is the first interleukin to be discovered (22). It is a 15,000-kDa, α-helical single protein with variable glycosylation. It has been implicated in almost all stages of adaptive immune response. In the sub-sections below, I will review the secretion of IL-2 and its functions during the primary response.

The receptor of IL-2, or IL-2R, is a hetero-trimeric protein expressed on the surface of lymphocytes. The α-subunit of IL-2R, CD25, is one of the earliest activation markers of T cell activation. In the experiments by Zehn et al., it was also one of the two surface markers (the other being CCR7) that showed different expression kinetics between high- and low-affinity APL experiments (5). This implicates CD25 as an important player in the model we seek to build. A few paragraphs will be devoted to reviewing the biology of CD25 in our discussions later.

IL-2 and the development of primary function

IL-2 has long been shown to increase the rate of division in activated T cells in vitro, as well as the differentiation of effector function (CTLs) (23). When examined in vivo, however, the picture is less definitive. Mice deficient in IL-2 or subunits of IL-2R have been used to study the impact of IL-2 on primary effector functions. Earlier studies tend to show that the proliferation of T cells appeared to only reduce marginally. Effector functions did not suffer much impairment, if any at all. These experiments used a range of different antigens, including lymphocytic choriomeningitis virus (LCMV)(24), OVA (25), vaccinia virus and LCMV (26), and male Ag (27). A caveat associated with these results is that the T cell proliferation may have resulted from an autoimmune response. IL-2 signaling is crucial for the suppression of autoimmunity. Thus, in experimental systems where transgenic T cells were adoptively transferred into the IL-2 or IL-2R-deficient hosts, autoimmunity may cause over-growth of T cells and mask the proliferation deficiency due to impaired IL-2 signaling (8, 28, 29).

More recent studies took care to circumvent this caveat. For example, Williams and coworkers devised a chimeric strategy, where CD25-deficiency is induced in mice with normal thymic development (29). This and some other similar studies argue that IL-2 deficiency mainly impacts the long term memory effect, while it influences the primary effector function in a quantitative, rather than qualitative, manner. IL-2 deficiency leads to less proliferation, rather than no proliferation.

The most direct evidence comes from the study by Turner et al. They measured the proliferation kinetics of the same set of APLs studied by Zehn et al., and found that IL-2

treatment allows T cell to divide for more rounds (30). Thus, IL-2 signal likely affects primary proliferation in a quantitative manner by altering the kinetics of cell division, rather than causing qualitative changes.

The kinetic profile of IL-2 during primary response

Satoguchi et al. have previously shown that the source of IL-2 during a primary response is confined to $CD25^{low}$ $CD4^{+}$ nonregulatory T cells (31). It can also come from activated CD8+ T cells, albeit to a much lesser extent. There is small amount of basal IL-2 present in secondary lymphoid organs (SLO) prior to the activation of CD4+ or CD8+ T cells, though the exact source of such IL-2 is unclear (6). Activated DCs have been implicated in an experimental study by Granucci et al (32). For our model, these less likely sources of IL-2 during primary proliferation will not be considered.

Sojka et al. recorded the time-course of IL-2 secretion in naïve T cells upon stimulation with Moth Cytochrome C (MCC) mixed with PBS buffer, both *in vitro* and *in vivo* (via adoptive transfer). They found that with potent Ag stimulation *in vivo*, activated CD4+ helper T cells began to secret IL-2 as early as within 1h of infection. Then the number of IL-2 secreting cells rose for 6h before reaching a plateau, which persisted for 4-5h. Afterward IL-2 secretion declined over a period of about 10h until barely detectable at 22h (33). In addition, at higher T cell density, the decline in IL-2 secretion began much earlier.

What intracellular mechanism turns up and down the IL-2 secretion? Though the pathway has not been fully delineated, several key molecules involved in the regulation of IL-2 secretion have been identified. There appears to be feedback regulation between IL-2 signal received by an active CD4+ T cell and its ability to further secret IL-2. For example, Gong and Malek showed that this IL-2 signaling, in addition to TCR signaling, is required for the expression of a transcription suppressor called Blimp-1. Blimp-1, in turn, may cause a decline in the transcription of IL-2 and CD25 genes (34). Martin et al. suggested that Blimp-1 dose so by directly suppressing the *il2* gene (35). Villarino et al. identified the STAT family transcription factors as important mediators of the negative feedback in IL-2 secretion (36). Unfortunately our current understanding of the JAK-

STAT pathway remains too rudimentary to allow for detailed modeling. Therefore, the model will reflect the connection between IL-2 signal and its own rate of synthesis without specifying the molecular mechanism.

IL-2 and T cell egress to periphery

IL-2 signaling may also play an important role in directing activated T cells away from SLO and toward peripheral tissues where they carry out effector functions. There is at least some indirect evidence to show that this is indeed the case. IL-2 appears to achieve this by contributing to the downregulation of CD62L (L-selectin) and C-Chemokine Receptor type 7 (CCR7) and the upregulation of receptors $S1P_1$.

Heavily expressed on the surface of naïve T cells, CD62L and CCR7 are two centrally important chemokine receptors in regulating T cell entry to LN and their migration within LN (37). To facilitate T cell egress from LN, CCR7 and CD62L expression need to be down-regulated (38). $S1P_1$ molecules are receptors for a lysophospholipid, phingosine-1-phosphotase (S1P). They are normally expressed on T cells but transiently downregulated after T cells are activated, in order to temporarily retain them in LN, where they can proliferate and mature. Then S1P1 is upregulated to enable the T cells to egress from LN (37, 39). Earlier experimental results implicate a feedback regulation as the cause of such down-regulation; namely, increasing S1P exposure leads to the down-regulation of S1P1 (37). More recent studies have shown that IL-2 is a very effective inducer in the down-regulation of CCR7, CD62-L and $S1P_1$ via the p100δ subunit of kinase PI3K (39, 40). These results are especially useful, as we recall that, in Zehn et al.'s assay of surface markers during primary proliferation, the only difference between T cells stimulated with high- and low-affinity APLs is the downregulation of CCR7 and CD25 (5).

The regulation of CD25 during primary response

The receptor of IL-2, or IL-2R, is a hetero-trimeric protein expressed on the surface of lymphocytes. The three protein subunits are the α, β and γ chains, which are alternatively known as CD25, CD122 and CD132. Importantly, all three subunits are required for the high affinity binding between IL-2 and IL-2R. Without the complete IL-2R complex, the binding is very weak and is unlikely to initiate much downstream activity (41).

The high-affinity hetero-trimer does not exist in the pre-assembled form in naïve T cells because the expression of the subunits varies significantly. CD132 is the most prevalent, being expressed by almost all hematopoeitic cells. CD122 is induced on Ag-activated CD4+ and CD8+ T cells, as well as regulatory T cells (Tregs). Both these units bind to other cytokines besides IL-2. CD25 is virtually absent in all naïve conventional CD4+ and CD8+ T cells (as opposed to Tregs), and is only induced by Ag-activation (6). CD25 on its own binds IL-2 with relatively low affinity ($K_d \sim 10^{-8}$M). But this association promotes the non-covalent binding with CD122 and CD132 to form the complete receptor, meanwhile stabilizing the binding of IL-2 ($K_d \sim 10^{-11}$M). Then the cytoplasmic tails of CD122 and CD132 associate with Janus kinase 1 (Jak-1) and Jak-3 (6). In this manner, IL-2 signaling enters the Jak-STAT signaling pathway, ultimately leading to relevant gene transcriptions in the nucleus. Newly formed IL2-IL2R complex formed on the surface of T cells are internalized very rapidly ($t_{1/2} \sim$10-20min). CD25 appears to recycle back to the surface, though the extent of which is unclear. Meanwhile the other subunits, along with IL-2, are degraded (42).

The expression and regulation of CD25 are intimately connected to how IL-2 is consumed in LN by activated T cells, thus CD25 kinetics influences how CD4+ and CD8+ T cells interact. However, a comprehensive understanding of how CD25 expression is regulated has yet to emerge. What we do know is that 1) CD25 is one of the earliest markers to be upregulated after T cell triggering; 2) a positive feedback between IL-2 signaling and IL-2R expression is likely (43). There appear to be multiple pathways leading to the enhanced gene transcription of CD25, including one via stimulation of STAT5 and one pathway that directly acts on the *cd25* gene to render the chromatin more accessible to transcription factors (44).

Additional comments on time delay and diffusion

A finite time delay exits between IL-2—IL-2R binding and the regulation of CD25 and IL-2 expression. This time delay corresponds to the time of signal transduction, as well as the transcription and translation of new genes. While this time delay most certainly exists, to

obtain an estimate for its duration requires better understanding of the underlying molecular mechanisms.

Finally, diffusion and distribution of IL-2 molecules in living SLO is important for assessing how localized or globalized CD4+ and CD8+ T cell interactions are. While it has not yet been directly addressed in available open literature, some indirect evidence suggests that its diffusion is a slow process. In earlier works, an estimate for the diffusivity based on molecular weight had been applied to various cytokines (45). Diffusivity estimated based on the physical characteristics of a collagen matrix were considered to closely mimic the diffusivity *in vivo*. Via this approach, IL-2 diffusivity is likely on the order of $10^{-7}cm^2/s$. One could then imagine that if potential "consumer" cells for IL-2 are widely distributed, IL-2 molecules will be restricted around its "producer" cells (i.e. activated CD4+ T cells). Indeed, Snyder performed immuno-histo-chemical staining of IL-2 producing tissues and observed a ring of IL-2 protein closely surrounding the secreting cells (46). This implies that transport limitation may come into play.

In summary, activated CD4+ T cells help the CD8+ T cell response via at least 2 channels: licensing of DCs and secretion of IL-2. Though most of the mechanistic details remain unavailable, there is a significant amount of qualitative understanding regarding processes such as the production, distribution and consumption of IL-2. Should any of these dynamical processes become relevant for modeling purposes, one can employ the strategy used in Chapter 2 by first postulating a simple, qualitatively correct "mechanism" (e.g. dose-response curve postulated in Chapter 2). As researchers uncover more signaling details, a more realistic version can be substituted in. Therefore, in the model development stage, we must also strive for greater flexibility in the computational framework, in anticipation for future expansion.

4.4 A hypothesis for CD8+ T cell proliferation

Guided by the modeling objective and model requirements described in the previous section, I constructed a hypothesis to describe CD8+ T cell proliferation *in vivo* given TCR-pMHC binding affinity. A "resource competition" is built into the model to capture some

key features of the experimental observations by Zehn et al. (5). The "resource" must possess the following characteristics:

1. It enhances T cell division.
2. The activated, dividing T cells need to have received a threshold dose of such "resource" to be able to leave LN and exit into the blood.
3. The total available amount of such "resource" is comparable in LN infected with different APLs.

The "competition" over such "resource" achieves the "dampening" effect observed when CD8+ T cell proliferation occurs *in vivo* as opposed to *in vitro*. The details are as follows:

1. Initially, due to lower TCR-pMHC binding affinity, fewer naïve CD8+ T cells are activated in an LN infected with low-affinity APL.
2. Since the total availability of the "resource" is the same, in the case of the lower-affinity APL, each activated T cell receives more such "resource", since their total number is smaller.
3. More intake of this "resource" per cell means the enhancement in cell division rate is greater, in T cells activated by the lower-affinity APL. Though initially fewer T cells begin to divide, these T cells divide more frequently. This compensates for the disadvantage of a lower TCR-pMHC binding affinity and allows for comparable initial growth kinetics.

The observations regarding the size and timing of expansion peak can be explained as follows:

1. Since the "resource" intake is higher for T cells activated with lower-affinity APLs, their cumulative exposure to such resource will reach the threshold dose required for exit earlier.
2. Earlier exit means that their residence time in LN is shorter, which means fewer rounds of total division, thus overall a small peak size.

Combining observations of several experimental studies, and also taking into consideration data availability, I found IL-2 to be the best candidate for such "resource". In a mouse infected with the lower-affinity Ag for CD8+ T cells, fewer naïve CD8+ T cells are activated initially. However, the mutations that generated the APLs do not affect the

epitopes for CD4+ T cells, thus we expect the number of CD4+ T cells initially activated to be about the same regardless of which APL is used. Thus the production of IL-2 is also comparable in all cases. Then if there are fewer T cells competing over a fixed amount of IL-2 in the LN, each T cell can form more IL-2 complexes. As reviewed in the previous section, IL-2 has been found to enhance the rate of division and increase the maximum rounds a cell can divide. Therefore T cells stimulated with low-affinity APL divide faster than those in a mouse infected with a higher-affinity APL, and in so doing compensate for their lower triggering rate. Thus the initial proliferation kinetics can appear comparable.

We can also explain why CCR7 and CD25 downregulation happens earlier on CD8+ T cells stimulated with the lower-affinity APL, and cell egress to periphery occurs slightly earlier. If a threshold amount of cumulative IL-2 signal is required for egress to begin, then T cells stimulated with lower-affinity Ag will reach this threshold faster, because the competition over the fixed amount of IL-2 is less severe. As T cells approach this threshold exposure, IL-2 signaling facilitates the upregulation of $S1P_1$, and downregulation of CD62L and CCR7, resulting in T cell egress from LN. The downregulation of CD25 can be seen as the consequence of reduced availability of IL-2. As more and more activated CD4+ T cells accumulate sufficient IL-2 exposure and exit LN, the number of IL-2 producers declines. On the other hand, a large number of IL-2 consumer cells still remain in LN, since in a typical primary response CD8+ T cells proliferates far more than CD4+ T cells. The combined result is a decline in IL-2 level while T cells exit LN. Since the expression of CD25 is positively correlated with IL-2 signaling, the expression of CD25 also decreases.

4.5 Model and parameters

After identifying IL-2 as the key "resource" in our hypothesis, the next step is to cast the hypothesis in mathematical language and implement the corresponding computer simulation to assess its veracity. In this section, I will first present the differential equations corresponding to the hypothesis, which is followed by a discussion of the parameters used.

4.5.1 Mathematical model

Ordinary Differential Equations (ODEs) have provided researchers with a powerful tool for studying the kinetics of cell proliferation, including the proliferation during an adaptive immune response (47, 48). Attempts have also been made to model the development of memory T cells using ODEs (49). On the molecular level, ODEs have long served as a primary tool for simulating the kinetics of molecular reactions, including those in biological systems. In this project, I opted for a model based on a system of coupled Delayed Differential Equations (DDEs). ODEs are a special case of DDEs with a zero time delay. The choice of DDEs instead of ODEs is motivated by the need for a signal-propagation time delay discussed at the end of the previous section. In the next few paragraphs, I will first describe the modeling of T cell activation, division, egress, as well as DC licensing. Then the dynamics for IL-2 production and consumption are presented, after which I will describe how to connect these two levels of dynamics.

The main types of cells simulated are naïve and activated CD4+ and CD8+ T cells, and DCs of different maturation stages. They are represented as N_4, N_8, T_4, T_8, and D, D^*, D^{**} respectively.

1. Activation of naïve T cells.

We postulate that a cognate DC can be in 3 states of different degrees of "licensing": unlicensed (D), partially licensed by inflammatory signals (D^*) and fully licensed via cognate interaction with a CD4+ T cell (D^{**}). The conversions can be represented by the following equations:

$$\begin{aligned} D &\xrightarrow{k_i} D^* \\ D + N_4 &\xrightarrow{p} D^{**} + T_4^0 \\ D^* + N_4 &\xrightarrow{p^*} D^{**} + T_4^0 \\ D^{**} + N_4 &\xrightarrow{p^{**}} D^{**} + T_4^0 \end{aligned} \qquad \text{Eq. 4. 1}$$

The first equation represents the "licensing" by inflammatory signals at a rate k_i. A cognate interaction between a DC and a naïve CD4+ T cell can lead to both the activation of the T cell and the full "licensing" of the DC, as represented by the next 3 reactions. The rates follow $p << p^* < p^{**}$.

CD8+ T cells, on the other hand, do not "license" DCs. The recruitment from the pool of naïve CD8+ T cell is represented by the following:

$$\begin{aligned} D + N_8 &\xrightarrow{q} D + T_8^0 \\ D^* + N_8 &\xrightarrow{q^*} D^* + T_8^0 \\ D^{**} + N_8 &\xrightarrow{q^{**}} D^{**} + T_8^0 \end{aligned} \qquad \text{Eq. 4. 2}$$

Note that these 3 reactions do not alter the states of DCs. To enforce the condition that CD8+ T cell can only be activated on licensed DCs, simply let $q \to 0$ and $q^{**} >> q^*$. We do not expect these rates (i.e. k_i, p, q) to change significantly with respect to IL-2 concentration in the LN, thus they remain constant throughout the simulation. Naïve T cells die at extremely low rates and can live for decades, which vastly exceeds the time horizon of this model (50). Thus, in this model we neglect the death of naïve T cells. Finally, the DCs may die at some rate:

$$D, D^*, D^{**} \xrightarrow{\varsigma_D} \varnothing$$

The associated differential equations for the DC population are the following:

$$\begin{aligned} \frac{dD}{dt} &= -k_i D - pDN_4 - \varsigma_D D \\ \frac{dD^*}{dt} &= k_i D + pDN_4 - p^* D^* N_4 - \varsigma_D D^* \\ \frac{dD^{**}}{dt} &= p^* D^* N_4 - \varsigma_D D^{**} \end{aligned} \qquad \text{Eq. 4. 3}$$

Differential equations for the naïve CD4+ and CD8+ T cells are the following:

$$\begin{aligned} \frac{dN_4}{dt} &= -(pD + p^* D^* + p^{**} D^{**}) N_4 \\ \frac{dN_8}{dt} &= -(q^* D^* + q^{**} D^{**}) N_8 \end{aligned} \qquad \text{Eq. 4. 4}$$

2. Division of activated T cells.

The division of individual T cell is a stochastic process. The time of division and the total rounds each cell may divide before stopping differ from cell to cell. In this mean-field treatment, however, we must specify the maximum rounds of divisions as M_4 and M_8. The activated T cell populations fall into different "generations", depending on how many times they have divided. This avoids the need to dynamically manage a variable number

of differential equations, thus significantly reducing the computational cost. Additionally, T cells may exit from LN into the periphery after a certain criterion (to be discussed later) is met. Finally, the activated T cells may die at rates ς_4 and ς_8 respectively.

$$\begin{aligned}
&T_4^i \xrightarrow{\lambda_i} 2T_4^{i+1} \quad i = 0..M_4 - 1 \\
&T_8^j \xrightarrow{\eta_j} 2T_8^{j+1} \quad j = 0..M_8 - 1 \\
&T_4^i \xrightarrow{\varepsilon_4} E_4 \quad i = 0..M_4 \\
&T_8^j \xrightarrow{\varepsilon_8} E_8 \quad j = 0..M_8 \\
&T_k \xrightarrow{\varsigma_k} \varnothing \quad k = 4,8
\end{aligned} \qquad \text{Eq. 4. 5}$$

The associated differential equations are

$$\begin{aligned}
\frac{dT_4^0}{dt} &= (pD + p^* D^* + p^{**} D^{**}) N_4 - (\lambda_0 + \varepsilon_4 + \varsigma_4) T_4^0 \\
\frac{dT_4^i}{dt} &= 2\lambda_{i-1} T_4^{i-1} - (\lambda_i + \varepsilon_4 + \varsigma_4) T_4^i \qquad i = 1 \ldots M_4 - 1 \\
\frac{dT_4^{M_4}}{dt} &= 2\lambda_{M_4 - 1} T_4^{M_4 - 1} - (\varepsilon_4 + \varsigma_4) T_4^{M_4} \\
\frac{dT_8^0}{dt} &= (qD + q^* D^* + q^{**} D^{**}) N_8 - (\eta_0 + \varepsilon_8 + \varsigma_8) T_8^0 \\
\frac{dT_8^j}{dt} &= 2\eta_{j-1} T_8^{j-1} - (\eta_j + \varepsilon_8 + \varsigma_8) T_8^j \qquad j = 1 \ldots M_8 - 1 \\
\frac{dT_8^{M_8}}{dt} &= 2\eta_{M_8 - 1} T_8^{M_8 - 1} - (\varepsilon_8 + \varsigma_8) T_8^{M_8}
\end{aligned} \qquad \text{Eq. 4. 6}$$

It's important to note that many of these rate parameters are not constant, and instead dependent on the dynamics of IL-2, which will be described next.

3. Dynamics of IL-2 and IL-2Rα (CD25).

We treat the formation and degradation of IL-2 – IL-2R complexes in a coarse-grained manner as follows:

$$R + L \underset{k_{off}}{\overset{k_{on}}{\leftrightarrow}} C \xrightarrow{k_d} \varnothing \qquad \text{Eq. 4. 7}$$

Here *R* denotes the concentration of CD25 (or the concentration of high-affinity, complete IL-2R) on a T cell. As discussed in the previous section, the number of high-affinity IL-2R is dictated by the number of CD25, because the other two subunits of IL-2R are constitutively expressed. L and C denote the number of IL-2 near the cell surface and the

number of IL-2 – IL-2R complexes, respectively. Here we assume the diffusion of IL-2 through the LN space is infinitely fast, compared to the other time-scales in the model, therefore the concentration near any T cell surface is the same as the concentration of IL-2 far away.

Also recall from the previous section that the production rates for IL-2 and CD25 depend on the IL-2 signal the cell has received. We postulate that the rate of IL-2 and CD25 production depend on the IL-2 complex concentration in a sigmoid manner. Busse et al. have used a Hill's equation-type formulation for the rates of IL-2 and IL-2R expression with some success (51). Here we apply a similar strategy as follows:

$$\frac{dR_k^i}{dt} = \gamma_k^i - k_{on}R_k^i L + k_{off}C_k^i - \varsigma_R R_k^i$$

$$\frac{dC_k^i}{dt} = k_{on}R_k^i L - k_{off}C_k^i - \varsigma_C C_k^i \qquad i = 1\ldots M_k, \quad k = 4,8 \qquad \text{Eq. 4. 8}$$

$$\sum_{k=4,8}\sum_i T_k^i \frac{dL}{dt} = \sum_{i=0..M_4}\left(\zeta_0 + \zeta^i\right)T_4^i - \sum_{k=4,8}\sum_i \left(k_{on}R_k^i L - k_{off}C_k^i\right)T_k^i - \varsigma_L L \sum_{k=4,8}\sum_i T_k^i$$

$$\gamma_k^i(t) = \gamma_0 \frac{1}{1+\left[\frac{K_\gamma^*}{C_k^i(t-\tau_\gamma)}\right]^{n_\gamma}} \qquad \zeta_k^i(t) = \zeta_0 \frac{1}{1+\left[\frac{K_\zeta^*}{C_k^i(t-\tau_\zeta)}\right]^{n_\zeta}} \qquad \text{Eq. 4. 9}$$

$$i = 1\ldots M_k, \quad k = 4,8$$

The first 2 sets of differential equations apply to both CD4 and CD8 T cells. The concentration of IL-2-IL-2R complexes, *C*, is used to measure the strength of IL-2 signal. The rate of CD25 production, γ, depends on *C* in a Hill's equation-manner with a time lag, τ_γ. This time lag accounts for the time required for IL-2 signal (initiated upon IL-2-IL2R binding on cell surface) to propagate through the intracellular signaling network until reaching the nucleus, and the time for IL-2 and CD25 mRNA transcription. And given that IL-2 and CD25 upregulation can begin within 10 min of stimulation, this time delay is likely very short. The rate for IL-2 production is calculated in an analogous manner with different parameters. The rate for cell division, λ and η, are also calculated in a similar manner as:

$$\lambda_k^i(t) = \lambda_0 \frac{1}{1+\left[\frac{K_\lambda^*}{C_k^i(t-\tau_\lambda)}\right]^{n_\lambda}} \qquad \eta_k^i(t) = \eta_0 \frac{1}{1+\left[\frac{K_\eta^*}{C_k^i(t-\tau_\eta)}\right]^{n_\eta}} \qquad \text{Eq. 4. 10}$$

This reflects the enhancement in cell division due to IL-2 signaling. An important difference is that only CD4+ T cells produce IL-2 after being activated. Therefore, in the final equation for the total IL-2 in the LN, the production term (the first summation) only has contributions from CD4+ T cells.

$$\sum_{k=4,8}\sum_i T_k^i \frac{dL}{dt} = \sum_{i=0..M_4} \zeta^i T_4^i - \sum_{k=4,9}\sum_i \left(k_{on} R_k^i L - k_{off} C_k^i\right) T_k^i - \varsigma_L L \sum_{k=4,8}\sum_i T_k^i \qquad \text{Eq. 4. 11}$$

The exit criterion is based on the total amount of IL-2 signal a cell has received, namely $\int_t C_k^i dt > Z^*$ where Z^* is a threshold for the cumulative IL-2 complexes. How much IL-2 signaling is necessary to turn off $S1P_1$, CCR7 or L-selectin (i.e. the value of this threshold Z^*) cannot be estimated from limited experimental data presently available. Thus its value requires tuning. More details can be found in the next subsection on parameters.

These equations are implemented as a system of Delayed Differential Equations (DDEs) and solved using a DDE solver available in MATLAB. The integrator keeps track of the previous steps (history) according to a time lag specified by the user.

Besides using DDEs rather than the more commonly used ODEs, this model contains another unusual feature, which concerns the initial conditions. As a zero-th generation T cell divides into two first-generation T cells, all cellular materials are divided between the two daughter cells. For simplicity, we assume the division of cellular materials is even between the 2 daughters. Then the initial value for R_k^1 and C_k^1 are half of $R_k^0(t_{0\to 1})$ and $C_k^0(t_{0\to 1})$ where $t_{0\to 1}$ is the time when the division takes place. Because of the coupling among these equations, it is impossible to know a priori the values of either $R_k^0(t_{0\to 1})$ or $t_{0\to 1}$. This also applies to the initial values of later generations. To address this issue, at the time when this division happens, the DDE integration of pauses, and the values of $R_k^1(t_{0\to 1})$ and $C_k^1(t_{0\to 1})$ at that time are updated as $R_k^1(t_{0\to 1}) = \frac{1}{2} R_k^0(t_{0\to 1})$ and

$C_k^1(t_{0\to 1}) = \frac{1}{2} C_k^0(t_{0\to 1})$. Using this newly updated initial condition, the same set of DDEs are integrated until the next division time.

One may ask: how is the "generation-crossing" time determined? While in reality, each cell of the same generation divides at different times (i.e. different values of $t_{i\to i+1}$), a mean-field model cannot accommodate that. In the model it is set to be the time when the cell number of the next generation exceeds a threshold. For example, if this threshold is 1, then the integrator stops as soon as the total cell number of the next generation exceeds 1. And the time is recorded as $t_{i->i+1}$. Such pause and updates are performed for each "generation crossing" for both CD4+ and CD8+ T cells, resulting in a total of M_4+M_8 pauses. The MATLAB® "event" function is used to locate these "generation-crossing" times. The other initial conditions are straightforward. An estimated 10% of the 3000 adoptively transferred T cells may arrive in the LN (Scott Weber and Paul Allen, personal communication). Thus the value of 300 is used as the initial number of naïve CD4+ and CD8+ T cells, N_4 and N_8. The initial amount of CD25 and IL-2 complex on newly recruited T cells are zero, i.e. $R_k^0(t=0) = C_k^0(t=0) = 0$. All DCs are initially in the un-licensed state, i.e. D^* and D^{**} are zero. The initial value of D is set to be of the same as T cells. The only knowledge regarding the initial value for IL-2 molecules available in the LN is that a low basal amount of IL-2 is present prior to primary response. Thus the initial value of IL-2 is another parameter that requires tuning.

4.5.2 Parameter estimation

Some of the kinetic parameters have been directly measured from experiments or estimated from experimental data. Although they apply to different experimental systems (types of cells and Ag used, in vitro vs. in vivo, etc), they at least provide an estimate for the order of magnitude of these parameters in the system we are concerned with. Table 4.1 lists the values of all parameters.

a)

Symbol	Significance	Value
k_i	Rate of DC licensing by inflammatory signals	5×10^{-5} min^{-1}
p	Activation propensity when a CD4+ T cell engages a cognate DC	5×10^{-6} cell^{-1} min^{-1}

p^* p^{**}	that is unlicensed, partially licensed by inflammation, and fully licensed via interactions with cognate CD4+ T cells	2.5×10^{-5} cell^{-1} min^{-1} 1.3×10^{-4} cell^{-1} min^{-1}
q q^* q^{**}	Activation propensity when a CD4+ T cell engages a cognate DC that is unlicensed, partially licensed by inflammation, and fully licensed via interactions with cognate CD4+ T cells	5×10^{-7} cell^{-1} min^{-1} 3×10^{-6} cell^{-1} min^{-1} 1.3×10^{-4} cell^{-1} min^{-1}
$\varepsilon_4, \varepsilon_8$	Rate of exit from LN to blood	1×10^{-4} min^{-1}
k_{on}	Rate of IL-2 binding to IL-2R	1.5×10^{-3}pM^{-1}min^{-1}
k_{off}	Rate of IL-2-IL-2R complex unbinding	0.14 min^{-1}
k_d	Rate of IL-2-IL-2R complex degrading	0.05 ~ 0.1 min^{-1}
Z^*	Threshold of cumulative IL-2 complex. Above which a T cell is qualified to exit from LN into periphery	2000 molecules
ς_D	Death rate of cognate DCs	0
ς_4, ς_4	Death rate of activated CD4+ and CD8+ T cells	0
ς_R	Rate of CD25 degradation	2×10^{-2} min^{-1}
ς_C	Rate of IL-2-IL-2R degradation	1×10^{-2} min^{-1}
ς_L	Rate of IL-2 clearance	1×10^{-3} min^{-1}

b)

Parameter & significance	Parameters in Hill's eq.	Value
λ: Rate of cell division for activated CD4+ T cells.	λ_0	5×10^{-4} cell^{-1} min^{-1}
	n_λ	0.5, 1, 1.5
	K_λ	20, 40, 60
η: Rate of cell division for activated CD8+ T cells.	η_0	5×10^{-4} cell^{-1} min^{-1}
	N_η	0.5, 1, 1.5
	K_η	20, 40, 60
γ: Rate of CD25 production	γ_0	500 molecules cell^{-1}min^{-1}
	N_γ	0.5, 1, 1.5
	K_γ	20, 40, 60
Θ: Rate of IL-2 production by activated CD4+ T cells	Θ_0	500 molecules cell^{-1}min^{-1}
	n_θ	0.5, 1, 1.5
	K_θ	20, 40, 60

Table 4. 1: a) Parameters used in the model. b) Parameters in the Hill's equations.

How the value of each parameter was determined is described below.

1. Rate of DC-licensing via inflammatory signals: No experimental data is available to allow for direct estimate of this rate. The activation rates of naïve CD4+ T cells by cognate DCs (i.e. the rates for DC-licensing via interaction with CD4+ T cells), p, provide an upper bound (see next), as it is significantly higher than k_i. Thus we choose k_i to be one order smaller than pN_4.

2. Rate of T cell activation, p and q: These rates can vary significantly depending on the quality and quantity of Ag present. Specific values are varied over a range to represent different Ag. However, the order of magnitude is maintained as specified in Table 4.1a
3. Exit rate: No direct experimental measurement is available for the kinetics of T cell exit into the periphery. Zehn et al. showed that in 3 days, intra-LN population size dropped by about 50% regardless of Ag used for stimulation (5). Assuming this reduction is mostly due to exit of activated T cells into the periphery, and assuming the exit is a first-order process with a $t_{1/2}$ = 3 days, then the rate is about 3×10^{-4} min^{-1}. Alternatively, we can use Young and cowokers' estimates for T cell population in LN and the total exit flux of T cells from LN. With ~10^8 T cells in LN and an exit flux about 10^6 cells per hour, the time to renew all the T cells in an LN is on average about 100h, which translates to a characteristic time of 3 days as well (details see Chapter 1 (52)). Varying the exit rate can affect when the peak of proliferation occur. The slower the exit rate, the more delayed the peak is.
4. Rate for IL-2 binding to high affinity IL-2R and the dissociation of their complex. The complex formed by IL-2 binding to high-affinity IL-2R has K_d~10nM (6).
5. Base rate of cell division (λ_0 and η_0): During a typical primary response, activated CD4 and CD8 T cells can divide about 7-8 rounds within the first 3 days, and for CD8+ T cells, up to 15 rounds in 7 days (8). The typical division rate is approximately one division per 6-8 hours. Activated CD8+ T cells may divide more rounds than do activated CD4+ T cells. Therefore, in the model, CD4+ cells can divide up to 13 rounds, while activated CD8+ T cells may divide up to 16 rounds. Note that the criteria for T cells to exit from LN into the blood stream do not directly depend on the rounds of divisions completed by a cell. It is possible for a cell that has divided fewer times than the maximum to exit from LN. The maximum number of possible division is set to a large number to ensure that T cell egress is solely due to their meeting the exit requirements.

6. Base rate of IL-2 expression used in the Hill's equation (θ_0): As there are no direct measurements of the rate of IL-2 or CD25 synthesis by active CD4+ and CD8+ T cells, I attempted to derive reasonable estimates from related experimental data and observations. The correct order of magnitude is very important to the validity of this model. Within a reasonable order of magnitude, sensitivity analyses can then be performed to see how the values of these rates affect the qualitative behaviors of the model. Kum et al. studied the kinetics of several anti-inflammatory cytokines induced by Toxic Shock Syndrome Toxin 1 (TSST-1) in human peripheral blood mononuclear cell (PBMC), which include lymphocytes and monocytes (53). About 2×10^6 fresh human PBMC were stimulated with TSST-1 to reach maximal T cell proliferation *in vitro*. Culture supernatants were collected every 0.5h for a total period of 3 days and assayed for cytokines. The resulted time-profile shows a 2-phase increase in IL-2. However, the *in vivo* growth kinetics may be different because of the following. First, the expression of IL-2 is accompanied by continuous cell division, as well as cell trafficking into and out of LN. Also, the *in vivo* IL-2 production by individual cells appears to be a short burst over about 24 hours (54), much shorter than *in vitro*. Therefore, the most relevant data in the time-course generated by Kun et al may be the initial time points only. These data points yield an estimate of 575pg/(ml·h), which corresponds to about 2.3×10^9 IL-2 molecules/(ml·h) (IL-2 molecule is about 155kDa or $\sim2.5\times10^{-7}$pg). Assuming these IL-2 molecules were produced by the 2×10^6 cells present in the sample, then each cell makes about 1100 molecules/(cell·h) or about 20 molecules per cell per min, during the initial phase of IL-2 production (about 12 hours).
7. Base rate of CD25 expression used in the Hill's equation (γ_0): There is no direct measurement in the open literature. A time profile similar to what was used for IL-2 expression was also unavailable. Therefore, I relied on an even more indirect set of measurements to obtain an order of magnitude estimate. The cysteine protease Der p1 has the ability to cleave CD25 on T cell surface and releasing the cleaved fragments from cell membrane. Schulz et al. performed an experiment where T cells were isolated from human blood and stimulated with anti-CD3 in vitro (55). Comparing the

amount of CD25 on untreated cells and cells treated with Der p 1, it appeared that the fluorescence level difference is about a factor of 1.25, i.e. the concentration of CD25 on untreated cells is about 1.25 times of those treated. In another set of experiments, 10^5 such stimulated cells were treated with Der p1. Then the supernatant, which totaled 200μl and contained cleaved CD25, was analyzed over time. The time-profile showed that in the supernatant, which contained cleaved CD25, by 24h, there was 1600pg/ml CD25 in the Der-p1-treated case, where there was only about 700pg/ml in the untreated case. Combining these two observations, one can deduce that the total number of CD25 at 24h is about (1600-700) × 1.25+700=1825pg/ml. Since there was no IL-2 present, CD25 internalization was unlikely to be significant. Thus, on average, there was 0.0037pg/cell. Since CD25 has a molecular weight of 55kDa, this number corresponds to approximately 30,000 molecules per cell. Since the rate of increase of soluble CD25 appears rather linear up to 24h, this rate translates to 21 molecules per min per cell.

8. EC_{50} (various K values) and the exponent (various n values) used in the Hill's equations: These parameters are dictated by the signaling network details and are difficult to estimate. Different values have been applied to see if they lead to qualitatively different behaviors. See next section for more details.

4.5.3 Some preliminary investigations and discussion

Parameter requirements for initial kinetics

First, I would like to examine the differential equations to see what Hill's-equation parameters should be used, in order for T cells stimulated by APLs of different avidities to grow at comparable rates in the first few days.

Adding the equations for CD8+ T cells through all the generations, one obtains an equation for the total number of CD8+ T cells:

$$\frac{dT_8^0}{dt}+\sum_{j=1..M_4}\frac{dT_8^j}{dt}+\frac{dT_8^{M_8}}{dt} = (qD+q^*D^*+q^{**}D^{**})N_8+\sum_{j=0..M_8}\eta_j T_8^j-(\varepsilon_8+\varsigma_8)\sum_{j=0..M_8}T_8^j \qquad \text{Eq. 4. 12}$$

The expressions for the total number of CD8+ T cells, weighted average of activation rates and division rates are as follows:

$$T_{tot} = \sum_{j=0..M_8} T_8^j \qquad \hat{q} = \frac{qD + q^* D^* + q^{**} D^{**}}{D + D^* + D^{**}} \qquad \hat{\eta} = \frac{\sum_{j=1..M_8} \eta_j T_8^j}{\sum_{j=0..M_8} T_8^j} \qquad \text{Eq. 4. 13}$$

Also note that in the very beginning of cell division, the number of naïve CD8+ T cells is much larger than the activated cells, and cell egress has not yet begun. Therefore, we can treat N_8 as a constant, and drop the egress term. Then Eq. 4.12 becomes the following:

$$\frac{dT_{tot}}{dt} = \hat{q} D N_8 + \hat{\eta} T_{tot} \qquad \text{Eq. 4. 14}$$

Now consider 2 APLs of high and low avidity for TCR, respectively. They are denoted using subscripts H and L respectively. If their initial growth kinetics are comparable, then with some algebraic re-arranging:

$$\left.\begin{array}{l} T_{tot}^H \sim T_{tot}^L \\ \dfrac{dT_{tot}^H / dt}{dT_{tot}^L / dt} \sim 1 \end{array}\right\} \Rightarrow \quad (\hat{\eta}_H - \hat{\eta}_L) = \frac{(\hat{q}_L - \hat{q}_H) N_8}{T_{tot}} \qquad \text{Eq. 4. 15}$$

Now using an average number of IL-2 complex per cell, C, and the expression for the rate of division, one obtains:

$$\frac{(\hat{q}_L - \hat{q}_H) N_8}{T_{tot}} \approx \eta_0 \frac{\left(\frac{K_L}{C_L}\right)^{n_\eta} - \left(\frac{K_H}{C_H}\right)^{n_\eta}}{\left[1 + \left(\frac{K_H}{C_H}\right)^{n_\eta}\right]\left[1 + \left(\frac{K_L}{C_L}\right)^{n_\eta}\right]} \qquad \text{Eq. 4. 16}$$

Ideally, if one were able to express K_H / K_L and C_H / C_L as a function of q_H / q_L, one obtains the necessary EC_{50} ratio for any given pair of APLs of known activation rates, such that their initial proliferation kinetics are comparable. Of course, the EC_{50} value is dictated by the actual signaling network, and not an input parameter one can arbitrarily vary. Nonetheless, one may compare the actual EC_{50} with the values that satisfy this equation. If they differ significantly, then this Hill's equation approximation is inappropriate. Experimentally, using appropriate IL-2 reporters, one may measure C. EC_{50} (i.e. K) may be determined using titration with different doses of IL-2 stimulation.

In simulations, it is difficult to predict the value of C a priori. We can, however, observe that in order for the initial kinetics to be comparable, it is required that $C_H/K_H < C_L/K_L<<1$. Simulation using the model shows that this is indeed the case. If the same value of EC_{50} (i.e. K) is used for both APLs, then though the temporal order in T cell egress was reproduced, the T cell stimulated by the high-affinity-APL case grows faster than the those stimulated with the low-affinity-APL case from the very beginning (Fig. 4.1a). By using a set of values that satisfies $K_H>K_L$, however, comparable initial growth kinetics are reproduced (Fig 4.1b).

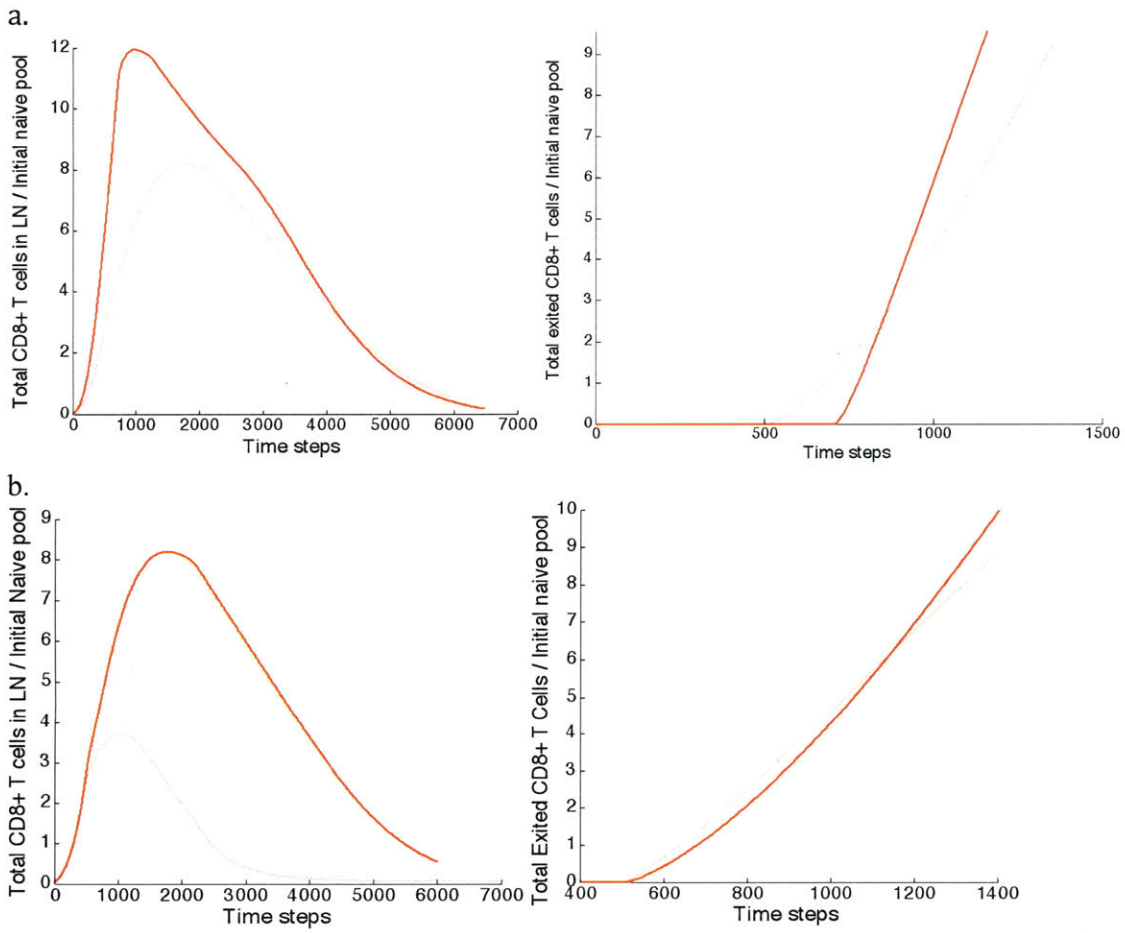

Figure 4. 1: The number of activated CD8+ T cells in the LN divided by the initial number of naïve CD8+ T cells (300) (a and c), and the number of activated CD8+ T cells that have exited from LN (b and d). There are also 200 naïve CD4+ T cells. The maximum numbers of generations an activated CD4+ or CD8+ T cell may divide up to are 13 and 16, respectively. For the high-affinity APL (solid line), the rate of recruitment on a fully matured DC is 10^{-4}/cell·s and 2×10^{-4}/cell·s.

Effect of varying the Hill's exponent, n

As shown in Fig. 4.2a, for IL-2 signal (C) less than the EC_{50} (K), smaller n values lead to higher rates. This trend is reversed if IL-2 signal is above the EC_{50}. It has no effect when the IL-2 signal exactly equals EC_{50}. Thus, the effect of this parameter depends on the EC_{50} value, which is dictated by the signaling network triggered by IL-2 binding to IL-2R. Fig. 4.2b and c demonstrate this point by showing 2 opposite trends. Three different values of n_η are used to calculate the rate of CD8+ T cell division, while this Hill's exponent for the rate of CD4+ T cell division, IL-2 production and CD25 expression are kept constant at 0.5. With a small value of EC_{50}=10, T cells proliferate faster and reach a higher peak size at larger values of n_η (Figure 4.2b), while the opposite is true with a large value of EC_{50} = 60 (Figure 4.2c).

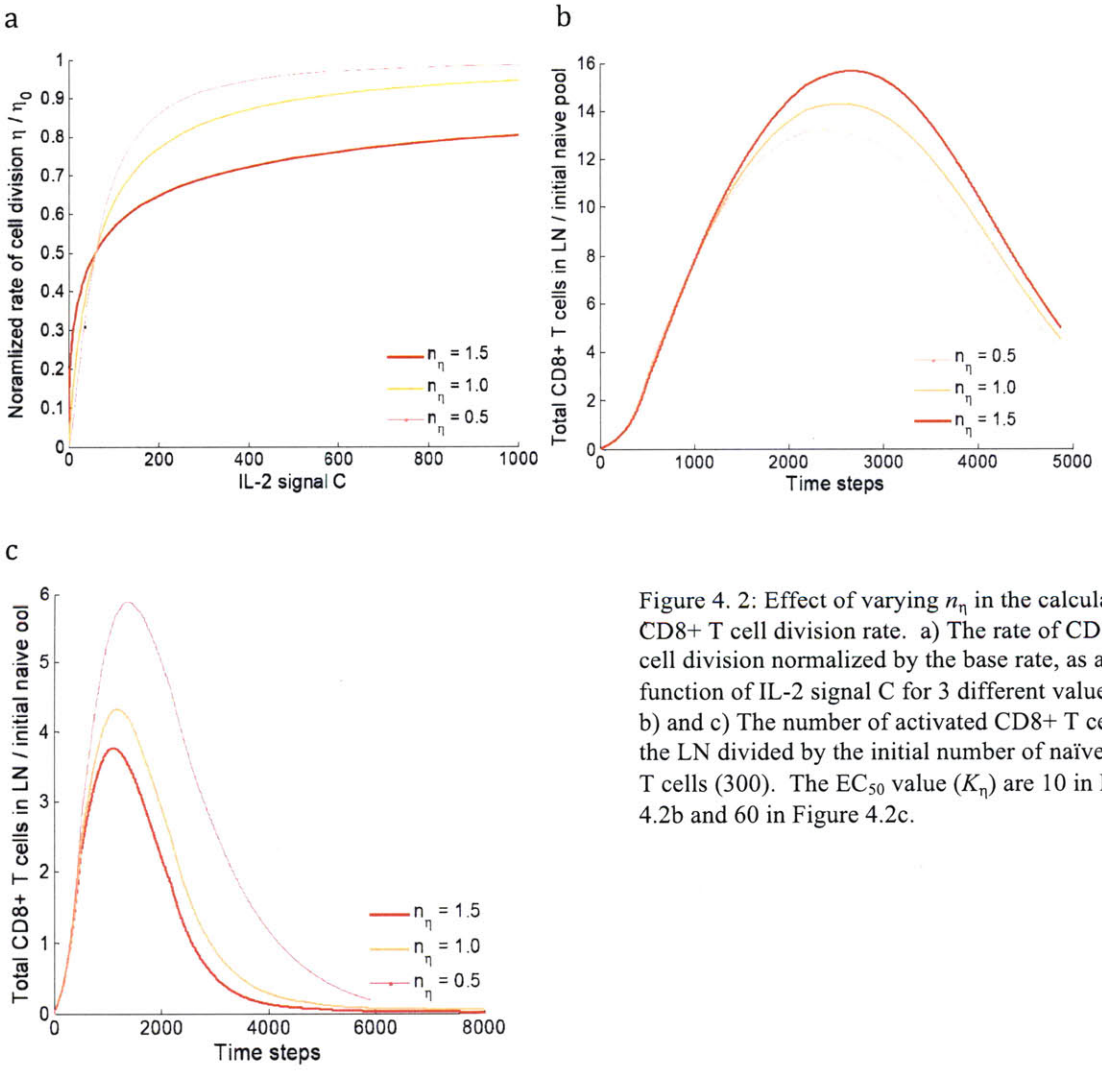

Figure 4. 2: Effect of varying n_η in the calculation of CD8+ T cell division rate. a) The rate of CD8+ T cell division normalized by the base rate, as a function of IL-2 signal C for 3 different values of n_η. b) and c) The number of activated CD8+ T cells in the LN divided by the initial number of naïve CD8+ T cells (300). The EC_{50} value (K_η) are 10 in Figure 4.2b and 60 in Figure 4.2c.

What if APLs are generated for a class-II epitope?

An interesting question is what happens if class-II-restricted epitope APLs are used instead? Consider a scenario analogous to what has been discussed so far, but with the amino acid substitution introduced to a class-II-restricted epitope. What would the proliferation time-course look like? The key differences between this case and the previous are listed below. Again the subscripts H and L denote parameters and variables for the high- and low-affinity-APL case.

Naïve CD4+ T cells initially activated	$T_H > T_L$
Total IL-2 produced	$L_H > L_L$
IL-2 available to each cell	$L_H > L_L$
Rate of cell division	$\lambda_H > \lambda_L$

Except for the first row, the rest of the trends are expected to be opposite of those in the previous case. An additional difference involves the activation and proliferation of CD8+ T cells. As CD8+ T cell activation may be heavily dependent on the licensing of DCs by CD4+ T cells, a lower-affinity class-II APL also means a slower pace in DC licensing. Thus the rate of CD8+ T cell recruitment is restricted, even though the class-I epitopes' affinities are not altered. The interplay of these competing forces would strongly depend on the specific parameters used.

Possible future directions

In the previous discussion, I have suggested some potential experimental tests. As the simulation and analytical results so far imply, the essential feature of this hypothesis lies in the ability of IL-2 signaling to enhance T cell division rate. Experimentally, one could perform a very straightforward titration test by supplying activated CD8+ T cells with different dosages of IL-2. If this hypothesis reflects to some degree the real mechanism, then activated T cells should divide faster at higher IL-2 doses up to some saturation level. Secondly, we must verify that in Zehn et al.'s experiments, CD4+ T cells responses were comparable in mice infected with different Ova APLs. This can be achieved by repeating

some of the experiments, where a time-course for the endogenous CD4+ T cell response is recorded.

Experiments are also needed to investigate the scenario where class-II-restricted epitopes are altered. In fact, such experiments are being conducted at our collaborators' lab at Washington University in St. Louis (Scott Weber and Paul Allen).

The *in silico* model can also be expanded in several directions, which I will briefly discuss below.

1. Regulatory T cells: Regulatory T cells are important in mediating peripheral tolerance. Unlike the conventional CD4+ T cells, they express a high level of CD25 and Foxp3 (a key transcription factor in the development of Tregs) (56). Currently this model only considers conventional CD4+ and CD8+ T cells. However, if experiments in the future verify that IL-2 indeed played an important role in producing the trends observed by Zehn et al., then it may become necessary to take into account the presence and activities of Tregs in the *in silico* model. This is because one of the main ways Tregs exert their influence is via a so-called "metabolic disruption". Since Tregs constitutively express high CD25, they are able to rapidly consume the IL-2 released by activated CD4+ T cells, in so doing "starve" the dividing conventional T cells of this important growth factor (56). This "metabolic disruption" will introduce additional "competition" over IL-2, thus altering the proliferation kinetics of T cells. Introducing Tregs to the model presented earlier is very straightforward.

2. Spatial considerations: The current model assumes instantaneous equilibration of IL-2 throughout the LN space. In other words, all cells are exposed to the same amount of IL-2 on their surfaces. Since LN possesses extraordinary structural complexity and is packed with hundreds of millions of cells, many of which are avid consumers of IL-2 (e.g. Tregs), this assumption may not be a realistic one. Busse and coworkers have shown that in certain parameter regimes, IL-2 diffusion limitation may lead to qualitatively different results (51). Earlier in the discussion of IL-2 diffusion, a diffusivity estimate was provided. One could potentially approximate the transport limitation using a characteristic "length of penetration", thus bypassing the need to simulate multi-scale reaction-diffusion equations.

3. Agent-based model: It is possible to implement the same model using an agent-based approach, where individual cells are explicitly simulated and their histories are tracked. The disadvantage of this approach is implementation difficulty and computational cost. Regarding the first difficulty, other agent-based models I have developed previously (see Chapter 2 and 3) share many common features and can provide readily usable library functions. The computational cost comes in 2 types. First, a very large memory is required to keep records of the history of individual cells. One can selectively record a smaller set of important variables to reduce the memory requirement. The other type of cost arises from the multi-scale nature of this model. Stochastic simulation of the molecular reactions may require extremely small time steps. This problem can be mitigated by using a hybrid approach. For example, the cellular level dynamics are simulated using a stochastic, agent-based approach, while the kinetics of IL-2 consumption and secretion for each cell are calculated using a mean-field solution. The benefit of such an agent-based approach compared to a mean-field one includes at least the following. First of all, it allows for the spatial considerations discussed above, since the diffusive motion of cells and molecules are now treated explicitly. Secondly, since cells divide at their own pace, depending on the DCs they encounter, the local cytokine and cellular environment they face, they will divide for different rounds. This will enable us to divide the active T cells into subsets, based on their rounds of division and IL-2 exposure. Recent experiments have shown that the more a cell divides, and the more IL-2 signaling it has received, the further it differentiates toward the effector lineage (57). The authors suggest that the stochastic trajectories taken by individual cells may be responsible for giving rise to the different functional subsets of activated CD8+ T cells, which later develop into different effector and memory subclasses. In light of these experimental observations and hypothesis, an agent-based approach described here may be very helpful in suggesting experimental designs to test this hypothesis.

4.6 Some concluding remarks

In conclusion, I would like to re-emphasize the necessity and efficacy of a multi-scale perspective toward the study of biological systems, which I elaborated on in the opening

chapter. Through the projects covered in the subsequent chapters, I hope that I succeeded to some extent in delivering this message. And in addition to that, provided some mechanistic insights on a few very important and difficult questions in immunology, and added new modeling tools for future explorations.

References

1. Henrickson, S. E., T. R. Mempel, I. B. Mazo, B. Liu, M. N. Artyomov, H. Zheng, A. Peixoto, M. P. Flynn, B. Senman, T. Junt, H. C. Wong, A. K. Chakraborty, and U. H. von Andrian. 2008. T cell sensing of antigen dose governs interactive behavior with dendritic cells and sets a threshold for T cell activation. *Nat. Immunol* 9:282-291.
2. Zheng, H., B. Jin, S. E. Henrickson, A. S. Perelson, U. H. von Andrian, and A. K. Chakraborty. 2008. How Antigen Quantity and Quality Determine T-Cell Decisions in Lymphoid Tissue *Mol. Cell. Biol.* 28:4040-4051.
3. Das, J., M. Ho, J. Zikherman, C. Govern, M. Yang, A. Weiss, A. K. Chakraborty, and J. P. Roose. 2009. Digital Signaling and Hysteresis Characterize Ras Activation in Lymphoid Cells. *Cell* 136:337-351.
4. Hugues, S., L. Fetler, L. Bonifaz, J. Helft, F. Amblard, and S. Amigorena. 2004. Distinct T cell dynamics in lymph nodes during the induction of tolerance and immunity. *Nat. Immunol.* 5:1235-1242.
5. Zehn, D., S. Y. Lee, and M. J. Bevan. 2009. Complete but curtailed T-cell response to very low-affinity antigen. *Nature* 458:211-214.
6. Malek, T. R. 2008. The Biology of Interleukin-2. *Annu. Rev. Immunol.* 26:453-479.
7. Villadangos, J. A., and P. Schnorrer. 2007. Intrinsic and cooperative antigen-presenting functions of dendritic-cell subsets in vivo. *Nat Rev Immunol* 7:543-555.
8. Bevan, M. J. 2004. Helping the CD8+ T-cell response. *Nat Rev Immunol* 4:595-602.
9. Quezada, S. A., L. Z. Jarvinen, E. F. Lind, and R. J. Noelle. 2004. CD40/CD154 Interactions at the Interface of Tolerance and Immunity. *Annu. Rev. Immunol.* 22:307-328.
10. Lee, B. O., L. Hartson, and T. D. Randall. 2003. CD40-deficient, Influenza-specific CD8 Memory T Cells Develop and Function Normally in a CD40-sufficient Environment. *The Journal of Experimental Medicine* 198:1759-1764.
11. Sun, J. C., and M. J. Bevan. 2003. Defective CD8 T Cell Memory Following Acute Infection Without CD4 T Cell Help. *Science* 300:339-342.
12. Bourgeois, C., B. Rocha, and C. Tanchot. 2002. A Role for CD40 Expression on CD8+ T Cells in the Generation of CD8+ T Cell Memory. *Science* 297:2060-2063.
13. Janssen, E. M., E. E. Lemmens, T. Wolfe, U. Christen, M. G. von Herrath, and S. P. Schoenberger. 2003. CD4+ T cells are required for secondary expansion and memory in CD8+ T lymphocytes. *Nature* 421:852-856.
14. Shedlock, D. J., and H. Shen. 2003. Requirement for CD4 T Cell Help in Generating Functional CD8 T Cell Memory. *Science* 300:337-339.
15. Smith, C. M., N. S. Wilson, J. Waithman, J. A. Villadangos, F. R. Carbone, W. R. Heath, and G. T. Belz. 2004. Cognate CD4+ T cell licensing of dendritic cells in CD8+ T cell immunity. *Nat Immunol* 5:1143-1148.
16. Williams, M. A., and M. J. Bevan. 2007. Effector and Memory CTL Differentiation. *Annu. Rev. Immunol.* 25:171-192.
17. Andreasen, S. O., J. E. Christensen, O. Marker, and A. R. Thomsen. 2000. Role of CD40 Ligand and CD28 in Induction and Maintenance of Antiviral CD8+ Effector T Cell Responses. *J Immunol* 164:3689-3697.

18. Ruedl, C., M. Kopf, and M. F. Bachmann. 1999. CD8+ T Cells Mediate CD40-independent Maturation of Dendritic Cells In Vivo. *The Journal of Experimental Medicine* 189:1875-1884.
19. Sarawar, S. R., B. J. Lee, S. K. Reiter, and S. P. Schoenberger. 2001. Stimulation via CD40 can substitute for CD4 T cell function in preventing reactivation of a latent herpesvirus. *Proceedings of the National Academy of Sciences of the United States of America* 98:6325-6329.
20. Zimmerli, S. C., A. Harari, C. Cellerai, F. Vallelian, P.-A. Bart, and G. Pantaleo. 2005. HIV-1-specific IFN-Œ≥/IL-2-secreting CD8 T cells support CD4-independent proliferation of HIV-1-specific CD8 T cells. *Proceedings of the National Academy of Sciences of the United States of America* 102:7239-7244.
21. Johnson, S., Y. Zhan, R. M. Sutherland, A. M. Mount, S. Bedoui, J. L. Brady, E. M. Carrington, L. E. Brown, G. T. Belz, W. R. Heath, and A. M. Lew. 2009. Selected Toll-like Receptor Ligands and Viruses Promote Helper-Independent Cytotoxic T Cell Priming by Upregulating CD40L on Dendritic Cells. 30:218-227.
22. Bohlen, P., F. Esch, D. Wegemer, P. Salk, and G. Dennert. 1983. Isolation and partial characterization of human T-cell growth factor. *Biochem. Biophys. Res. Commun.* 117:623-630.
23. Smith, K. 1988. Interleukin-2: inception, impact, and implications. *Science* 240:1169-1176.
24. Bachmann, M. F., and A. Oxenius. 2007. Interleukin 2: from immunostimulation to immunoregulation and back again. *EMBO Rep* 8:1142-1148.
25. Yu, A., J. Zhou, N. Marten, C. C. Bergmann, M. Mammolenti, R. B. Levy, and T. R. Malek. 2003. Efficient Induction of Primary and Secondary T Cell-Dependent Immune Responses In Vivo in the Absence of Functional IL-2 and IL-15 Receptors. *J Immunol* 170:236-242.
26. Kundig, T., H. Schorle, M. Bachmann, H. Hengartner, R. Zinkernagel, and I. Horak. 1993. Immune responses in interleukin-2-deficient mice. *Science* 262:1059-1061.
27. Carlow, D. A., M. J. Williams, and H. J. Ziltener. 2005. Inducing P-Selectin Ligand Formation in CD8 T Cells: IL-2 and IL-12 Are Active In Vitro but Not Required In Vivo. *J Immunol* 174:3959-3966.
28. Pipkin, M. E., J. A. Sacks, F. Cruz-Guilloty, M. G. Lichtenheld, M. J. Bevan, and A. Rao. 2010. Interleukin-2 and Inflammation Induce Distinct Transcriptional Programs that Promote the Differentiation of Effector Cytolytic T Cells. 32:79-90.
29. Williams, M. A., A. J. Tyznik, and M. J. Bevan. 2006. Interleukin-2 signals during priming are required for secondary expansion of CD8+ memory T cells. *Nature* 441:890-893.
30. Turner, M. L., E. D. Hawkins, and P. D. Hodgkin. 2008. Quantitative Regulation of B Cell Division Destiny by Signal Strength. *J Immunol* 181:374-382.
31. Setoguchi, R., S. Hori, T. Takahashi, and S. Sakaguchi. 2005. Homeostatic maintenance of natural Foxp3+ CD25+ CD4+ regulatory T cells by interleukin (IL)-2 and induction of autoimmune disease by IL-2 neutralization. *The Journal of Experimental Medicine* 201:723-735.

32. Granucci, F., C. Vizzardelli, N. Pavelka, S. Feau, M. Persico, E. Virzi, M. Rescigno, G. Moro, and P. Ricciardi-Castagnoli. 2001. Inducible IL-2 production by dendritic cells revealed by global gene expression analysis. *Nat Immunol* 2:882-888.
33. Sojka, D. K., D. Bruniquel, R. H. Schwartz, and N. J. Singh. 2004. IL-2 Secretion by CD4+ T Cells In Vivo Is Rapid, Transient, and Influenced by TCR-Specific Competition. *J Immunol* 172:6136-6143.
34. Gong, D., and T. R. Malek. 2007. Cytokine-Dependent Blimp-1 Expression in Activated T Cells Inhibits IL-2 Production. *J Immunol* 178:242-252.
35. Martins, G. i. A., L. Cimmino, J. Liao, E. Magnusdottir, and K. Calame. 2008. Blimp-1 directly represses Il2 and the Il2 activator Fos, attenuating T cell proliferation and survival. *The Journal of Experimental Medicine* 205:1959-1965.
36. Villarino, A. V., C. M. Tato, J. S. Stumhofer, Z. Yao, Y. K. Cui, L. Hennighausen, J. J. O'Shea, and C. A. Hunter. 2007. Helper T cell IL-2 production is limited by negative feedback and STAT-dependent cytokine signals. *The Journal of Experimental Medicine* 204:65-71.
37. Cyster, J. G. 2005. CHEMOKINES, SPHINGOSINE-1-PHOSPHATE, AND CELL MIGRATION IN SECONDARY LYMPHOID ORGANS. *Annu. Rev. Immunol.* 23:127-159.
38. Mora, J. R., and U. H. von Andrian. 2006. T-cell homing specificity and plasticity: new concepts and future challenges. *Trends Immunol.* 27:235-243.
39. Berstein, G., and R. T. Abraham. 2008. Moving out: mobilizing activated T cells from lymphoid tissues. *Nat Immunol* 9:455-457.
40. Sinclair, L. V., D. Finlay, C. Feijoo, G. H. Cornish, A. Gray, A. Ager, K. Okkenhaug, T. J. Hagenbeek, H. Spits, and D. A. Cantrell. 2008. Phosphatidylinositol-3-OH kinase and nutrient-sensing mTOR pathways control T lymphocyte trafficking. *Nat Immunol* 9:513-521.
41. Liparoto, S. F., D. G. Myszka, Z. Wu, B. Goldstein, T. M. Laue, and T. L. Ciardelli. 2002. Analysis of the Role of the Interleukin-2 Receptor Œ≥ Chain in Ligand Binding,Ä†. *Biochemistry* 41:2543-2551.
42. Stauber, D. J., E. W. Debler, P. A. Horton, K. A. Smith, and I. A. Wilson. 2006. Crystal structure of the IL-2 signaling complex: Paradigm for a heterotrimeric cytokine receptor. *Proceedings of the National Academy of Sciences of the United States of America* 103:2788-2793.
43. Kim, H.-P., J. Kelly, and W. J. Leonard. 2001. The Basis for IL-2-Induced IL-2 Receptor [alpha] Chain Gene Regulation: Importance of Two Widely Separated IL-2 Response Elements. *Immunity* 15:159-172.
44. Meyer, W. K.-H., P. Reichenbach, U. Schindler, E. Soldaini, and M. Nabholz. 1997. Interaction of STAT5 Dimers on Two Low Affinity Binding Sites Mediates Interleukin 2 (IL-2) Stimulation of IL-2 Receptor Œ± Gene Transcription. *J. Biol. Chem.* 272:31821-31828.
45. Francis, K., and B. O. Palsson. 1997. Effective intercellular communication distances are determined by the relative time constants for cyto/chemokine secretion and,Äâdiffusion. *Proceedings of the National Academy of Sciences of the United States of America* 94:12258-12262.

46. Yang-Snyder, J. a. R., Ellen V. 1998. Spontaneous Expression of Interleukin-2 In Vivo in Specific Tissues of Young Mice. *Dev. Immunol.* 5:223-245.
47. De Boer, R. J., M. Oprea, R. Antia, K. Murali-Krishna, R. Ahmed, and A. S. Perelson. 2001. Recruitment Times, Proliferation, and Apoptosis Rates during the CD8+ T-Cell Response to Lymphocytic Choriomeningitis Virus. *J. Virol.* 75:10663-10669.
48. De Boer, R. J., and A. S. Perelson. 1995. Towards a general function describing t cell proliferation. *Journal of Theoretical Biology* 175:567-576.
49. Antia, R., V. V. Ganusov, and R. Ahmed. 2005. The role of models in understanding CD8+ T-cell memory. *Nat Rev Immunol* 5:101-111.
50. De Boer, R. J. 2007. Time Scales of CD4⁺ T Cell Depletion in HIV Infection. *PLoS Med* 4:e193.
51. Busse, D., M. de la Rosa, K. Hobiger, K. Thurley, M. Flossdorf, A. Scheffold, and T. H√∂fer. 2010. Competing feedback loops shape IL-2 signaling between helper and regulatory T lymphocytes in cellular microenvironments. *Proc. Natl. Acad. Sci. USA* 107:3058-3063.
52. Young, A. J. 1999. The physiology of lymphocyte migration through the single lymph node in vivo. *Semin. Immunol.* 11:73-83.
53. Kum, W. W. S., S. B. Cameron, R. W. Y. Hung, S. Kalyan, and A. W. Chow. 2001. Temporal Sequence and Kinetics of Proinflammatory and Anti-Inflammatory Cytokine Secretion Induced by Toxic Shock Syndrome Toxin 1 in Human Peripheral Blood Mononuclear Cells. *Infect. Immun.* 69:7544-7549.
54. Lowenthal, J. W., R. H. Zubler, M. Nabholz, and H. R. MacDonald. 1985. Similarities between interleukin-2 receptor number and affinity on activated B and T lymphocytes. *Nature* 315:669-672.
55. Schulz, O., H. F. Sewell, and F. Shakib. 1998. Proteolytic Cleavage of CD25, the Œ± Subunit of the Human T Cell Interleukin 2 Receptor, by Der p 1, a Major Mite Allergen with Cysteine Protease Activity. *The Journal of Experimental Medicine* 187:271-275.
56. Vignali, D. A. A., L. W. Collison, and C. J. Workman. 2008. How regulatory T cells work. *Nat Rev Immunol* 8:523-532.
57. Kalia, V., S. Sarkar, S. Subramaniam, W. N. Haining, K. A. Smith, and R. Ahmed. Prolonged Interleukin-2R[alpha] Expression on Virus-Specific CD8+ T Cells Favors Terminal-Effector Differentiation In Vivo. *Immunity* 32:91-103.